SCIENTIFIC CONFERENCE

Le Bourget-du-Lac – July 2022

PRE-PRINT 2021

SYMPOSIUM 05
Karst hydrogeology, physical Chemistry

Hydrogeology and water chemistry of Hin Nam No National Park, Laos

Terry BOLGER (1) & Gheorghe M. L. PONTA (2)

(1) Cave and Karst Specialist, Vientiane, Laos, laocaves@gmail.com

(2) Geological Survey of Alabama, 420 Hackberry Lane, Tuscaloosa, Alabama 35401 U.S.A., gponta@gsa.state.al.us

Abstract

The Hin Nam No National Park (HNN NP) covers 94,000 ha of mainly limestone landscape in the central Laos province of Khammouane, where the Central Indochina Limestone meets the Annamite Mountain Chain. The karst landscape of HNN NP is contiguous with that of Phong Nha-Ke Bang NP in Vietnam. A nomination for listing HNN NP as a UNESCO natural World Heritage site is in progress. The main features of the hydrographic network are the Xe Bang Fai River in the southern and central areas, including a 6.4 km underground section, and the Nam Ngo and Nam Heu rivers in the northern portion of HNN NP. In February 2020 (dry season), a field survey was conducted to evaluate the karst landscape and to collect fourteen water samples from karst springs, caves, and main river systems of HNN NP. A karst hydrogeological map, which displays the spatial distribution of water in soil and rocks with distinctive permeability was created. Additional information obtained during the karst inventory including springs, caves, sinkholes, sinking streams, are shown on the map to help define the recharge area of the aquifers.

1. Introduction

The Hin Nam No NP is bounded in the South and East by the Xe Bang Fai River and its tributaries, to the West by Nam Ngo and Nam Heu rivers, and in the Northeast with the Phong Nha-Ke Bang National Park, Vietnam (Figure 1. Inset 1a and 1b).

The characteristic landscape style of Hin Nam No is that of a dissected plateau of karst massifs that are bordered by bare limestone walls or cliffs rising to 500 m above intervening alluvial plains developed along Xe Bang Fai and Nam Ngo rivers (BOLGER et al. 2017). The limestone massifs have been eroded into a classic fengcong karst of clustered cones, with pinnacles and deep fissures, making them virtually inaccessible. The sharp-edged and spectacular pinnacles up to 10 m high are signature features of the karst landscape, from which Hin Nam No derives its name i.e., spiky rocks in English (BOLGER 2019).

2. Hydrogeological Map

A karst hydrogeological map of the area is presented in Figure 1. The availability of ground water in the Hin Nam No NP varies widely largely due to the geologic complexity of the area as in other parts of Laos (PONTA & AHARON 2014). The hydrogeologic units are represented according to the legend and symbols used in the Cave and Karst Systems of Romania (PONTA 2019).

The hydrogeological map shows that the availability of ground water in Hin Nam No NP varies widely due to the geologic complexity of the area. Extensive and productive karst aquifers occur in the Khammouane Formation (C-P_1 km) of the upper Xe Bang Fai and Nam Ngo Rivers basins. The mean annual discharge rate from the Xe Bang Fai Cave is 76 m^3/sec. It reaches a maximum monthly average of 480 m^3/sec in August during the wet-season and decreases to a minimum of 2 m^3/sec during the dry-season months of March and April (BOLGER 2019). The Khammouane Formation, consisting of Carboniferous-Lower Permian age carbonate rocks exhibits little or no intercrystalline porosity. Groundwater flow occurs along solutionally enlarged fractures, cavities, joints, and along the bedding planes.

A remarkable finding is the lack of perennial large springs at the base of the cliffs surrounding the HNN karst plateau (the Xe Bang Fai Cave being a notable exception). One explanation for this may be a high degree of secondary porosity (dissolved conduits) providing very efficient drainage and resulting in springs and caves ceasing flow during the dry season. Also, a portion of the HNN karst may be in the recharge area of some large springs in the neighboring Phong Nha-Ke Bang karst area of Vietnam. More studies are required to better understand these observations and the overall hydrogeology of HNN NP.

The hydrogeological map is a useful tool for the management of karst and caves of HNN and the upstream catchment areas draining into HNN NP. The hydrogeological map highlights the catchment areas critical to the environmental management and protection of HNN NP.

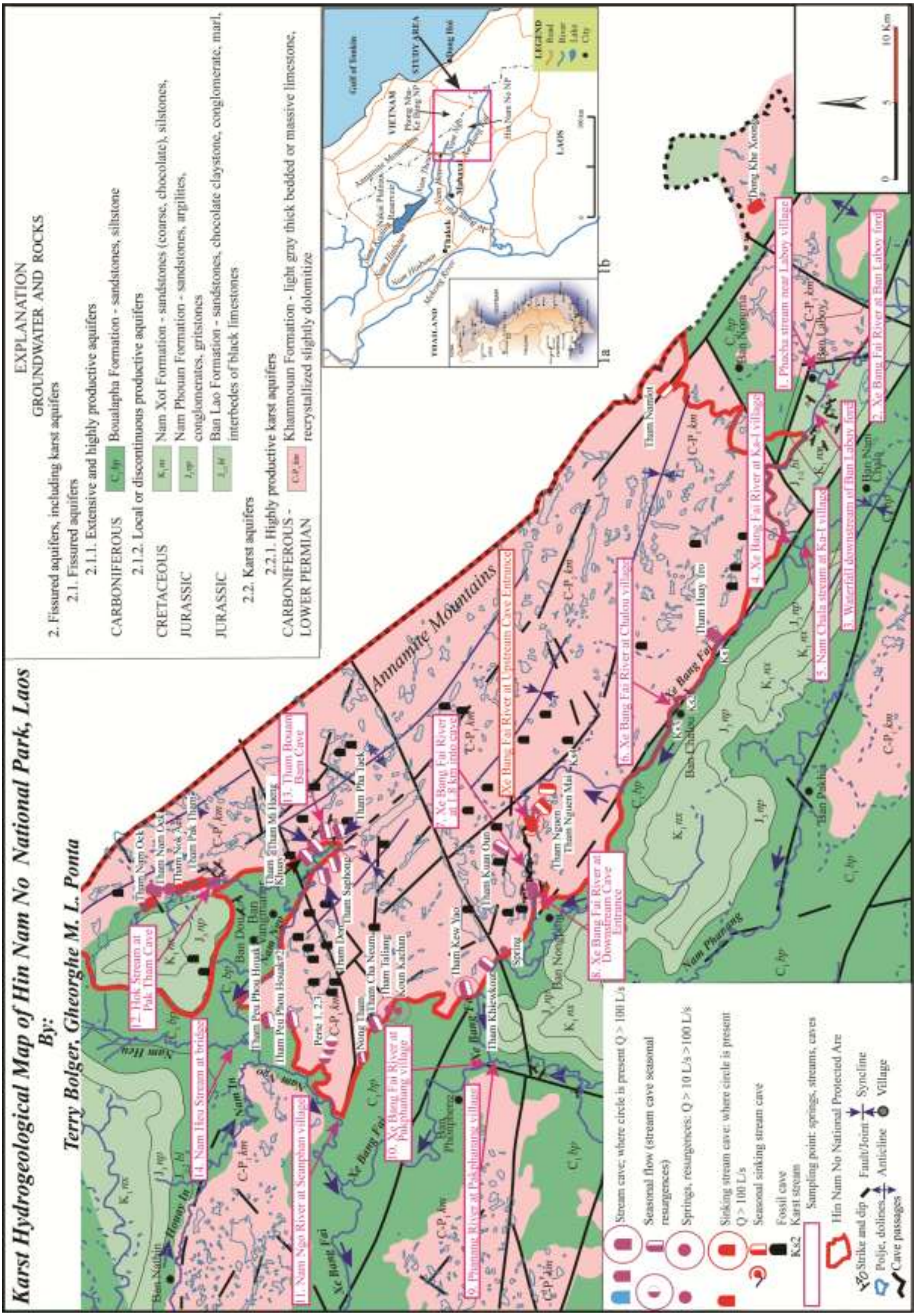

Figure 1: Hydrogeological Map of Hin Nam No National Park (Geology modified after TRAN VAN BAN et al., 2000).

3. Sampling and Water Quality Methods

In February 2020, during base flow, water samples were collected from fourteen locations in and around HNN NP as shown on Figure 1. Geographic coordinates (UTM, WGS84) and elevation were recorded with a GPS (Garmin 62S) at each sampling point. The water samples were analyzed for anions and cations (both major and trace), from caves streams and pools, springs, and rivers. Selected water-quality parameters were monitored at each sampling point with a Hach HQ11d and YSI 63 instrument (pH, temperature, specific conductance, and salinity). Additionally, a digital titrator (Hach Model 16900) was used in the field to determine total hardness as alkalinity, total hardness as calcium, and carbon dioxide.

Groundwater samples from each source were collected and treated as shown below. Samples for cations were collected in 40 ml glass vials treated with nitric acid (concentration 50%) after filtration. Samples for anions were collected in 40 ml vials with no preservatives. Both water samples were filtered to 0.45µm using Mixed Cellulose Esters Sterile membranes, attached to a 60 ml syringe, to remove sediments and microorganisms.

4. Results and Discussions

Fourteen sets of water samples were collected from Hin Nam No NP. The elevations of sampling points ranged between 141m and 323m (AMSL). The estimated flow rates ranged from 0.01 m^3/s to 5 m^3/s. The observations were recorded in February 2020, during the dry season, so these values are characteristic for base flow.

There is a significant variation between sites in water chemistry baselines, conductivity and temperature. The water samples had slightly basic pH values (7.09 – 8.48), and moderate conductivity (C) values 200 to 346 µS/cm.

Temperatures varied from 22.50 to 28.10 ºC. Total alkalinity as $CaCO_3$ varies between 108.6 mg/L (Sample 4) and 230 mg/L (Sample 5).

Total hardness is expressed as the total concentration of Ca^{2+} and Mg^{2+} as mg/L equivalent of $CaCO_3$. Measured water total hardness varies between 142 mg/L (Samples 4 and 6) and 204 mg/L $CaCO_3$ (Sample 5): ten samples fall into the hard category (121 to 180 mg/L $CaCO_3$) and four into the very hard category (>181 mg/L $CaCO_3$). The elevated total hardness values in all study sites indicate large amounts of carbonate rock have been taken into solution.

Anions and cations

Chloride ranged from 0.68 to 2.19 mg/L, with the highest concentration in the Xe Bang Fai River at Ka-I village (2.19 mg/L). Chloride values 2 mg/L or less are naturally occurring. Concentrations of nitrite and nitrate as nitrogen (NO_2+NO_3 as N) ranged from 0 to 1.55 mg/L were found in 13 of 14 study sites, the highest being recorded at Tham Bouam Bam Cave (Sample 13).

Sulfate concentrations ranged from 0.97 to 5.27 mg/L. Calcium concentrations varied from 31 (Xe Bang Fai River before entering the main limestone area) to 81.6 mg/L. The highest recorded values were collected from samples 3 (Waterfall 1.6 km downstream of Ban Laboy ford) and 13 (Tham Bouam Bam Cave).

The concentrations of sodium ranged between 1.72 and 3.58 mg/L. The presence of Mg^{2+} (ranged between 2.30 to 12.80 mg/L), in low concentrations compared to Ca^{2+}, except Sample 1/12.80 mg/L suggesting that the stream traverses dolomitic layers.

In natural waters unaffected by pollution, trace metals occur in low concentrations, generally <0.001 mg/L. Elevated trace metal concentrations may indicate the presence of a pollution source or a nearby ore deposit. Chromium was detected in all 14 samples and ranged from 0.0019 to 0.034 mg/L. The drinking water MCL (USEPA National Primary and Secondary Drinking Water Standard) for chromium (III) is 0.1 mg/L. Manganese was detected in all 14 samples and ranged from 0.0019 to 0.0536 mg/L. Water sample 14 is the only one with manganese above US drinking water standards. The drinking water MCL for manganese is 0.05 mg/L. Cadmium was not detected in any of the 14 samples.

Two of the highest values of the volume of calcite per liter (PALMER, 2007) that has been dissolved/removed in all study sites were calculated in samples 3 (Waterfall 1.6 km downstream of Ban Laboy ford) and 13 (Tham Bouam Bam Cave) both at 0.073 cm^3/L of dissolved calcite. Unexpectedly, the highest value was found in sample 5 (Nam Chala stream at Ka-I village/ 0.084 cm^3/L of dissolved calcite)

The CO_2 concentration in the water samples ranged from 34.4 to 72.4 mg/L, with the highest value being in sample 13 (Tham Bouam Bam Cave). Waters replenishing aquifers near the ground surface are rich in CO_2 originating from the atmosphere and from the oxidation of organic matter by bacteria.

The tendency of a water system to dissolve or precipitate carbonates can be determined by calculating the calcite saturation index or Langelier Index (LI). The LI has been used to evaluate the degree of saturation of waters with respect to $CaCO_3$ based on the pH of the water and the pH at which water becomes saturated pH_s: $LI = pH\text{-}pH_s$

For the investigated groundwaters, LI values range from -0.40 to +0.60. The negative values indicate that groundwater is under saturated with respect to calcite and tends to dissolve carbonate minerals from the host rock. The most negative indexes are for the samples 7 (Xe Bang Fai River at 1.8 km into cave) and 13 (Tham Bouam Bam Cave). Waters collected from eight sites have a positive LI, and all are saturated with respect of calcite. From the samples with LI positive index, the highest values were recorded in samples 6 (Nam Heu Stream at bridge/0.60) and 10 (Xe Bang Fai River at Pakphanang village/0.54), from high $CaCO_3$ concentration limestones.

Geochemical analyses are displayed graphically on the Schoeller Berkaloff diagram in Figure 2. The major cation (Ca^{2+}, Na^{2+}, and Mg^{2+}) and anions (HCO_3^-, Cl^-, $SO_4^{2-}$and NO_3^-) determine water types, which are used to characterize

groundwater quality in specific areas. The major ionic composition of water collected from 14 locations is dominated by calcium, magnesium and bicarbonate ions, typical of karst groundwater.

5. Conclusions

In the Hin Nam No National Park, the Carboniferous to Lower Permian Khammouane Formation (C-P_1km) is exposed in a series of faulted synclines and anticlines, structural strike-oriented northwest to southeast, and forms a highly productive karst aquifer.

The major ionic composition of water collected from 14 locations is dominated by calcium, magnesium and bicarbonate ions, typical of karst groundwater.

Langelier Index values ranged from -0.40 to +0.60. Water collected from eight sites has a positive LI range, all these waters are saturated with respect to calcite. This enrichment was only possible due to the high purity of the limestone. The most negative LI indexes are from samples 7 (Xe Bang Fai River at 1.8 km into cave) and 13 (Tham Bouam Bam Cave).

The hydrogeological map is a useful tool for the management of the HNN karst and the upstream catchment areas draining into the HNN NP. The hydrogeological map highlights the catchment areas critical to the environmental management and protection of HNN NP. These upstream catchment areas should be included in the World Heritage buffer zone, with appropriate regulations and restrictions on land use and development to protect the quality of the water draining from these areas.

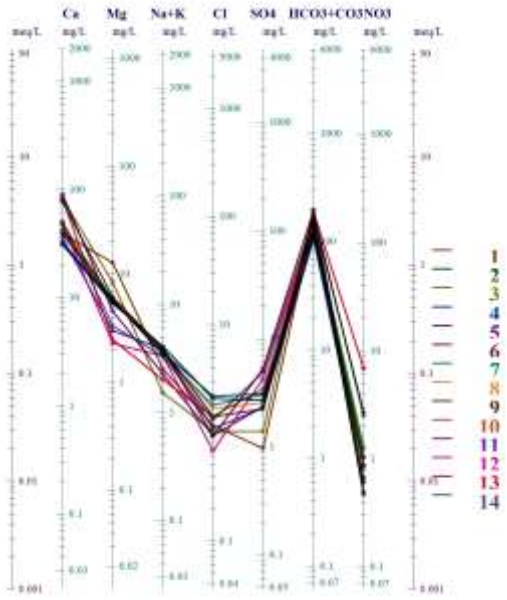

Figure 2: Schöeller Berkaloff diagram illustrating the distribution of the major ions of 14 water samples collected in Hin Nam No NP (dry season). Sample names and locations are shown on Fig. 1.

Acknowledgments

We are grateful to Rick Wagner and Aubrey Prior for performing the water samples analyses in the Geological Survey of Alabama's lab, and to James LaMoreaux with PELA GeoEnvironmental, for the loan a pH meter. We thank the GIZ-Hin Nam No Project and the Hin Nam No National Park for providing logistical support and assistance in the field.

References

BOLGER T., de Koning, M. & Soudthichak S., 2017, Ecotourism Development at the Xe Bang Fai Cave. NSS News, 75(5), 4–7.

BOLGER T., 2019, Xe Bang Fai Cave, Laos in Encyclopedia of Caves Third Edition White W.B., Culver D. V., and Pipan T. (eds), p. 1185-1192.

PALMER A.N., 2007, Cave Geology, Cave Books, U.S.A., p. 454

PONTA G.M.L, 2019, Karst Hydrogeology. In Ponta GML and Onac B.P. (eds.) Cave and Karst Systems of Romania. Springer International Publishing, Cham, pp 41-47

PONTA G. M., and AHARON P., 2014, Karst geology and isotope hydrology of the upstream section of Nam Hinboun River, Khammouane Province (Central Laos), Carbonates and Evaporites 29:1 DOI 10.1007/s13146-014-0195-4, p.127-139

TRAN VAN BAN, VU DINH CHAU, LE VAN DIEU, TRAN SUNG, TA QUOC DAT, BOUNTHEUNG PHENGTHAVONGSA, SIPHANDON VILAYHACK, BOUNTHEUNG SAYASENG, THONGKHANH THOUMMARATH, 2000, Geological Map of Mid - Central Laos Region, sheets E-48-XXII (B. Mahaxai) and E-48-XXVII (B. DonHen), scale 1:200,000

Maillet or not Maillet? What the recession curves of the Fontaine de Vaucluse (France) tell us about the structure of karst

Bernard COLLIGNON

HYDROCONSEIL, 198 chemin d'Avignon, 84470, Chateauneuf de Gadagne, France, collignon@hyroconseil.com ,

Abstract

Following the publication of Maillet's model (1905), hydrologists became accustomed to using decreasing exponentials to model river flows after floods (recession). This law has the advantage of being very simple and it allows us to characterize drying-up using only two numbers: the flow at the beginning of the recession curve and the rate of decrease (expressed in % per day). Due to its simplicity, this model is commonly applied by hydrogeologists in karstic aquifers. However, this is not justified from a theoretical point of view (this type of exponential behaviour does not construe the emptying of a karstic aquifer). We will show that it is also not justified from the observations made on the largest spring in Europe: the Fontaine de Vaucluse (France). The drying curves there are better modelled by the succession of straight lines and hyperboles, accompanied by abrupt variations in flow. We then propose a hydraulic interpretation of this behaviour, which is due to the drainage of the karstic massif by a limited number of main channels in which the flow conditions vary with the water level and saturation of karst conduits. Recession curve details then represent a kind of X-ray of this network.

Résumé

Maillet ou pas Maillet ? Ce que les courbes de récession de la Fontaine de Vaucluse (France) nous apprennent sur la structure du karst. A la suite d'une publication de Maillet (en 1905), les hydrologues ont pris l'habitude d'utiliser des exponentielles décroissantes pour modéliser les écoulements des cours d'eau après les crues (décrue et tarissement). Cette loi a l'avantage d'être très simple et elle permet de caractériser le tarissement par seulement deux nombres : le débit de début de décrue et le taux de décroissance (exprimé en % par jour). A cause de sa simplicité, ce modèle est couramment appliqué par les hydrogéologues dans les aquifères karstiques. Nous allons montrer que ce n'est pas justifié d'un point de vue théorique (ce type de comportement exponentiel ne traduit pas la vidange d'un aquifère karstique). Nous allons montrer que ce n'est pas non plus justifié par les observations réalisées sur la plus grande source d'Europe : la Fontaine de Vaucluse (France). Les courbes de tarissement y sont mieux modélisées par la succession de plusieurs segments de droite ou d'hyperboles, accompagnés de brusques variations de débit. On propose alors une interprétation hydraulique de ce comportement, qui est dû au drainage du massif karstique par un nombre limités de chenaux principaux, dans lesquels les conditions d'écoulements varient avec la hauteur d'eau (et notamment avec les transitions entre un écoulement en charge et un écoulement à surface libre). Les détails de la courbe de décrue constituent alors une radiographie de ce réseau.

1. Introduction

For a century, it has been common practice to analyse recession and drying curves using a decreasing exponential model ($Q=Q_0\ e^{-\alpha t}$) (MAILLET, 1905). This model has the advantage of simplicity: the hydraulic behaviour of a watershed is characterised by a single number: the recession coefficient α.

This model has other advantages:

- it is very simple to implement (you just have to measure the slope of a straight line on a diagram established in semi-logarithmic coordinates);
- it is very eloquent (drying up is simply expressed in %/day, similar to what is used to describe the decrease in activity of a radioactive element, for example).
- it is suitable for direct comparison between different floods or different watersheds.

The same model is still used today, not only by surface water specialists, but also by hydrogeologists who seek to characterise the drying up of springs, including in karstic regions. Maillet's model, developed to simply characterise the recession curves, does not fit with any physical model of karstic structure (and this was not Maillet's ambition).

We will take the example of the Fontaine de Vaucluse (France) to show that a decreasing exponential law has a very low predictive value in the case of a karstic aquifer and that other forms of modelling provide richer information on the flow mechanisms inside the karstic reservoir.

2. Materials and methods

This study focuses on the Fontaine de Vaucluse, which is the most powerful spring in Europe. Its average flow rate is 20m³/s and the most powerful floods exceed 80 m³/s. It is the unique outlet of an aquifer that extends over 1,100 km². This karstic-type aquifer developed in a layer of limestone of Urgonian facies with a thickness exceeding 800m (MUDRY & PUIG, 1991).

The Fontaine de Vaucluse is a spectacular spring that has been explored by divers and robots to a depth of 310 m (Figure 1). In summer, water flows through a scree, 200 m downstream of a wide porch, which gives a view to the water table (Figure 3 - right). At high water, the water level rises until it overflows above the scree (Figure 3 - left).

The Fontaine de Vaucluse is equipped with a very interesting measuring device consisting of two elements:

- A classic gauging station located 300 m downstream of the resurgence, with hourly time step measurements that have been collected since 1996 (Grand Delta organisation manages the database - http://www.hydro.eaufrance.fr);
- A water level gauge (called *Sorgometre* - Table 1) fixed on the wall of the resurgence (Figure 1), with 2-3 measures per week, which has been in service since 1869 (database BRGM).

This device makes it possible to simultaneously measure the total flow rate of the aquifer and the hydraulic head of the aquifer.

Thanks to the records taken with these two measuring devices, we have been able to conduct a detailed analysis of 30 major floods that have occurred over the last 20 years. Each of these floods corresponds to a total discharged volume of several tens of millions of m³.

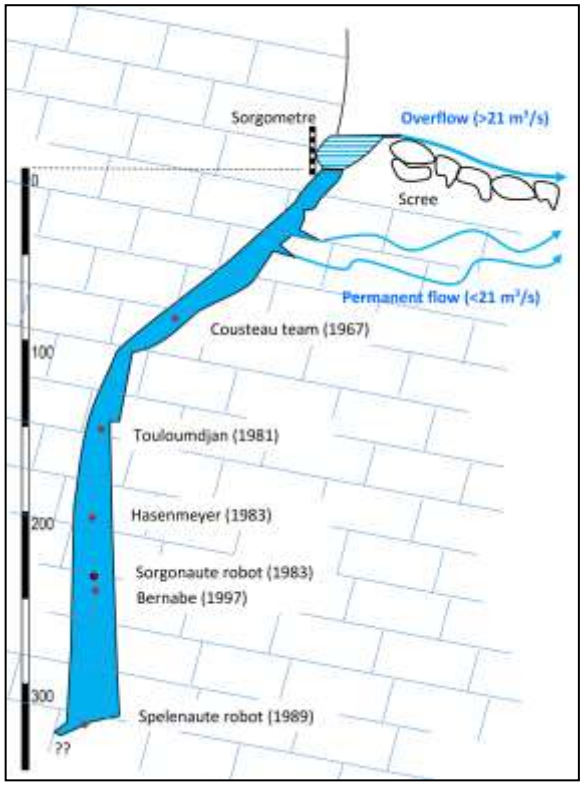

Figure 1: Cross-section of the Fontaine de Vaucluse and main exploration steps

3. Results

Maillet's model does not fit well with the recession curves of the Fontaine de Vaucluse. These curves are closer to a succession of two straight sections than to a decreasing exponential. You could try to frame the family of flood recession curves by two exponentials (Figure 2), but this only underlines the very artificial nature of such an analysis.

In order to better take data into account, we will successively analyse the three main elements of these recession curves and look for a hydraulic interpretation of each of them:

A. The break in the recession curve (net change in slope) that occurs for all the recessionary flows at about 21 m³/s.

B. Recession curves that are very different from each other, for a flow rate higher than 21m³/s.

C. Recession curves that are close to each other, for a flow rate lower than 21 m³/s.

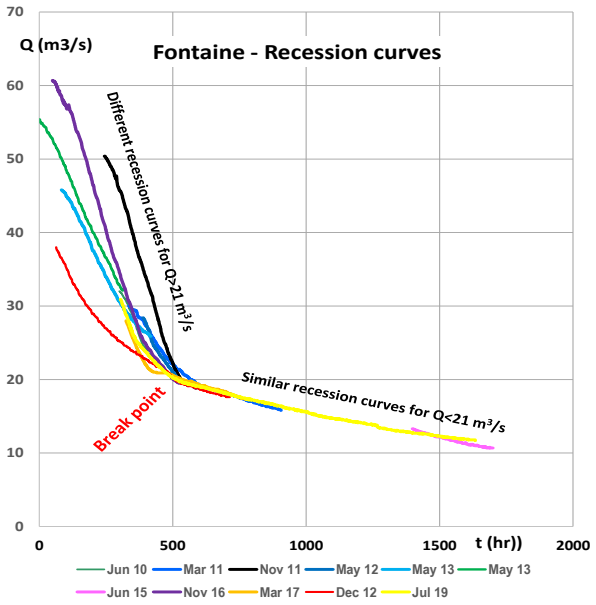

Figure 2: Multiple recession curves for Fontaine de Vaucluse.

For Q>21m3/s, recession curves differ greatly in their shape and slope. Modelling is rather complex.	For Q<21m3/s, recession curve are similar and can be modelled as Q = ((14050 / (t+1485))4/3.
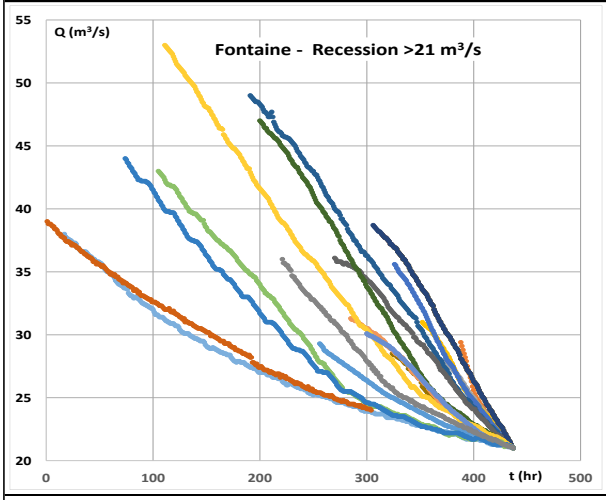	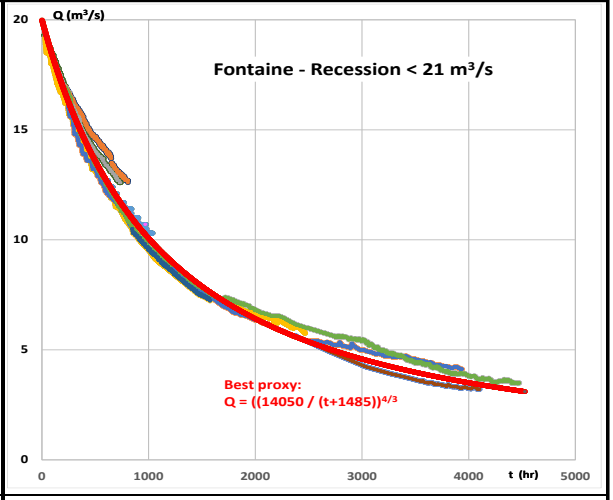
Duration: <15 days / Flowrate: 80 to 21m^3/s	Duration: up to 180 days / Flowrate: 21 to 3m^3/s
This section of the recession curve corresponds to the beginning of recession, with a predominance of free surface flows in a set of channels that change depending on the distribution of rainfall over the catchment area.	This section of the recession curve corresponds to the slow emptying of the epiphreatic reservoir that was filled with water during the floods. The head losses reflect the predominance of pressure flow in the scree.
	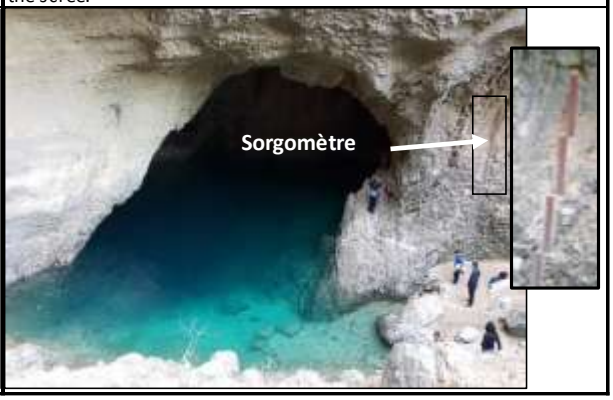

Figure 3: Comparing the two main recession phases - >21 m³/s (left) - <21 m³/s (right)

4. Discussion

A. The break in the recession curve

Many authors have already proposed breaking down the recession curve of a karstic source into several portions that are analysed separately (BONACCI, 1993; MALIK, 2015). This breakdown is easily applied to the Fontaine de Vaucluse, where the slope break is obvious on all the recession curves regardless of the season or intensity of the flood. It is therefore an intrinsic feature of the hydraulics of the karst conduit network, with little dependency on the rain signal. The flow rate of 21 m^3/s corresponds to a physical feature of the system: it is exactly equal to the overflow rate of the basin (MUDRY & PUIG, 1991).

We have highlighted a similar slope break during recession, for Q=25.5 m^3/s (Figure 4) and another slope break on the flood rise curves, for an identical flow rate of 21 m^3/s.

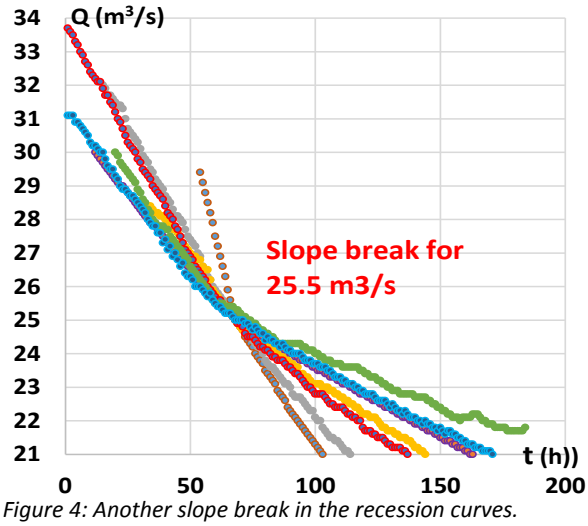

Figure 4: Another slope break in the recession curves.

B. The recession curves that are very different from each other, for Q>21 m³/s

For a flowrate exceeding 21 m³/s, the basin of the Fontaine de Vaucluse overflows. 3 to 5 days after the rainfall episode, the water discharge begins to fall at a rate that differs greatly from one flood to the next (Figure 3 - right). The recession coefficient (as defined by Maillet) varies between 3.5 and 14 % per day. This portion of the recession curve and the recession coefficient are therefore not a direct signature of the drainage network, but the transformation by this network of a rainfall signal that differs from one flood to another, according to the intensity and location of rainfall in the vast catchment area

C. The recession curves that are close to each other, for Q<21 m³/s

When the flowrate falls below 21 m³/s, the spring stops overflowing and all the water flows through the scree. The large porch that acts as an overflow spring in high water conditions then becomes a simple piezometer showing head variations in the main conduit feeding the scree.

This phase can last up to 5 months. This section of the recession curve is almost the same for all floods, which means that it reflects an intrinsic feature of this karstic system: the volume of water stored in the aquifer system.

When Q<21 m³/s, the best proxy for the recession curve is not an exponential (as proposed with Maillet's model) but rather a hyperbolic law ($Q=14000/(t+1500)^{4/3}$) as proposed by DROGUE (1972) (Figure 5). This relation does not claim to be a universal physical law. It is simply a good approximation for Fontaine de Vaucluse recession curve.

This phase illustrates the progressive emptying of the aquifer slice between 85 and 103 m.a.s.l. (Figure 1).

By comparing the two sets of data, we can calculate the permanent aquifer reserves for each meter of aquifer using a method similar to the one we use borehole monitoring (COLLIGNON, 1988). The reserves of the Fontaine de Vaucluse store are 4 million m³ per meter of drawdown in the 85-103 m asl range. This corresponds to <1% of the rock volume.

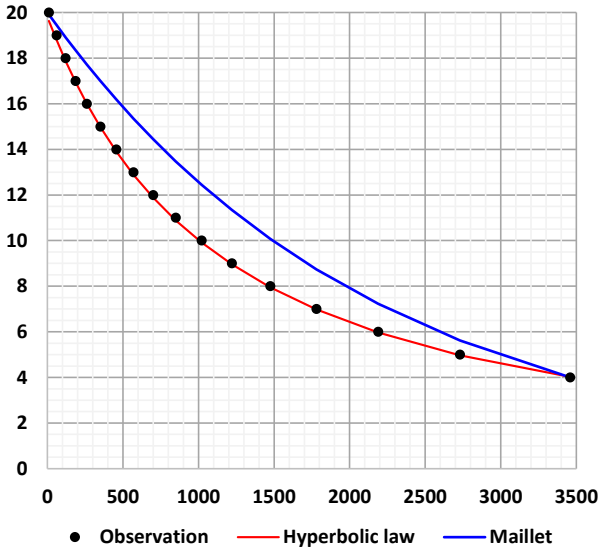

Figure 5: Best proxy for the recession curves

5. Conclusion

The main interest of Maillet's law is its simplicity of use. It allows us to quickly make comparisons between floods or between karstic springs from limited data. However, it must always be borne in mind that the karstic environment is too heterogeneous for water circulation to obey such simple laws as Maillet's or Darcy's.

During floods, most of the flow passes through a limited number of conduits where the flow regime is turbulent. The shape of the recession curves then reflects the progressive dewatering of a portion of these channels. When the recession hydrograph shows several sections separated by a clear break in the slope, it is important to study each section separately. If this break always occurs for the same flow rate, it is likely that it reflects a threshold effect: below this flow rate, one of the main karstic channels is dewatered. This is the case for the Fontaine de Vaucluse, where the two clearly visible sections on the recession curves correspond exactly to the geometry of the resurgence. The first section varies from one flood to another, depending on the characteristics of the rainfall event. The second section, common to all floods, is a signature of the karst reservoir. It is a sound basis to estimate the storage in the karst reservoir: 4 Mm³ per meter (<1% of the rock volume).

References

BONACCI, O. (1993). Karst spring hydrographs as indicators of karst aquifers. *Hydrological Sciences Journal*, 53-62.

COLLIGNON, B. (1988). Evaluation des réserves permanentes et renouvelables des aquifères karstiques de l'Ouest de l'Algérie à partir du suivi des forages en exploitation. 4ème Colloque d'hydrologie en pays calcaire, (pp. 99-105). Besançon.

DROGUE, C. (1972). Statistical analysis of hydrographs of karstic springs. J.Hydrology. 15,1, pp 49-68.

MAILLET. (1905). Essais d'hydraulique souterraine et fluviale. Paris: Herman.

MALIK, P. (2015). Evaluating discharge regimes of karst aquifer. In Z. Stevanovic, Karst aquifers (pp. 205-249). Cham: Springer.

MUDRY, J., & PUIG, J.-M. (1991). Le karst de la Fontaine de Vaucluse. Karstologia, 29-38.

Hydrology of the El Convento Tropical Karst Stream, Puerto Rico

Carlos CONDE-COSTAS

Puerto Rico Speleological Society; Sacred Heart University, Puerto Rico; Tierra Linda Consultants, condecostas@yahoo.com

Abstract

The hydrological regime of the El Convento cave stream was characterized over one hydrological year. Instantaneous discharge measurements were conducted and a continuous record obtained by an automatic water-level logger. A stage-discharge relation (r2 = 0.92) was correlated to the logger record and a mean daily discharge hydrograph constructed. The hydrograph, which included groundwater and surface water inputs, averaged a discharge of 0.106 m3/s and related well to the seasonal precipitation regime. The prevailing base-flow dynamics of the system as well as the percentage of the time that a particular flow is equaled or exceeded was assessed by a flow-duration curve. Particularly relevant is that the hydrograph median value (0.014 m3/s) is comparable to the ground water contribution as given by the median of the instantaneous discharge measurements (0.013 m3/s) conducted under base-flow. Thus, the difference between the average and median values of the hydrograph provided a sound approximation of the annual surface water contribution to the stream. The assessment offers an insight on methods and analytical techniques that can be applied to characterize the hydrology of a tropical karst cave stream.

Résumé

Hydrologie de la rivière souterraine tropicale d'El Convento, Puerto-Rico. Le régime de la rivière souterraine d'El Convento a été étudié sur plus d'une année hydrologique. Des mesures de débits instantanés ont été effectuées et un enregistrement en continu du niveau d'eau a été obtenu par un logger automatique. La relation hauteur-débit (r2 = 0.92) a été établie par les données du logger et un hydrogramme du débit moyen journalier a été construit. Cet hydrogramme, qui prend en compte les apports des eaux souterraines et de surface, met en évidence un débit moyen de 0,106 m^3/s, bien corrélé avec le régime saisonnier des précipitations. Il est significatif que la valeur médiane de l'hydrogramme (0,014 m^3/s) est comparable à la contribution des eaux souterraines indiquée par la médiane des débits instantanés (0,013 m^3/s). Ainsi, la différence entre les débits moyens et médians fournit une solide approximation de la contribution des eaux de surface au débit de la rivière. Cette estimation donne un aperçu des méthodes et techniques analytiques capables de caractériser l'hydrologie d'une rivière souterraine dans un karst tropical.

1. Introduction

Karst terrains are characterized by subsurface drainage, where linkages between surface and groundwater are strong. These underground drainage systems may discharge into streams, emerge as springs or as cave resurgences, becoming the "headwaters" of many karst surface streams. Recognizing that the hydrological condition of the stream can be a major factor influencing aspects of the cycling of nitrogen (BRYCE, 1983), the hydrology of the El Convento cave system (Fig. 1) was characterized over one hydrological year in order to support an investigation concerning the dynamics of nitrogen in a tropical karst stream. The El Convento cave stream is a representative tropical system located on the southwestern coast of Puerto Rico. The cave stream maintains a perennial flow due to groundwater inputs from the limestone aquifer. The following paper summarizes fundamental hydrological aspects included in (CONDE-COSTAS, 2011).

2. Methods and Procedures

It has been shown that concepts and models of nutrient dynamics, as well as methods developed for surface streams are applicable and useful in the study of cave streams (GRAENING & BROWN, 2000); (SIMON & BENFIELD, 2002). Instantaneous discharge measurements were conducted at the upstream reach (Sta. C2) and at the surface reach (Sta. SR) (Fig. 1), 25 at each site using the velocity-area method as described by (GORE, 1996).

To obtain a continuous discharge record, an automatic water-level logger (Hobo U20™) and a staff gage (i.e. long ruler) were installed at the surface reach monitoring pool (Sta. SR) and operated from January 2007 to February 2008. The logger pressure readings were fixed to the appropriate interval of 15 minutes and converted to water levels using the HOBOware™ software.

Figure 1: Plan-view map of the El Convento cave system, Guayanilla-Peñuelas, Puerto Rico

For the construction of the mean daily discharge hydrograph the stage - instantaneous discharge relation ($y = 0.9759x + 0.2365$; $r^2 = 0.92$) was correlated to the logger continuous water level record. To assess flow-occurrence probabilities with a strong degree of certainty, the U.S. Geological Survey long-term data (29 years of record) from the nearby Rio Guayanilla was utilized. A discharge correlation was established between the Rio Guayanilla station and the surface reach monitoring station ($r^2 = 0.90$) of the cave stream, from which a flow-duration curve was constructed for the cave stream.

3. Results

A statistical summary of the mean daily discharge for the study period is provided in Table 1. The mean daily discharge hydrograph (Fig. 3) integrates the perennial base-flow provided by the limestone aquifer and the periodic short-term surface water inputs of the El Cedro creek, which discharges into the cave stream only during storm events through a connecting sinkhole. Such events are responsible for the periodic flooding of the cave and mean daily discharge extremes or peak flows.

Mean Daily Discharge (m^3/s)				
Period Total	**Average**	**Median (Q_{50})**	**Minimun**	**Maximun**
45.36	**0.106**	**0.014**	**0.003**	**5.94**

Figure 2: Statistical summary of mean daily discharges (m^3/s) recorded at the El Convento cave stream from January 2007 to February 2008

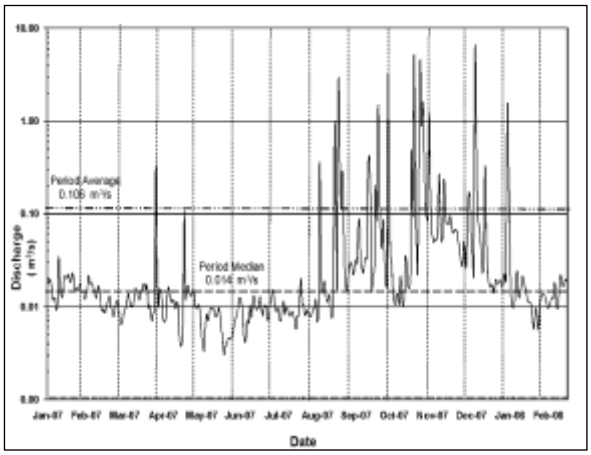

Figure 3: Mean daily discharge hydrograph of the El Convento cave stream.

The monthly discharge partition was provided for assessing the precipitation-discharge relation under the groundwater drainage regime and during surface water inputs (Fig. 4). When the monthly median trend is compared to the total rainfall distribution, a slower and delayed response to the rainfall recharge events is observed, particularly within August-September and October-November, where the stream monthly discharge increases the following month after a high precipitation period. In contrast, during the wet-period (i.e. from August to November) the distribution of monthly averages (which integrates surface water inputs) followed the monthly precipitation trend. The observation is consistent with the expected hydrologic response of ground and surface water drainage systems to precipitation.

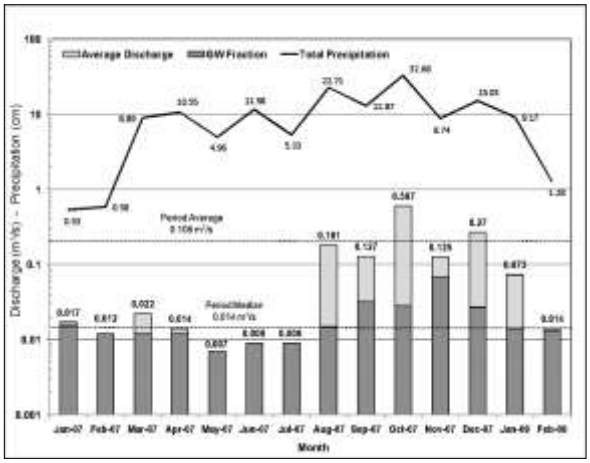

Figure 4: Relative groundwater (GW) contribution to the average monthly discharge of the El Convento cave stream and total monthly precipitation recorded at the Peñuelas 1 NE climate station (NWS).

As expected, the flow-duration analysis or percentage of the time that a particular flow is equaled or exceeded (Fig. 5), showed that the period median discharge (0.014 m^3/s) had a duration of 50 percent. This is, during half of the annual cycle the stream discharge is greater than 0.014 m^3/s, but

conversely 50 percent of the time the flow is equal or less than the median. The flow-duration analysis anticipates if water-quality determinations are representative of base-flow dynamics.

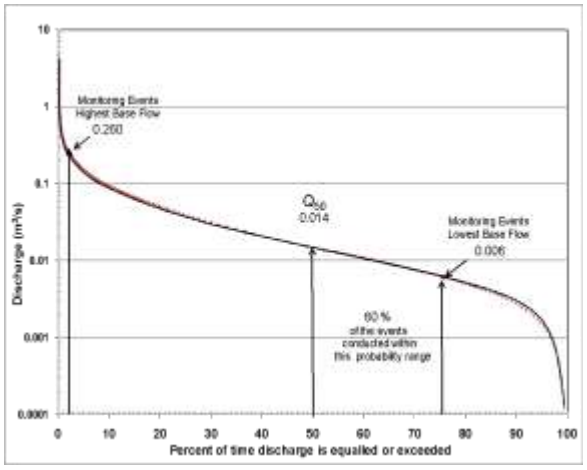

Figure 5: Annual flow-duration curve for the El Convento cave stream showing occurrence probabilities for the highest and lowest base flow discharge recorded during the monitoring events.

The discharge relation between the headwater input and the surface reach outflow (Fig. 6) showed that about 85 percent of the time the stream flow increased along the cave waterway. The prevailing *gaining* condition suggests that most of the time the water-table is above the stream bed. However, during the monitoring events of March, April, May and July 2007, the system became mostly a *losing* stream, indicating that the water-table was below the stream bed. This results in a leakage.

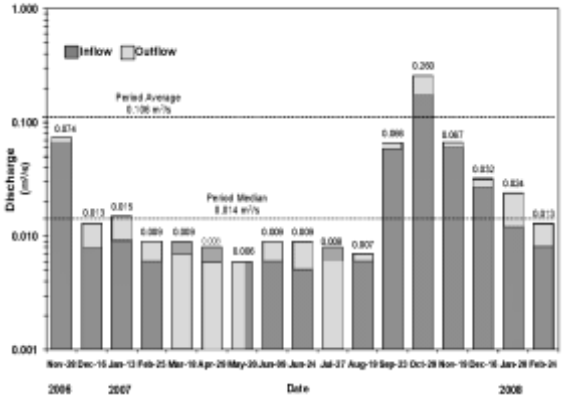

Figure 6: Relation between the El Convento cave stream headwater inflow and outflow discharges.

4. Discussions

During the 14 months monitoring period, total precipitation within the area (134.5 cm) was comparable to the historic annual average (139.3 cm), as recorded by the nearest climate station (NOAA, Peñuelas 1 NE). Consequently, the hydrological measurements made over this period can be considered as representative of average annual hydrological conditions. The steep recessions of the hydrograph evidenced that surface water inputs are short-term events.

The median value of the daily discharge rates for the period (0.014 m^3/s) is comparable to the cave stream annual base-flow outflow of 0.016 m^3/s asserted for the local karst drainage system using the MODFLOW-96 groundwater model (QUIÑONES, 2001). Moreover, it almost matches the median (0.013 m^3/s) of the 25 base-flow direct discharge measurements conducted at the surface reach (SR) during the monitoring period. Consequently and considering that the median is not sensitive to *outliers* (such as, periodic short-term flood events caused by surface water inputs), it is reasonable to accept the median value of the monthly mean daily discharge as representative of the relative monthly contribution of groundwater inputs to the cave stream. Thus, it can be deduced that the difference between the average and median values provides a sound approximation of surface water contributions. The fact that during the months of February, May, June and July (where no surface water inputs occurred), the average and median values were equal supports the relation. In our case, such partition evidenced that as a groundwater drainage system the cave stream exhibits a slower and delayed response to rainfall recharge events. Such response provides for a smoother transition between low and high base-flow discharges, damping the impact of high flow disturbances in the benthic community and ecological processes.

Although groundwater is the perennial recharge source (providing for an annual base-flow discharge of about 0.014 m^3/s), the dynamic of the stream discharge is notably influenced by the periodic short-term surface water inputs of the El Cedro creek, which accounts for about 85 percent of the annual average mean daily discharge (0.106 m^3/s). Considering the annual base-flow (0.63 m^3/s) and average mean daily discharge (3.31 m^3/s) of the largest cave stream in Puerto Rico (Rio Camuy Cave System) (Torres-Gonzalez, et al. 1983), the water contribution of the El Convento cave stream to the surface environment can be regarded as relatively small. Nevertheless, due to its perennial character in such a dry region its ecological importance stands-out as a key element in the transport of nutrients and integration of biogeochemical processes along the downstream portion of the karst watershed.

The observed water gaining-losing condition of the cave stream is a function of the rise and decline of the aquifer water table due to seasonal changes in precipitation. During dry periods (i.e. from December to March) the cave stream drains the aquifer storage, while in the wet season (i.e. from August to November) the storage is replenished and the aquifer water table rise, increasing groundwater inputs and the base flow of the cave stream. The relative gentle slope of the flow-duration curve (Fig. 5) indicates a substantial groundwater storage within the karst catchment basin (MORISAWA, 1968). If the annual aquifer recharge of 0.022

m^3/s (QUIÑONES, 2001) and base-flow discharge (0.014 m^3/s) are considered, about 0.008 m^3/s of groundwater (36 percent of the recharge) are found to be in transient storage within the aquifer. The fact is that the non-gaining events were associated with outflow discharges of 0.007 and 0.006 m^3/s (less than the computed transient storage), while gaining events were observed when output discharges were higher than the aquifer transient storage. Based on the observed relation and considering that the probability of exceedance for such discharges is about 75 percent, it can be stated that about 25 percent of the annual hydrologic cycle the cave stream turns into a losing stream, mostly during spring and summer.

5. Conclusion

The assessment offers an insight on methods and analytical techniques that can be applied to characterize the hydrology of a tropical karst cave stream. The finding that the median and average values of the annual mean daily discharge record can be related to the monthly contribution of ground and surface water inputs to the cave stream constitute a practical instrument for characterizing recharge dynamics in similar cave systems.

The study corroborated that the El Convento cave stream constitutes the main groundwater discharge point for the local karst conduit drainage system. The observed hydrological relation between the cave and surface drainages evidenced that cave systems can play a major role in the integration of nutrient cycles in karst

Acknowledgments

Special recognition to my doctoral advisor, Dr Jorge Ortiz-Zayas (Graduate Program of Biology, University of Puerto Rico, Rio Piedras Campus) and to the members of the dissertation committee, Dr. Elvira Cuevas, Dr. Gary Toranzos, Dr. Alonso Ramírez and Dr. Armando Rodríguez for their commitment and valuable support.

References

BECK, B. F. (1974). *Geology and hydrology of the Convento Cave Spring System, Southwestern Puerto Rico.* International Journal of Speleology, Vole 6, pp. 93-107.

BRYCE COOPER, A. (1983). *Effect of Storm Events on Benthic Nitrifying Activity.* Applied Environmental Microbiology, American Society for Microbiology, p. 957-960.

CONDE-COSTAS, C. (2011). Nitrogen Dynamics in a Tropical Cave Stream. Doctoral Dissertation, UPR RRP SB Ciencias Naturales (551.49 C745n 2011), 152 p.

GORE, J.A. (1996). *Discharge measurements and streamflow analysis.* Methods in Stream Ecology. Edited by F.R. Hauer and G.A. Lamberti. Academic Press. San Diego: 145-160.

GRAENING, G.O. and BROWN, A.V. (2000). *Trophic dynamics and pollution effects in Cave Springs cave, Arkansas.* Arkansas Water Resources Center, University of Arkansas. Publication No. MSC-285.

MORISAWA, M. (1968). Streams: Their dynamics and morphology. McGraw-Hill. New York, N.Y.

QUIÑONES-APONTE, V. (2001). Geohydrologic investigation, Parque de Miramontes, Peñuelas, P.R. Planning Board, Report 2001-62-0392-JPU-ISV.

SIMON, K.S. and E.F. BENFIELD. 2002. Ammonium retention and whole-stream metabolism in cave streams. Hydrobiologia 482: 31-39.

TORRES GONZALEZ, A., E. AGUILAR and G. PANNELLA. (1983). Geohydrology of the Rio Camuy Cave System Puerto Rico. Journal of Engineering Research, University of Puerto Rico, Mayaguez.

The experimental station in the Trebiciano Abyss

Sergio DAMBROSI

Società Adriatica di Speleologia, 34100 Trieste, Italy, www.sastrieste.it

Abstract

The aim of this work is to illustrate the origin and evolution of a Hypogeal Experimentation Station for Environmental Monitoring in a peculiar speleological site in Italy, the **Grotta di Trebiciano;** this cave was the deepest in the world for over 70 years. The station provides the real-time data collection of physical and physical-chemical parameters of the site and is capable of interfacing with other sites in the territory and with the Internet networking. Structure and methods may be reproduced in other contexts and the **Società Adriatica di Speleologia** that manages the project will be pleased to provide collaboration and technical support to everyone, individual or groups, who want to carry out research in this field.

Résumé

La station expérimentale de l'abysse Trebiciano. Le but de ce travail est d'illustrer l'origine et l'évolution d'une station d'expérimentation hypogée pour la surveillance environnementale dans un site spéléologique particulier en Italie, la Grotta di Trebiciano. Cette grotte a été la plus profonde du monde pendant plus de 70 ans. La station assure la collecte de données en temps réel des paramètres physiques et physico-chimiques du site et est capable de s'interfacer avec d'autres sites du territoire et avec le réseau Internet. La structure et les méthodes peuvent être reproduites dans d'autres contextes et la Società Adriatica di Speleologia, qui gère le projet, sera heureuse de fournir une collaboration et un soutien technique à tous ceux, individus ou groupes, qui veulent mener des recherches dans ce domaine.

1. Introduction

The **Grotta di Trebiciano** (Trebiciano Cave, near Trieste, NE Italy) also known as **Abisso di Trebiciano** (Trebiciano Abyss) was discovered in April 1841 and considered the deepest cave in the world for over 70 years. Its exploration was not the result of a scientific initiative but a private initiative aimed at finding new water supplies for the then booming city of Trieste. Water was indeed found, but the excessive depth (-329 m) couldn't justify the huge financial costs involved in pumping it to the surface.

In 1876 the **Società Adriatica di Scienze Naturali** (Adriatic Society of Natural Sciences), at the time the most important scientific institution of Trieste, proposed using the cave as a geological and biological research laboratory. The proposal was not carried out, but since then the site has nevertheless been the site of countless adaptations, studies and researches that are still ongoing.

In 1971 the Adriatic Society of Speleology obtained the licence to manage the Trebiciano cave from the Municipality of Trieste along with a run-down building nearby, for the purpose of scientific research.

Since that time the group has continued without interruption to invest resources, time, and (much) money to plan and realize a **Stazione Sperimentale Ipogea di Monitoraggio Ambientale** (Hypogeal Experimentation Station for Environmental Monitoring) in Trebiciano Cave, capable of interfacing with other sites in the territory and the Internet networking. Our goal is the real-time data collection of physical and physical-chemical parameters from a series of interesting caves in the area.

Figure 1: Interior set-up. Photo Danieli

The work has followed several stages. The first step was to clean the cave of the remains of the old wooden ladders; subsequently, the rockfall containment walls were rebuilt, new metal ladders were installed right down to the bottom, and a power line and a telephone for maintenance works were set up. Later, the run-down building 500 meters from the cave was completely restored and we obtained the connection to the public power grid and to the Internet. We activated a first overhead line for data transmission between the cave and the building. The next steps were the laying of an underground cable for optical fiber and the construction of a branching module (a small building in reinforced concrete) to protect the entrance to the cave and allow the transfer of signals to the building.

2. Underground laboratory equipment

The basic idea behind the project has been the creation of an extremely flexible system, expandable if necessary in future. Most of the investment has been directed to the installation of the necessary support to power instruments (sensors/transmitters), transfer the collected data, allow internal communication and protect the devices from electric discharges.

The Station is now equipped with an internal data transmission line consisting of optical fiber (6 pairs), two cat. 5 twisted-pair cables, two tubes for gas withdrawing, a telephone/Internet line and a power line. Some junction/switching control cabinets are located at -70 (**C2**), -170 (**C3**), -220 m. (**C4**).

Each of these is equipped with a spare battery charge loaded in a buffer, a phone and an analogue-to-digital signal converter.

All the converters are connected in parallel operating in RS-485 mode; each one is provided with its own address. The 4-20mA standard was adopted for transmission between sensors/transmitters and control cabinets.

This standard allows easy maintenance in difficult environments. Two racks are positioned at the entrance (**C1**), in the sorting module and provide power for the entire system, for the management of signals from the control cabinets and to transfer them to the building located 500 meters away from the cave (**C0**).

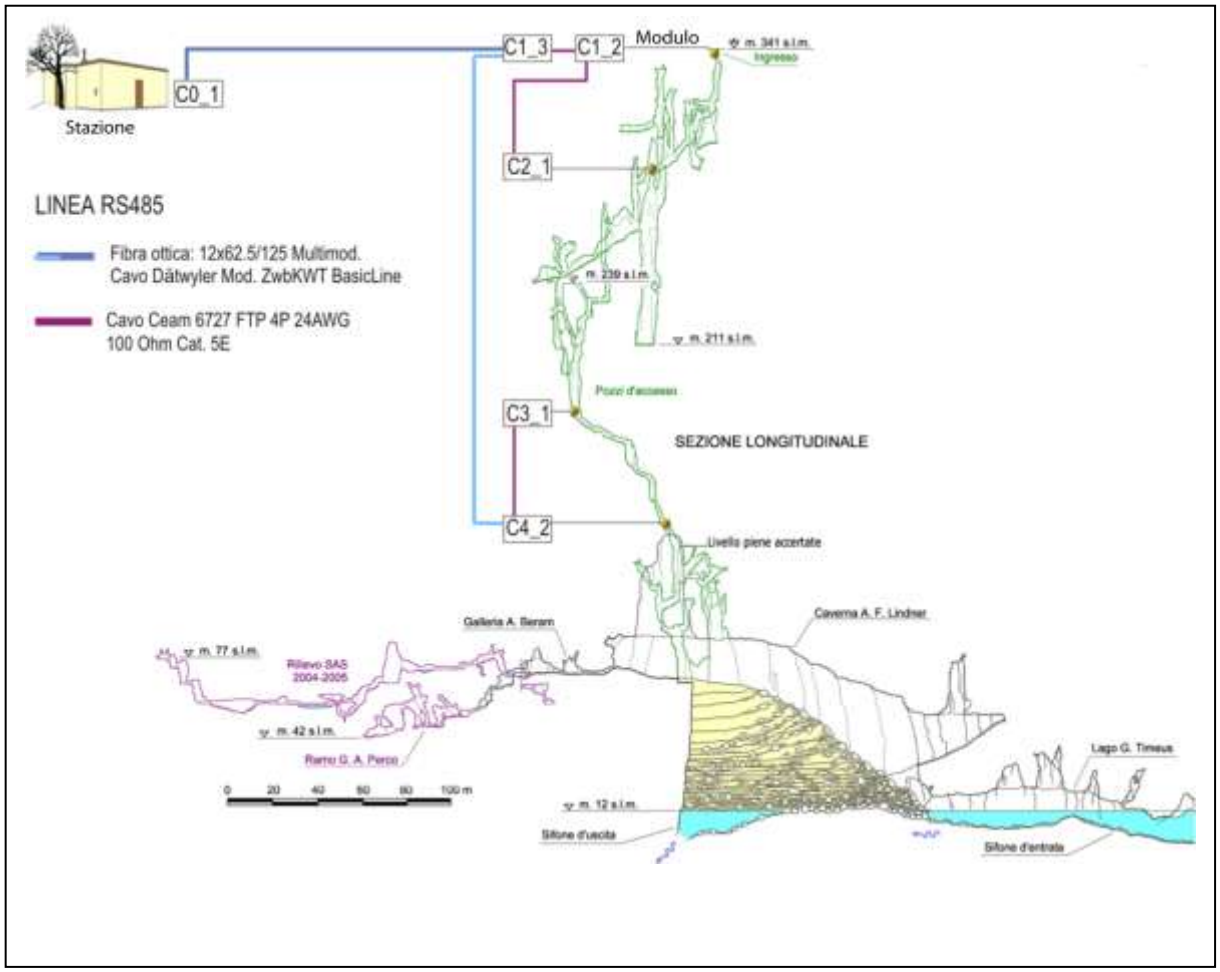

Figure 2: Transmission connection diagram

At the moment, public subsidies cover only electricity costs and Internet connection. The agreements we have with research institutes are all free of charge. Sensors and transmitters were purchased or privately built with our great sacrifice. Any support from research even different from ours, would definitely be welcome.

3. Current and planned surveys

At present we are recording the levels of the river flowing into the cave (Timavo River) and correlating them to the times of the floods in the Škocijanske Jame, Slovenija, 20 km upstream and at the mouth of the river (at Duino), 20 km from Trebiciano. At the same time, we register the changes in water temperature at the bottom of Trebiciano Cave. The pressure variations that occur inside the cave when it floods, are used in another cave to monitor the floods of Timavo River in good time. This phenomenon is evident in large, deep caves.
We have started to measure the concentration of CO_2 in Trebiciano Cave: it has been seen to exceed the atmospheric concentration by two orders of magnitude. Another immediate task is to identify the origin of the CO_2 we have found in the caves. We need to compare the CO_2 concentration in the environment with the one dissolved in water and verify the abundance of ^{13}C to identify the source. Another long-term investigation can be carried out to determine with a laser interferometer the dissolution of limestone that occurs at different depths along wells, combined with a constant measurement of CO_2. The matters are still in project but promise interesting developments.

Figure 3: The river in the terminal cavern. Photo Danieli

There is a factor that limits our work: the rising river level - up to 100 m - during the floods; this occurrence obliges us to use sensors capable of withstanding about 10 Atm. At present we are thinking of adding a new conductivity meter induction probe to our devices which should eliminate oxidation problems in the usual metal contacts. We have planned to double the transmission systems between the cave and the building located at 500 m, using radio transmitters in UHF, in the case of dormouses eating our fiber optics.
There are still so many projects: anyone who wants to work with us will always be welcome. I can assure you that any scientific (non-commercial) research will be able to rely on our station and our assistance.

References

ADVANTECH CO. LTD (2018) *"User manual for ADAM-4000 series"*https://www.advantech.eu/support/details/manual?id=1adv-plus__GEadv-plus__715

BOEGAN E. (1909-1910) *"La Grotta di Trebiciano,* Alpi Giulie.

BOEGAN E. (1921) *"La Grotta di Trebiciano, studi e rilievi dal 1910 al 1921"*, Alpi Giulie. http://www.boegan.it/wpcontent/uploads/2011/08/LaGrottadiTrebicianoWEB.pdf

DAMBROSI S. (2016) *"Indagine sulla presenza del Diossido di Carbonio in alcune cavità naturali del Carso Classico"*. Degree Thesis in Geology, Università degli Studi di Trieste.

DOUCHET M. (2017) *"Au coeur du Karst primitif",* Le Fil, Bulletin de liason de la Commission Nationale de Plongee Souterraine.

FORTI F., SEMERARO R., ULCIGRAI F. (1978) *"Carsogenesi e morfologia dell'Abisso di Trebiciano"*, Atti e memorie della Commissione E. Boegan, vol. XVIII. https://sastrieste.it/index.php/2019/11/15/forti-f-semeraro-r-ulcigrai-f-carsogenesi-e-geomorfologia-dell'abisso-di-trebiciano/

MAUCCI W. (1953)*"Organizzazione tecnica e risultati delle ricerche sul corso ipogeo del Timavo",* Atti del I Congr. Intern. de Speleologie, Paris. https://sastrieste.it/index.php/2019/11/15/maucci-w-1953-organizzazione-tecnica-e-risultati-delle-ricerche-sul-corso-ipogeo-del-timavo/

MORPURGO E. (1892) *" La Grotta di Trebiciano*", Atti e Memorie della Società Alpina delle Giulie https://www.boegan.it/wpcontent/uploads/2020/11/02-%E2%80%93-La-Grotta-di-Trebiciano.pdf

SEMERARO R., BALLARIN L., BRUN C., DAMBROSI S., FORTI F. (2006) *"Tracer test in the vadose Zone of the Trebiciano Abyss near an Uncontrolled Landfill (the Karst of Trieste)",* Intern. Conf. "The quality of Life and Environment: a Must for European Integration", Constanta. https://sastrieste.it/index.php/2019/11/15/rinosemeraro-luciano-ballarin-clarissa-brun-sergio-dambrosi-fulvio-forti-2006-tracer-test-in-the-vadose- zone-of-the-trebiciano-abyss-near-an-uncontrolled- landfil-the-karst-of-trieste/

TIMEUS G. (1910) "*Sui mezzi d'indagine nell'idrologia sotterranea. Nuovi metod"*. Boll. della Soc. Adriatica di Sc. Nat., Trieste.
TIMEUS G., VORTMANN G. (1910) "*L'applicazione del cloruro di litio nelle indagini di idrologia sotterrane".* Boll. della Soc. Adriatica di Sc. Nat., vol. 25, Trieste.

TOMASINI M., (1876) *"Memoria letta nella radunanza generale della Società Adriatica di Scienze naturali, il dì 7 gennaio 1877.* Bollettino della S.A.S.N., Tipografia del Lloyd Austro-Ungarico, - https://sastrieste.it/index.php/2019/11/15/tommasini-m-1876-memoria-letta-nella-radunanza-denerale-della-societa-adriatica-di-scienze-naturali-il-di-7-gennaio-1877/

ULCIGRAI F. (1976) "Successione stratigrafica dell'Abisso di Trebiciano", Atti e memorie della Commissione E. Boegan, vol. XVI- https://sastrieste.it/index.php/2019/11/15/ulcigrai-f-1976-successione-stratigrafica-dellabisso-di-trebiciano/

Hydrogeological Behaviour Characterization of the Foussoubie Karst Network using Statistical Approaches

Manon ERGUY [(1)], Judicaël ARNAUD [(4)], Anne JOHANNET [(1)], Séverin PISTRE [(1)], Didier CAILHOL [(3)], Guillaume ARTIGUE [(1)] & Stéphane JAILLET [(2)]

(1) HydroSciences Montpellier, Université de Montpellier, IMT MINES ALES, CNRS, IRD, Place Eugène Bataillon, 34095 Montpellier, France, anne.johannet@mines-ales.fr (corresponding author)
(2) Laboratoire EDYTEM, Université de Savoie /CNRS, Pôle Montagne, 73376 Le Bourget-du-Lac cedex, France
(3) Laboratoire TRACES (UMR5608) Université Toulouse Jean Jaurès, 5, allées Antonio Machado F 31058 Toulouse cedex 9
(4) Comité départemental de Spéléologie de l'Ardèche, les Blaches, 07120 Chauzon, France

Abstract

The *Foussoubie* karst, located on the right bank of the *Ardèche Gorges* (France), is the second longest network in the *Bas Vivarais* (23 km of recognized galleries). The *Foussoubie* system is fed by a main sinkhole: "*la Goule*" towards an outlet: "*l'évent de Foussoubie*". The *Foussoubie* system, influenced by a Mediterranean climate, is known for its violent and dangerous floods having caused several casualties. The network is mainly shallow (average depth from "*la Goule*": 82 m) and partially submerged. Sensors distributed along the network acquired measurements of temperature and water level between 2010 and 2018. These measurements, combined with the good speleological knowledge of the conduits, allowed carrying out statistical and systemic analysis. Correlations, as well as sorted discharges have been calculated on different floods to improve knowledge of the network's hydraulic characteristics. The system appeared as very reactive and transmissive. It was shown that the reactivity of this dominant conduit-type system is linked to the soil and karst saturation. In addition, a "threshold" swallowed flow, constrained by the conduit section, was approached at the sinkhole "*la Goule*".

Résumé

Caractérisation du fonctionnement hydrogéologique du réseau karstique de Foussoubie. Approches statistiques. Le karst de Foussoubie, situé sur la rive droite des gorges de l'Ardèche, est le second plus long réseau du Bas Vivarais (23 km de galeries reconnues). Le système karstique est alimenté par une perte principale : la Goule jusqu'à une exsurgence : l'évent de Foussoubie. Le système de Foussoubie, influencé par un climat méditerranéen, est connu pour ses crues violentes ayant fait plusieurs victimes. Le réseau est peu profond (profondeur moyenne depuis la Goule : 82 m) et partiellement submergé. Différentes sondes réparties sur le réseau ont permis l'acquisition d'une base de données des températures et des hauteurs d'eau entre 2010 et 2018. Ces mesures, associées à la bonne connaissance spéléologique des conduits, ont permis de réaliser des analyses statistiques. Les analyses corrélatoires ainsi que les débits classés ont été calculés pour différentes crues afin d'améliorer les connaissances des caractéristiques hydrauliques du réseau. En plus du caractère très transmissif du réseau, il est apparu que la réactivité de ce système de type conduit dominant est lié à la saturation des sols et du karst. De plus, une valeur seuil du débit d'entrée du système, contraint par la section du conduit, a été approché à la Goule de Foussoubie.

1. Introduction

Karst aquifers represent about 25% of the water used for drinking water supply in the world FORD & WILLIAMS, (2007). These aquifers are very complex and often under-exploited because of their non-linear and heterogeneous functioning. In addition, as the karst flow may be extremely fast, this makes them difficult to study, particularly regarding the prediction of floods.

The *Foussoubie* system is subject to heavy precipitation called "*cévenols*" episodes, which can lead to flash floods particularly during autumn and spring seasons. On June 3rd, 1963, one of these violent underground floods caused the death of 2 speleologists: Jean Dupont and Bernard Raffy. This event brought a baneful reputation to the "*Goule de Foussoubie*" described as dangerous.

It is a binary system of limited size (14,4 km²) and complexity that allows the study of the response of the unsaturated karst zone during intense rainfall events and its relationship with surface runoff.

This paper proposes, in the next section, a presentation of the karst system of *Foussoubie* and of the measurement network. In the following section we present the methods, results, and discussion on statistical approaches. First, simple, and cross correlation analyses were used on the water levels sampled on the different measurement stations during floods in the 2010-2011 period (July 2010 to July 2011). In addition, sorted discharges were calculated, for several floods, to constrain a "threshold" discharge at the system entry in order to better apprehend flooding at "*la Goule*".

2. The *Foussoubie* system

2.1. Presentation of the *Foussoubie* network

The catchment of the *Foussoubie* karst system develops in the Eocene molassic PASCAL et al. (1989; 1989b). The sinkhole: "*La Goule*" opens at the contact with the Barremian limestone, and the outlet of the system is the karst spring: "*l'évent de Foussoubie*" located on the right bank of the *Ardèche Gorges*. The karst network (Fig. 1) is developed in Urgonian limestone containing fossils specific to warm, shallow marine environments, like rudist PASCAL et al. (1989b).

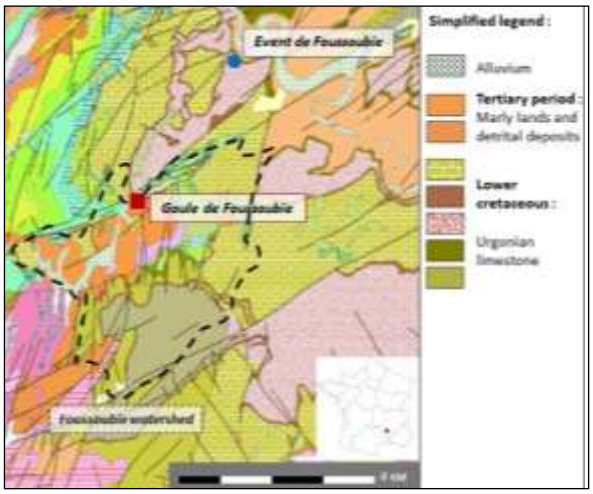

Figure 1: Localisation of the Foussoubie system. Harmonized geological map (InfoTerre, 2021 ; PASCAL et al. (1989b))

The *Foussoubie* catchment area is estimated at 14.4 km² and is mainly made up of impermeable tertiary detrital deposits from the synclinal depression of *Labastide-de-Virac* JAILLET et al. 2012. Thus, the *Foussoubie* impluvium is a binary system made up of karst and impermeable non-karst grounds. The karst network shows a conduit-dominant type functioning SADIER (2013) ; JAILLET et al. (2012).

The system is quite "simple" from the network inlet ("*Base des puits*") to the network outlet ("*Siphon A*"). It becomes more complex near the outlet with the junction with "*Siphon B2*" and "*Siphon C2*" (paleo-conduits with a slightly different behaviour) (Fig.2).

The climate of the *Cévennes* border is Mediterranean, with intense rainy episodes in autumn and spring that can cause flash floods. On the contrary, the summer period is marked by long droughts.

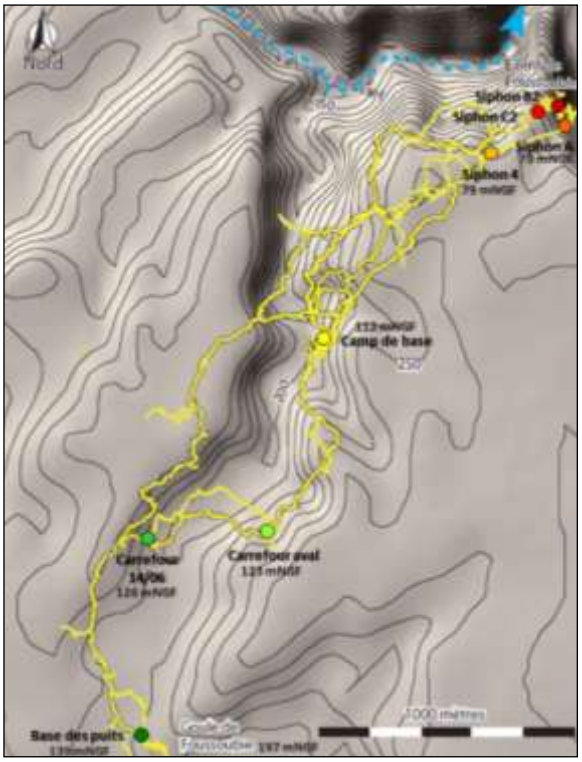

Figure 2: Foussoubie karst network and measurement stations. Base map from SADIER (2013)

2.2. Measurement network

The *Foussoubie* system database consists of a discontinuous set of temperatures and water levels data, with a sampling time-step of 15 minutes, from 2010 to 2018 at different measurement locations, depending on the period. Acquisition periods run from July of one year to July of the following year. Here the statistical analysis will be carried out over the 2010-2011 period, for which data are available at all the measurement stations (fig. 2). Also, many floods occurred during this hydrological year.

The rainfall data used for this study were provided by the Grand Delta Flood Forecasting Service station in Vallon-Pont-d'Arc, at 4.5 km from the sinkhole, with a time-step of 5 minutes (Fig. 1).

3. Statistical approaches

3.1. Correlations analyses

a. Methods

Cross-correlation is the correlation coefficient of two distinct time-series shifted in time. The correlation coefficient is calculated with the following equation MANGIN (1975):

$$r_k = \frac{\frac{1}{n}\sum_{i=1}^{n-k}(x_i-\bar{x})(y_{i+k}-\bar{y})}{\sigma_x\sigma_y} \qquad \text{(eq.1)}$$

With: x the time-series of the input signal, the pluviometry; $\bar{x}$ its mean, $\bar{x}$ its standard deviation; y the time-series of the output signal, the water level; $\bar{y}$ its mean; σ_y its standard deviation; n is the number of samples; k is the discrete-time delay (15 minutes). To prevent results degradation k must vary between 0 and $n/3$ MANGIN (1975). Cross-correlogram is the graphic representation of r_k versus k. It allows getting the response-time of the system. The response-time is the value of k corresponding to the peak of the correlogram. For

simple correlation, the eq. 1 is similar, replacing *y* by *x*. The simple correlogram allows determining the system memory effect. It corresponds to the time interval for r_k to be inferior to 0.2. It corresponds to the time that input takes to influence the output, while memory effect corresponds to the duration of correlation between one value and the following. The *Foussoubie* response-times between rain and water levels for different floods and the various stations during the 2010-2011 years were shown in fig.3.

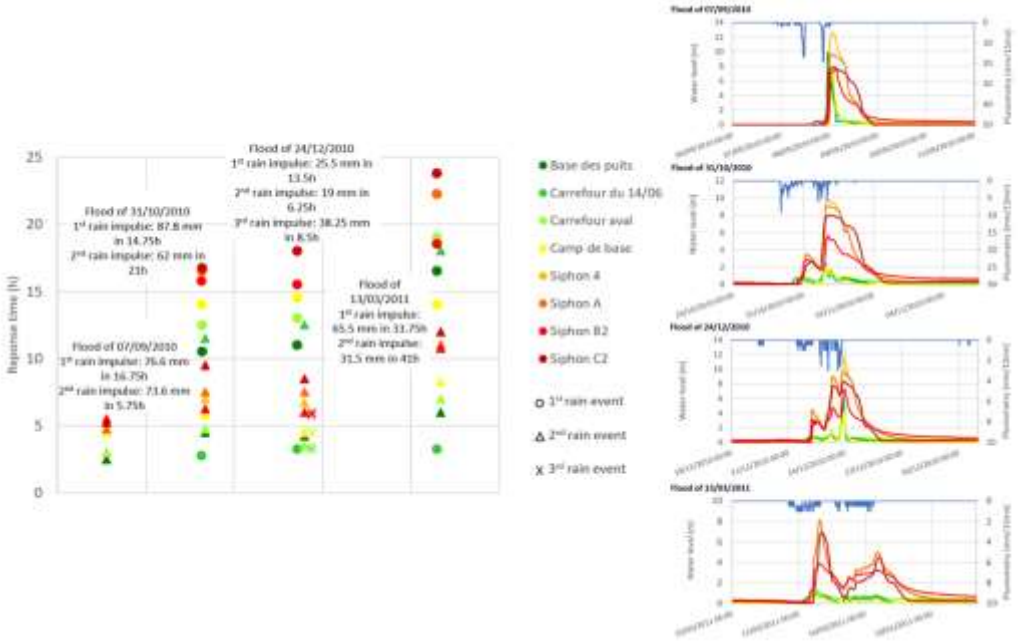

Figure 3: Graph of response times at different points in the system for different floods in the 2010-2011 period. The colour code goes from the green (system upstream) to the orange (system downstream), red is for the paleo-conduits.

b. Results

Cross correlations were calculated for three major rain episodes and eight stations along the underground network for the period 2010-2011. For all the floods, it is possible to observe an upstream/downstream logic with response-times increasing downstream ("*Siphon A*"). In addition, the "*Siphon B2*" and *"Siphon C2*" show longer response times because they are not linked directly to the main network.

Regarding the flood of September that was composed of two rain impulses, it appears that the first impulse of rain had no effect on the water level. This flood took place after the summer drought; it is likely that this first water volume was stored by the soils. So, only the second rain impulse caused the flood, considering that it occurs on saturated soils. For this event, there is a difference of 2 hours between upstream and downstream peaks.

The flood at the end of October is also caused by two rain impulses that led to two water levels peaks, unlike the previous flood. The month of September 2010 has been rainy (cumulative precipitations of September 2010: 185.8 mm), these precipitations met the soils and vegetation water needs. Indeed, according to figure 3, the difference between the response times at "*Base des puits*" (upstream) and the "*Siphon A*" (downstream) is 6 hours for the first rain event and 1.75 hours for the second one. Therefore, it appears that when the soils are wet the upstream/downstream response is faster. In addition, the system response-times are roughly divided by two when the network is saturated. The same behaviours with several rain episodes were observed for the following floods.

The December flood is composed of three rain impulses. Response times between upstream and downstream is almost three times faster for the second and third pulses compared to the first. The system response-times are more than three times shorter for a saturated system (second and third rain events).

The last flood was in March during the spring and the growth of the vegetation. The two rain impulses were not intense but rather long. The system response-time of the first impulse was important (16.5 hours at the inlet and 22.25 hours at the outlet). This may be related to the low rain intensity and the soil moistening. The system response is twice as fast for the second rain peak.

Therefore, according to figure 3, the *Foussoubie* karst system is very responsive and transmissive. In addition, it appears that the reactivity is linked with: (*i*) the moisture of soil, and (*ii*) the saturation of the karst. When the network is saturated, the system response-time decreases greatly. This information helps to explain the particularly sudden and violent floods that affect the *Foussoubie* system, they can constitute a significant risk, especially for speleologists.

3.2. Sorted discharges

a. Methods

Sorted discharge graphs are made by putting flow values into classes and calculating the empirical cumulated probability for each one. Then, the cumulated probability is represented in function of the flow classes. Ruptures in hydrological behaviour or "threshold" flow can be estimated by studying the curve slope variations DORFLIGER (2010).

There is no existing rating curve for the Foussoubie system. Flow rates were estimated in the saturated zone, using the

linear pressure drops between the "*Siphon 4*" and "*Siphon A*" sensors. The maximum pressure drop recorded in the conduit is 3.05 m. The length of the conduit is 340 m without difference in altitude and the minimum section is 3 m² . To calculate the Reynolds number ($2x10^6$), the velocity is estimated to be 1.5 m/s from the solid transport. This estimation supposes that the conduit between the two sensors is considered rectilinear, of constant diameter and that the flow rate is equal at the two measurement stations. These conditions are not rigorously verified implying thus important uncertainty. Nevertheless, establishing a rating curve in underground karst also generates important uncertainties. We thus considered that the study could be done, considering it as a feasibility step.

b. Results

As explained previously, flow rates are estimated at the "*Siphon A*", it is the system outlet. If we consider the system as a single simple conduit, it is possible to estimate that the flow at the "*Base des puits*" (network inlet) is the same as at the "*Siphon A*". This is an important assumption, so the threshold discharge obtained should be considered with caution.

According to figure 4, the limiting absorption flow rate of the conduit is estimated thanks to the four floods presented previously at around 1.60 ± 1.45 m3/s. When this flow is reached at the "*Base des puits*", the water level increases in the inlet well: "*la Goule*". One can distinguish three zones in the Fig. 4: (1) non saturation on conduit (absorption without limit); (2) threshold flow; (3) saturation: flow increase due to the pressure increase at the bottom of the inlet vertical conduit.

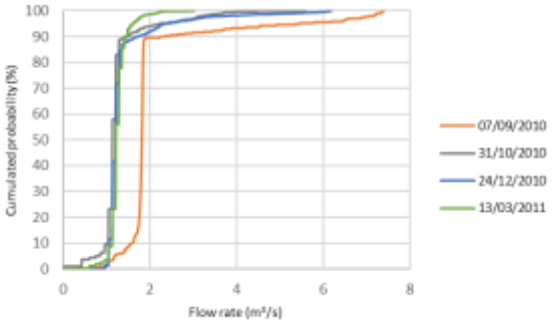

Figure 1: Sorted discharges at the "Siphon 4" during several floods. The red dotted lines separate the different zones and the purple indicates the mean limiting flow.

5. Conclusion

The *Foussoubie* karst system dynamics is marked by floods, themselves conditioned by thresholds and site effects. Statistical approaches allow to quantify the important transmissivity and reactivity of the system. The comparison of different floods during the 2010-2011 period allowed to state the importance of the soil moisture and karst saturation on the reactivity of the system with regards to the precipitations.

This system gives a good example of floods in binary karsts dominated by conduit behaviour in Mediterranean climate. However, many questions remain unanswered regarding the *Foussoubie* system. The behaviour of the conduit B and C, not directly linked with the rest of the system and only submerged during floods, remains unclear. In addition, a study on the site effects as well as the thresholds, would allow a better understanding of the variations in the flood wave propagation.

As the *Foussoubie* database also contains temperatures, a simulation model of water levels and temperatures using artificial neural networks is planned. It could also help to improve the knowledge about the *Foussoubie* hydrogeological behaviour.

Acknowledgments

The authors would like to thank the SPCGD Flood Warning Service for providing the rainfall dataset.

References

DORFLIGER N. (2010) Guide méthodologique, les outils de l'hydrogéologie karstique pour la caractérisation de la structure et du fonctionnement des systèmes karstiques et l'évaluation de leur ressource (RP-58237-FR). BRGM, 246 p.

FORD D., WILLIAMS P. (2007) Karst Hydrogeology and Geomorphology, John Wiley & Sons, 562 p.

JAILLET S., CAILHOL D., ARNAUD J. et al. (2012) Les crues du système karstique de Foussoubie (Ardèche, France). Une analyse géomorphologique et hydrodynamique des circulations dans la zone épinoyée du karst. Karsts Paysages Préhistoire, (13), 115-138.

MANGIN A. (1975) Contribution à l'étude hydrodynamique des aquifères karstiques. (Thèse de doctorat, Sciences de la Terre). Université de Dijon, 268 p.

PASCAL M., ELMI S., BUSNARDO R., LAFARGE D., TRUC G., VALLERON M.-M., CHEDHOMME J., ET COMBIER J. (1989a) Carte géologique de la France 1:50 000, feuille Bourg-Saint-Andéol (889).

PASCAL M., LAFARGE D., CHEDHOMME J. et al. (1989b) Notice explicative de la carte géologique de la France 1:50 000, feuille Bourg-Saint-Andéol, 889.

SADIER B. (2013) 3D et géomorphologie karstique : La grotte Chauvet et les cavités des Gorges de l'Ardèche. (Thèse de doctorat). Université de Grenoble, 476 p

Le karst de Tsanfleuron (Valais, Suisse) : Dynamique des écoulements souterrains dans le karst et le glacier

Gérald FAVRE

Route de Crassier 16, 1277 Borex, Suisse, geologos@bluewin.ch - +41 22 367 22 59

Résumé

Au même titre que le célèbre Désert de Platé en Haute-Savoie, le plateau calcaire de Tsanfleuron fait partie des grands massifs karstiques de la chaîne alpine. Son originalité est d'être, encore aujourd'hui, recouvert en partie par un glacier. Mis à part un potentiel spéléologique réel (-1 500 m), il représente un sujet d'étude captivant pour les hydrogéologues, les géomorphologues ou les spéléologues. Pour faire suite aux 38 expériences de traçages réalisées depuis plus de 20 ans, nous présentons ici quelques types d'écoulements souterrains observés qui révèlent une dynamique hydraulique changeante, en relation avec un contexte géologique, tectonique et glaciologique varié. Les allures des courbes de restitution des traceurs nous ont permis de mieux comprendre le fonctionnement de ce karst haut-alpin et ainsi de pouvoir réaliser une carte des zones de protection des eaux de la source de Glarey qui alimente la commune de Conthey.

Abstract

The plateau of Tsanfleuron (Wallis, Switzerland): Dynamics of underground flows inside karst and inside glacier. Like the famous Platé Desert in Haute-Savoie, the limestone plateau of Tsanfleuron is one of the great karstic massifs of the Alpine chain. Its originality is that it is, even today, partly covered by a glacier. Aside from a real speleological potential (-1,500 m), it represents a fascinating subject of study for hydrogeologists, geomorphologists or cavers. Following the 38 tracing experiments carried out for more than 20 years, we will present some types of underground flows observed which reveal a changing hydraulic dynamic in relation to a varied geological, tectonic and glaciological context. The shape of the plotters' restitution curves allowed us to better understand the functioning of this high-alpine karst and thus to be able to draw a map of the water protection zones of the Glarey spring which feeds the town of Conthey.

1. Cadre

Dès 1976, des recherches spéléologiques ont été menées sur ce massif et depuis 1998 des études (Réf.1) hydrogéologiques (Geologos SA) ont été réalisées pour le compte de la Commune de Conthey (Valais) qui utilise l'eau de la source de Glarey, principal exutoire du massif

Mis à part le fait d'obtenir une meilleure connaissance des écoulements souterrains dans le karst, toujours utile pour l'exploration spéléologique, le but principal de ces études est d'identifier les sources de pollutions existantes et de les éliminer (carte des zones de protection).

2. Situation

Le karst de Tsanfleuron est situé en Suisse, à la limite des trois cantons du Valais, de Vaud et de Berne. Son altitude moyenne (2 500m) et ses caractéristiques en font un karst haut-alpin typique. Il est aussi l'un des derniers dans les Alpes à être recouvert par un glacier.

La **source de Glarey** est une émergence alpine (exsurgence et résurgence) karstique typique, caractérisée par des importantes variations de débits et de caractéristiques physico-chimiques et biologiques. Les volumes d'eau restitués sont importants à l'échelle locale. Les aquifères de la source sont constitués par l'épaisse série calcaire massive d'âge barrémien et par les formations calcaires et gréseuses du Tertiaire inférieur. Ces formations font partie de l'ensemble tectonique de la nappe des Diablerets, qui présente pour le karst de Tsanfleuron un pendage général de 10° à 30° en direction de l'est et une inclinaison axiale d'environ 10° en direction du nord-est. Le bassin d'alimentation de la source est constitué en grande partie par un karst bien développé et très perméable, avec certaines zones recouvertes par des dépôts glaciaires ou alluvionnaires. Le glacier de Tsanfleuron, qui occupe en surface une partie du bassin versant, joue un rôle particulier en ce qui concerne le régime des eaux souterraines. Le but de ce court article est de considérer quelques expériences de traçages symboliques qui représentent bien les écoulements souterrains dans ce karst et permettent d'en tirer des conclusions quant au potentiel spéléologique réel. Comme la situation le permet, quelques parallèles sont tirés entre les écoulements endokarstiques et intra-glaciaires. Dans l'ordre, nous décrirons un traçage (Fig. 2), qui illustre bien les écoulements rapides dans des drains majeurs à partir des zones d'alimentation éloignées de l'émergence. Puis, nous commenterons le traçage effectué depuis la cabane de Prarochet (Fig. 3) qui montre le transit vertical de l'eau dans l'endokarst et la dilution du traceur en fonction de la fonte journalière du glacier. Dans

le gouffre G 16, un affluent du collecteur souterrain a été mis en évidence, avec un passage rapide du traceur jusqu'à la source (Fig. 4). Un autre traçage très instructif, au col du Sanetsch (Fig. 5) met en évidence un aquifère perché dont les eaux s'écoulent à la fois à la source de Glarey et à celle de la Sarine. Enfin, il a été très instructif de comparer ces traçages avec ceux réalisés directement sur et au travers du glacier de Tsanfleuron (Fig. 6).

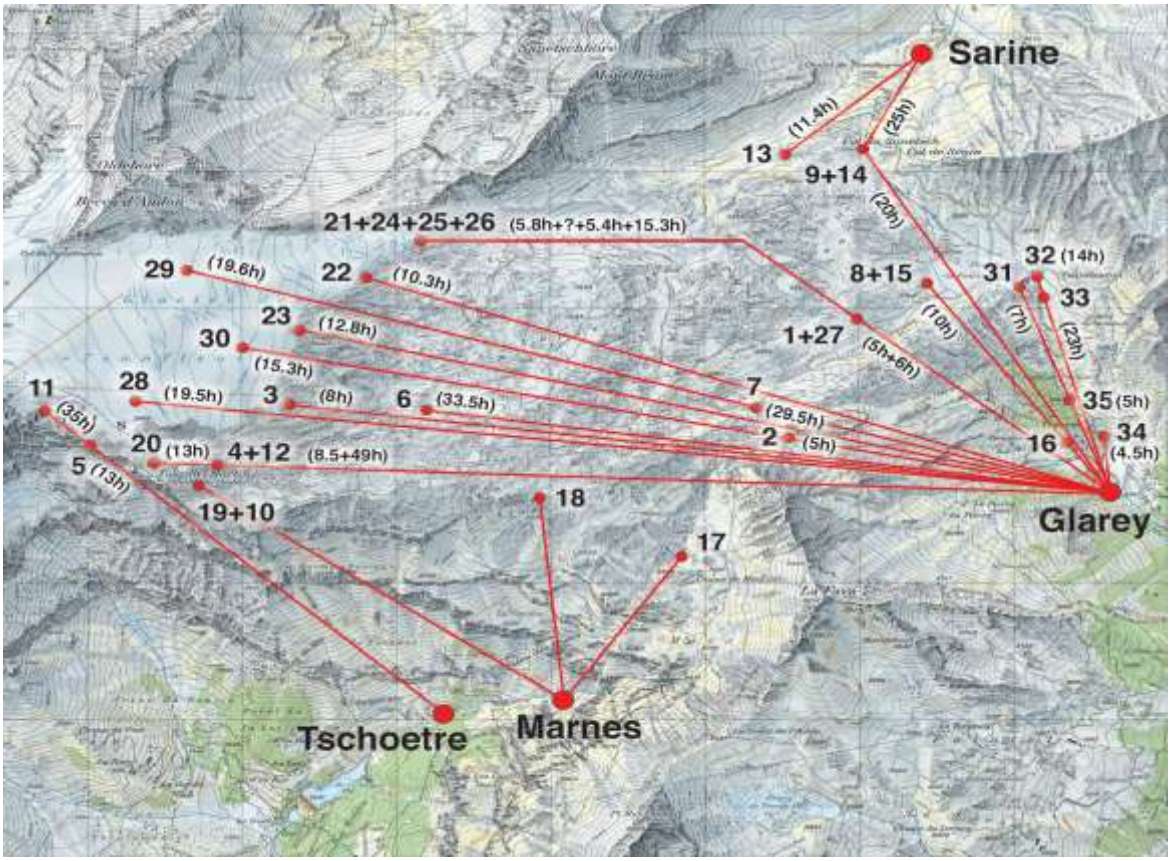

Figure 1 : Carte des traçages (G. Favre)

3. Traçages

Traçage 20 au téléski de la Quille (Fig. 2)

Toujours pour préciser les limites des bassins dans ce secteur, nous avons injecté 1 kg d'uranine dans un petit actif qui s'écoule en direction de l'est, juste sous l'arrivée du téléski de «La Quille» de Glacier 3000 et qui disparaît dans le gouffre D5. Les appareils placés à la source de Glarey ont détecté le colorant 8 h après l'injection, avec un taux de restitution particulièrement élevé de 58 %. Ces deux valeurs sont maximales pour le massif et représentent le temps de passage le plus rapide pour le point le plus éloigné de la résurgence.

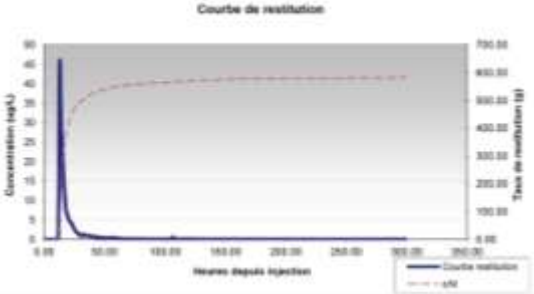

Figure 2 : Courbe de restitution de l'uranine de La Quille (V. Gremaud)

Traçage 6 à la Cabane de Prarochet (Fig. 3)

Afin de confirmer les relations hydrogéologiques en aval du front du glacier de Tsanfleuron, une injection d'uranine a été effectuée directement dans l'évier de la cuisine de la cabane. Dans ce cas, il s'agit d'élucider le destin des eaux « grises » (évier, lavabo), ainsi que des eaux usées des toilettes pouvant déborder de la cuve de biodigestion.

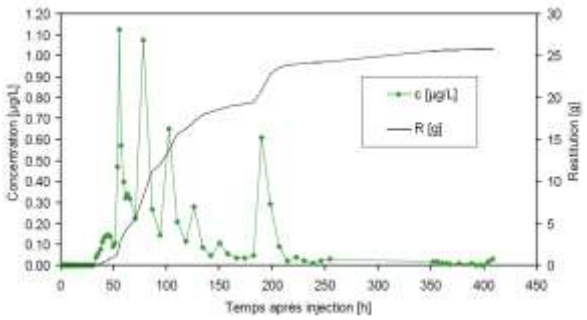

Figure 3 : Courbe de restitution de l'uranine de Prarochet (L. Savoy)

Le traceur utilisé (uranine, 200 g) est ressorti 131 heures après l'injection à la source de Glarey située à 4,4 km à l'est du point d'injection. La zone non saturée de l'endokarst

traversée est assez importante quant à son épaisseur (120 m environ).
L'allure de la courbe de restitution à pics multiples sur plus de 10 jours fait penser qu'un drain important se développe à la verticale du point d'injection selon le pendage général du massif. Il est intéressant de constater les variations de concentrations liées aux cycles nycthéméraux en relation avec la fonte journalière du glacier (peu d'eau = plus forte concentration et beaucoup d'eau = dilution du traceur) (Fig. 3) Le colorant a alimenté cet écoulement régulièrement durant plusieurs cycles quotidiens par un réseau de fractures moyennement développées.

Traçage 7 au gouffre G16 (Fig. 4)
Sa position entre la cabane de Prarochet et la source de Glarey ainsi que l'opportunité d'avoir accès directement à l'un des drains du massif nous a poussé à injecter un traceur à cet emplacement. Les spéléologues ont injecté le traceur à 150 m de profondeur dans un actif qui est un affluent du collecteur principal du massif. Le traceur utilisé (Tinopal, 2 kg) est ressorti 30 heures après l'injection à la source de Glarey située 2,5 km à l'est du point d'injection. L'allure de la courbe de restitution indique un transit dans des chenaux bien développés. Ce fait découle de l'observation de la courbe de restitution, qui montre un premier pic correspondant à l'arrivée du colorant dans la rivière principale à partir de l'affluent du G16 et un deuxième petit pic, 24 heures plus tard, qui correspond au solde du colorant entraîné par l'onde de crue journalière en provenance du glacier. L'affluent du G16 n'est, quant à lui, pas touché par ces cycles journaliers, vu sa zone d'alimentation typiquement karstique et non glacio-karstique.

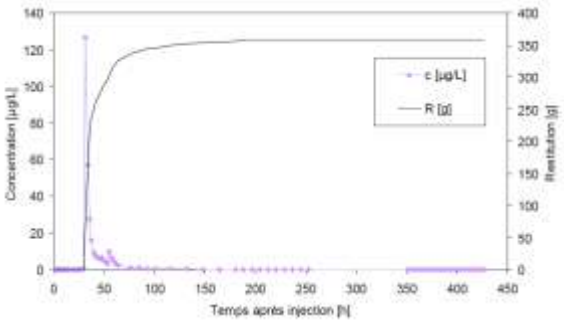

Figure4 : Courbe de restitution du Tinopal du G 16 (L. Savoy)

Traçage 14 à la Perte du col du Sanetsch (Fig. 5)
Nous sommes ici à la frontière du bassin d'alimentation de la source de Glarey, car ce point d'injection est situé à la limite des calcaires de l'Urgonien de la nappe des Diablerets et des marnes du Valanginien de la nappe du Wildhorn. Topographiquement, le col du Sanetsch représente aussi la ligne de partage des eaux entre le Rhin et le Rhône. L'émergence pérenne de la Sarine est située seulement 500 m au nord-nord-est en contrebas. Le traceur utilisé (uranine, 0,3 kg) est ressorti à la fois à la source de la Sarine et à celle de Glarey. Dans le premier cas, le transit a duré 37 heures pour une distance de 600 m à vol d'oiseau. Dans le deuxième cas, le transit a duré 30 heures pour une distance de 3150 m à vol d'oiseau. Cette injection met en évidence une diffluence des eaux d'infiltration dans la région du col du Sanetsch. Malgré la distance 5 fois plus courte jusqu'à la source de la Sarine par rapport à la source de Glarey, le traceur met plus ou moins le même temps pour y parvenir. Les faibles restitutions peuvent être expliquées de plusieurs manières : au contact des nappes (Diablerets, Wildhorn) est située une zone noyée importante en milieu fortement fracturé. Ce réservoir, par débordement, alimente les sources de Glarey et de la Sarine.

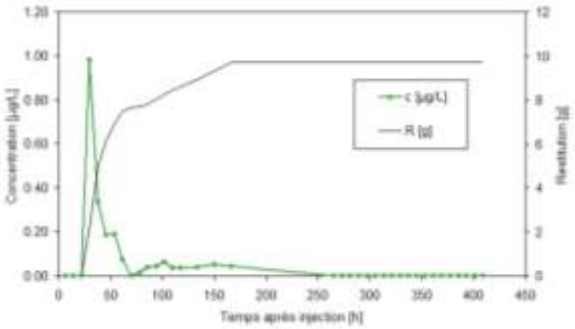

Figure 5 : Restitution à Glarey de l'uranine du col du Sanetsch (L. Savoy)

Traçages sur le glacier de Tsanfleuron (Fig. 6)
Dans le cadre de son travail de thèse au CHYN, Vivian Gremaud a réalisé des traçages sur le glacier de Tsanfleuron, dans le but de mettre en évidence la dynamique qui existe entre un karst alpin typique et l'appareil glaciaire qui le recouvre.
Les trois traçages effectués sur le glacier (n° 28, 29, 30), directement à la surface du glacier de Tsanfleuron, avaient pour but de déterminer les relations qui existent entre les écoulements superficiels sur ce substrat et les écoulements dans le karst sous-jacent et à l'interface entre la glace basale et le calcaire. Ils ont permis de mettre en évidence les différents modes d'écoulement des eaux à l'interface glace-karst, ainsi que des temps de transfert également rapides.

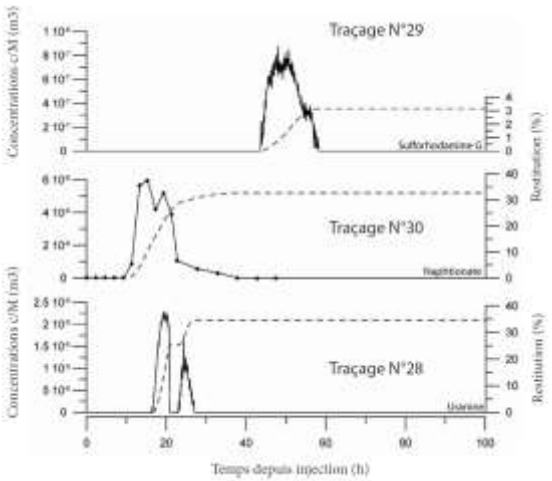

Figure 6 : Restitution des traceurs sur le glacier (V. Gremaud)

Pour le premier traçage (n° 28, 500 m au nord de la Tour Saint-Martin), le traceur a disparu dans une perte ponctuelle et a rejoint directement la base du glacier. L'actif de ce moulin glaciaire a poursuivi son cheminement directement dans l'endokarst. Sa réapparition à la source de Glarey, après 18h de transit, confirme cette observation. Le

deuxième traçage (n° 29, 500 m au sud-ouest du col de L'Olden) présente des résultats différents. Le traceur (sulfo G) a été détecté aussi bien dans le Lachon que dans deux fluocapteurs au front du glacier, proche du Lachon, et à la source de Glarey. Le troisième traçage (n° 30, au centre aval du glacier) présente des caractéristiques de restitution intermédiaires par rapport aux deux traçages précédents. Comme le point d'enfouissement du traceur (naphtionate) dans un moulin se situe proche du front du glacier, nous assistons à une diffluence des écoulements sous-glaciaires à l'interface glace-roche. Le traceur a été retrouvé dans trois fluocapteurs placés au front du glacier répartis sur une distance latérale de plus de 500 m. Ces écoulements disparaissent tous, plus en aval, dans les fractures ou pertes du lapiaz. Le fait de retrouver le colorant à la source de Glarey 15 h après l'injection est tout à fait normal et correspond aux autres traçages réalisés dans ce secteur (Fig.1). Par contre, il n'est pas possible de savoir, pour l'instant avant que le glacier n'ait fondu, s'il existe des pertes karstiques directement à la verticale du moulin où le colorant a été injecté. Ces trois traçages démontrent bien le passage rapide des écoulements de surface au travers du glacier, ainsi que leur absorption, directement dans le karst sous-jacent, de façon « déportée » dans des pertes proches ou directement dans le torrent sous-glaciaire (le Lachon).

4. Le glacier de Tsanfleuron et son fonctionnement hydrologique

Le karst de Tsanfleuron constitue la plus grande partie du bassin d'alimentation en eau de la source de Glarey. L'appareil glaciaire de Tsanfleuron présente, du point de vue des écoulements hydrauliques, de fortes similitudes avec le fonctionnement d'un karst alpin bien développé. Si un glacier ne présente pas une microfissuration, comme c'est très souvent le cas dans un massif calcaire, il développe par contre dans les secteurs soumis à des contraintes mécaniques importantes, une macrofracturation sous la forme de crevasses ouvertes ou fermées, qui le traversent souvent jusqu'à sa base. Ces fractures permettent aux eaux qui s'écoulent à la surface de la calotte glaciaire de rejoindre très rapidement le karst sous-jacent. Dans ce cas, les vitesses d'écoulement sont en tous points comparables à celles des écoulements karstiques, qui empruntent des diaclases ou des gouffres dans un bloc calcaire. L'eau de ruissellement supra-glaciaire ne s'engouffre pas, la plupart du temps, directement dans des crevasses.

Sur des glaciers peu pentus, elles forment souvent des ruisseaux ou même des rivières de surface qui creusent de véritables chenaux tortueux dans la glace (méandres et bédières). Ces écoulements peuvent ensuite disparaître dans un moulin glaciaire qui a comme origine une fracture tectonique, comme c'est le cas à Tsanfleuron, se perdre dans une fissure du karst. Dans un moulin glaciaire, en profondeur, les sections des conduits diminuent pour cause d'équilibre thermique et mécanique. L'eau, pour sa part, trouve très souvent un passage le long de la fracture tectonique pour poursuivre son chemin vers la base du glacier. Les écoulements se font de façon rapide et ponctuelle en fonction des conditions météorologiques et du rythme nycthéméral (jour / nuit).

5. Conclusions

Par rapport aux 38 expériences de traçages réalisées à ce jour (les dernières en 2020) nous avons considéré 7 cas représentatifs qui permettent de se faire une meilleure idée des écoulements souterrains du karst de Tsanfleuron. Quel que soit le contexte (Fig. 1) on constate que le transit de l'eau dans le glacier et le karst se fait de façon rapide jusqu'à la source de Glarey et ceci, sans zones de stockage intermédiaire. Certains écoulements souterrains sont un peu plus rapides que d'autres, mais dans l'ensemble l'eau souterraine s'écoule dans des fractures bien ouvertes qui lui permettent de parvenir à l'émergence en moins de 20 heures (8 h au minimum).

Ces observations vont dans le sens de ce que nous présentions en ce qui concerne l'exploration spéléologique, soit un excellent potentiel pour découvrir un réseau souterrain de plusieurs kilomètres pour une dénivellation pouvant dépasser les 1000 mètres. À ce jour, les cavités explorées, telles le D 16 et le réseau du Tranpirateur (2 km de développement dans des galeries fossiles et actives) n'ont pas encore permis d'atteindre un drain majeur.

En tenant compte de ces expériences de traçages, il existe donc un bon espoir de trouver des conduits accessibles à l'homme et de pouvoir suivre le chemin de l'eau à l'intérieur du massif. Juste une question de persévérance…

Remerciements

Aux membres de la Société Spéléologique Genevoise, du Groupe Spéléo Rhodanien et du spéléo club du Jura

Références

FAVRE G., SAVOY L. (2017) Source de Glarey, Détermination des zones de protection, pour la commune de Conthey, Valais.

GREMAUD, V. (2011) Relations between retreating alpine glacier and karst aquifer dynamics. Tsanfleuron-Sanetsch experimental test site, Swiss Alps » PhD thesis, UNINE, CHYN.

CAVES, PALEOSPRINGS AND TROP-PLEINS IN SLOPE AQUIFERS. THE CASE OF THE GUARDAL RIVER SOURCES (SE SPAIN)

Antonio GONZÁLEZ-RAMÓN[(1)(4)], Antonio Lope MORALES-GONZÁLEZ[(2)], Sergio MARTOS-ROSILLO[(1)], Francisco MORAL-MARTOS[(3)], D. Raul GEA-LÓPEZ[(4)], Pedro PÉREZ-MARTÍNEZ[(4)], Iván MOLINA-MOLINA[(4)], Tomás PEINADO[(1)] & Gema ALCAÍN[(5)]

(1) Geological and Mining Institute of Spain, Urb. Alcázar del Genil, 4 Edf. Zulema bajo, 18006 Granada, Spain. antonio.gonzalez@igme.es (corresponding author); s.martos@igme.es; t.peinado@igme.es
(2) University of Jaén. Antonio.lopemorales.ext@juntadeandalucia.es
(3) Pablo de Olavide University,Seville, Spain. fmormar@upo.es
(4) Asociación Espeleológica Velezana (AEV), C/ Levante, 1. Vélez Rubio, Almería, Spain. espeleovelez@gmail.com
(5) Diputación de Granada. Periodista Barrios Talavera, 1, 18014 Granada. galcain@dipgra.es

Abstract

The evolution from Pleistocene to the Present of the main springs in a slope karstic aquifer (with an altitudinal difference and where the phreatic zone affects only the base of the slope) is studied in two different systems: Fuente Alta and La Natividad. The consequence of the evolution of the slope in Fuente Alta area is the existence of successive perched paleo springs associated with caves that show a characteristic *trop-plein* (overflow) functioning. In the La Natividad system there is only one permanent spring. Fuente Alta and La Natividad permanent springs show the water table level position in the aquifer, with a saturated zone under marly materials of low permeability, but, the permeable outcrops where recharge occurs are completely unsaturated. These outcrops have a great exo- and endokarstic development with a fast recharge system (few days of duration), related to high rainfall episodes. Nival recharge is also important. One of the caves reaches the water table, and this has been used to install pressure and temperature sensors for the water table control. The study of the cave systems and the relationships between fast floods and the evolution of levels show that most of the fast-flowing water is expelled across the paleo springs before reaching the saturated zone. This water flows through the vadose karst conduits, directly connected to the paleo springs. This can explain that the peak of the flood in Fuente Alta spring has little importance in relation to the great flow in the associated overflows. In La Natividad the fast component of the water flow reaches the saturated zone, and, in consequence, the temporal evolution of the spring flow shows significant differences.

1. Introduction

Development of karstification in a carbonate aquifer is linked to the action of water and CO_2 infiltrated from the surface and other factors such as geological structure of the rock, mineralogical composition, presence or not of interlayers levels of different hydraulic conductivity and tectonic or geomorphological evolution (FORD & WILLIAMS, 1989). Sierra Seca (Granada province, SE of Spain), where the study area is located, is a good example where all the mentioned factors are determinant in the distribution of karst conduits and the evolution of karstification. This can be appreciated while studying the hydrodynamic functioning of springs and karst conduits directly associated with localized recharge areas (ponors and sinkhole fields). The climate is Mediterranean with an annual precipitation of 900 mm in the highest peaks (Morro del Buitre, 2138 m). The objective of this work is to describe the way these factors influence karstification and fast flow of groundwater after strong storms in Sierra Seca aquifers.

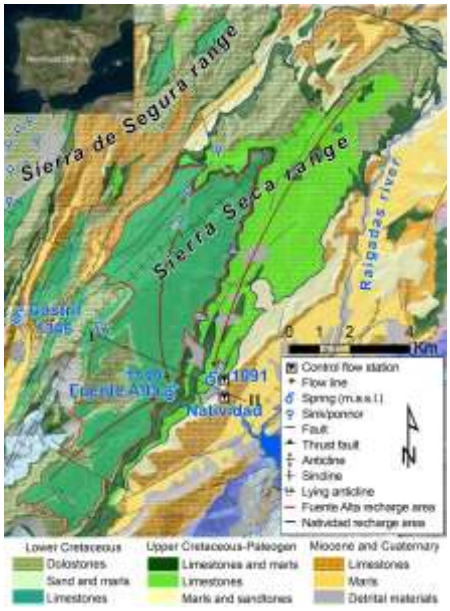

Figure 1: Geographical and geological context of Fuentes del Guardal. GEODE cartography (www.igme.es).

Sierra Seca is a NNE-SSW mountainous range formed by a carbonate sequence of Cretaceous-Miocene age (Fig. 1). It is structured in an asymmetric anticline with the eastern flank dipping around 30° (LUPIANI et al. 2007).

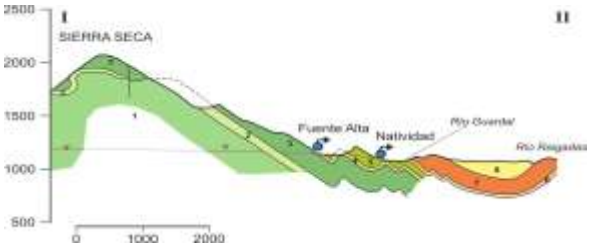

Figure 2: Hydrogeological cross-section. Located in Fig.1.

Lower Cretaceous dolomites and dolomitized calcarenites outcrop in the core of the anticline. Above them, a 20 to 70 m thick layer of marls and sands are present (Fig. 2). The Lower Cretaceous ends with a stretch of limestone, with rudists in the upper part, where the cavities of the Fuente Alta overflows are located. These carbonates are sealed by a layer of this marly limestone. Fuente Alta rises in the contact between these two layers. Towards the top, the loamy layer passes into Upper Cretaceous limestone where La Natividad spring emerges. The Cretaceous limestone outcrops are highly karstified. In the highlands, a well-developed exokarst is observed with numerous sinkholes, uvalas and small poljes with temporary flooding and blind sinkholes (ponor) (MORAL MARTOS, 2019). Both systems discharge the infiltrated underground water in the same area, giving rise to the Fuentes del Guardal. The stretch of Lower Cretaceous limestone drains at Fuente Alta (1140 m a.s.l.), and the stretch of Upper Cretaceous drains at La Natividad (1090 m a.s.l.). Above Fuente Alta there are two caves (Upper and Lower "Cuevas del Nacimiento del Guardal-CNG") that function as overflow during floods.

2. Materials and methods

There is a flow monitoring of a gauging station that records all the water drained by the Fuentes del Guardal. Another station controls La Natividad discharges (Fig. 1). Both are monitored with sensors such as Seba SlimLogCom the first and OTT EcoLog 500 the second, which measure the variation of the water column with a ten minutes time steps. The CNG were explored and surveyed by the AEV speleological group in 2006 and completed by the GEG in 2006 and the GEI in 2014 by diving under the water table level discovered in 2006 (GONZÁLEZ RAMÓN et al., 2016). The difference in the records between the two flow control stations allows calculating the discharges from Fuente Alta; the whole discharging flows are integrated in addition to the permanent spring discharge and the -overflow, when they are active. On 10/19/2019, a LevelSCOUT® sensor (Van Walt) was installed in the CNG, where the water level coincides with the level of the permanent source of Fuente Alta. The sensor was programmed to measure the variation of water level and temperature every hour. The data obtained in the period from 10/19/2019 to 02/12/2020 shows several floods that allow a preliminary assessment of the functioning of the karst system. Lastly, in a fish farm that uses the waters of La Natividad spring, a weather station was installed, programmed to collect hourly data on rainfall, air temperature and atmospheric pressure.

3. Results

The decomposition of the Fuente Alta and La Natividad hydrographs makes it possible to differentiate fast-circulating groundwater from those of slow circulation (Fig. 2A and B). Both springs have a very karstic behavior but differ in that the Fuente Alta hydrograph presents sharper peaks and a faster recession. The flood recorded on 19-25 December 2019 has made it possible to calculate the recession coefficients (α). In Fuente Alta, two lines can be adjusted that would characterize the fast-flow (α = 9.18E-1) of vadose circulation and a slower-flow (α = 2.17E-1) that corresponds to depletion of saturated zone (eg. BONACCI, 1993). In La Natividad the coefficients are lower in both cases (α = 7.61E-1 and α = 5.62E-2), which suggest a different karst system behavior (Fig 3D). The α coefficients show that the response to rainfall in Fuente Alta is faster and the recession is less inertial than La Natividad spring. From the record obtained in the CNG (Fig. 4C), it has been possible to document that much of the fast flow draining through the overflows does not reach the saturated zone (ZS) of the aquifer and is expelled through the epikarstic conduits without influencing permanent spring discharge (Fig. 3C and 4B). The four overflow water points of the CNG are located 25 m of height difference between them. However, surprisingly, in the December 2019 flood, when all of them were activated, the CNG sensor only recorded a 15.4 cm rise (Fig. 3C). This shows that during floods, a large part of the groundwater flow is drained by the overflows before it reaches the ZS, where the sensor is placed (Fig. 4B). La Natividad, instead, does not present associated overflows and its hydrodynamic functioning differs from Fuente Alta, since the entire volume of the flood water is drained by a single point. It is interpreted that, in this case, the fast flow reaches the ZS. As a consequence, this spring has a less pronounced hydrograph, with the rain input signal more attenuated in relation to Fuente Alta spring, although it also shows a markedly karstic behavior. These differences were clearly observed between the dates 01/19/2019 and 02/02/2020, where after snow precipitation in the recharge areas of both springs, only got response in Fuente Alta (Figs. 3A and B).

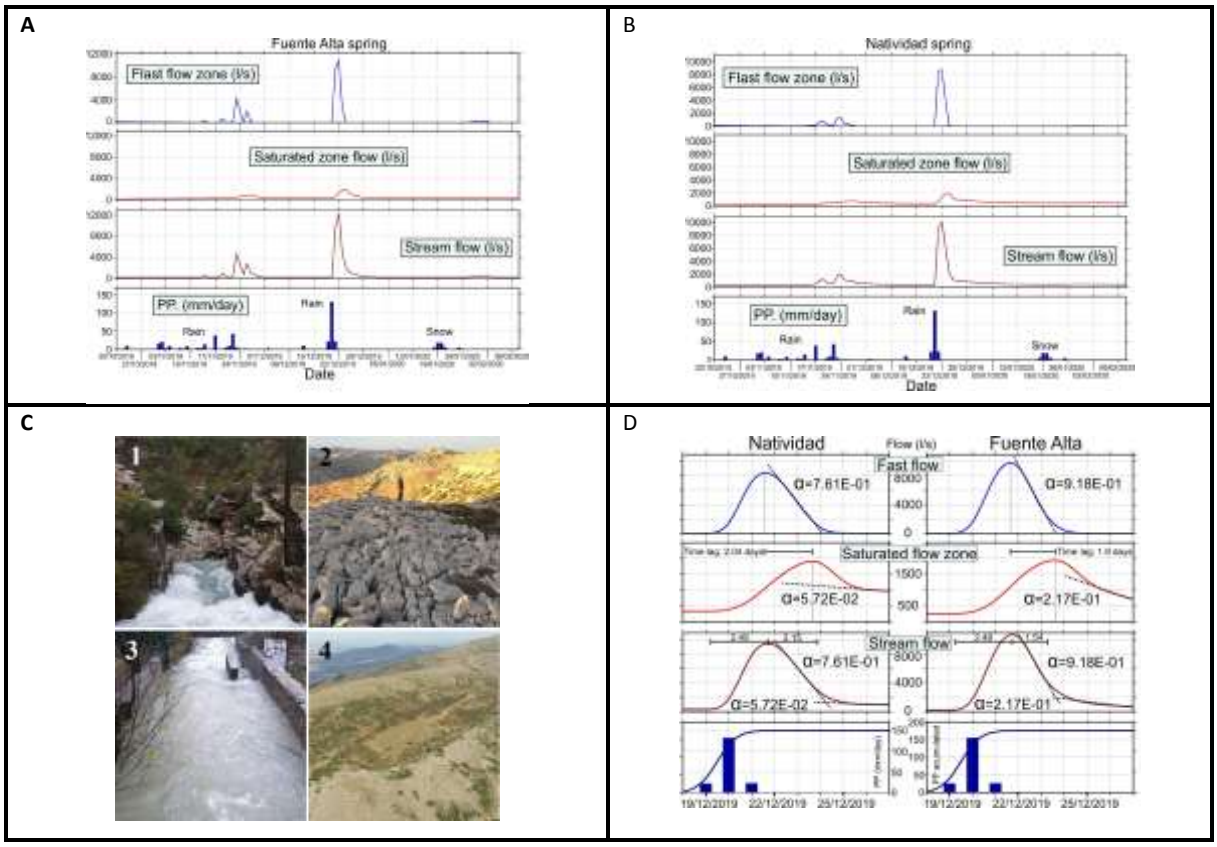

*Figure 3: Hydrograph of Fuente Alta (A) and La Natividad (B). C) 1-*Overflow *of Fuente Alta (CNG), 2-Karren in the recharge area, 3-La Natividad gauging station in flood, 4-Uvala and associated sinkhole in the recharge area. D; Decomposition of the recession curves and recession coefficients obtained in the 19-25 of December 2019 flood.*

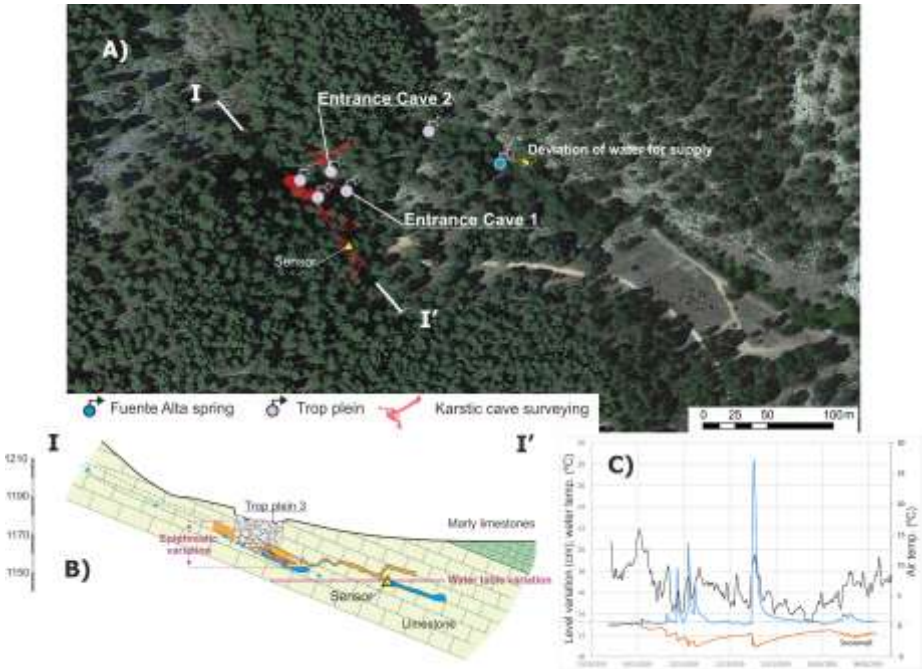

Figure 4: A) Location of the trop-pleins *and caves (in red) in the Fuente Alta area. B) Hydrogeological section of the CNG. C) Records obtained from the CNG sensor, the black line corresponds to the mean daily air temperature in the climate station of the fish farm, the blue line to the water level and the orange line to the groundwater temperature.*

4. Discussion and conclusions

The results show that both springs, despite being less than 1000 m away from each other, present different hydrodynamic functioning (MORALES-GONZÁLEZ et al. 2019). Fuente Alta responds to the infiltration of rainwater more quickly than La Natividad. The slope of the decline curve, corresponding to the vadose zone (USZ) flow, is very steep, with a coefficient α of 9.18E-01, and the recession curve, which represents the drainage of the phreatic zone, shows a steeper slope than in La Natividad, 2.17E-01 and 5.72E-02, respectively (Fig. 2D). This difference in response is due to, firstly, the geological factors; Fuente Alta recharge area is made up of limestone rock outcrops, highly karstified, with fields of karren and other karst landforms, as sinkholes and uvalas (Fig. 3C). Five overflows associated with Fuente Alta spring have been located, which are activated successively depending on the volume of recharge. In addition, the roof of the materials that make up the Fuente Alta aquifer are marly limestones from the Upper Cretaceous. These materials act as a hydrogeological barrier between the Fuente Alta and La Natividad aquifers, reducing the hydrogeological connection between them. While the Fuente Alta recharge zone extends to the W-SW. La Natividad recharge area does it towards the N and NE (Fig. 1) and the lithological layers that outcrop on its recharge area are limestones and dolomites of Upper Cretaceous-Paleogene age. The area related to La Natividad is also highly karstified in the higher areas, where there are fields of sinkholes however, no functional sinkholes are known in which concentrated infiltration could occur, as in the case of Fuente Alta. In the area of lower altitude, towards the NE, the permeable outcrops are covered by a dense mass of vegetation, which can influence the type of infiltration produced, being less concentrated than in the higher altitude area. The hydrodynamic response of La Natividad is more inertial than that of Fuente Alta. As we observed in the November 2019 floods, the peaks are attenuated by the modulating effect produced by the associated aquifer, which presents an important phreatic zone that be able of filtering the input signal produced by the recharge. Another evidence of this functioning was observed after snow precipitation produced in January 2020, when only the Fuente Alta spring responded to this event, days later when there was a rise in temperatures (Figs. 3 and 4). Both springs have a lag time between their responses of approximately 6 hours, depending on the intensity of the precipitation. The first to respond is Fuente Alta, whose maximum registered flood is 11,500 l/s; instead, its flow barely reaches 100 l/s in low water. This spring has an important karst network, which has been partially explored, reaching only about 350 m development of galleries topography since, for now, it has not been possible to access the conduits located upstream of the collapse observed in the CNG (Fig 4B). The five overflows work for a few hours and drain waters that have only passed through the vadose zone, without much of the water reaching the phreatic zone of the aquifer. Temperature control (Fig. 4C) shows a fast cooling of the water during floods. It has not been possible to access to the karst network associated with the La Natividad spring, although the difference in flows between the maximum (8000 l/s) and the minimum flow (230 l/s), despite the lack of overflows, shows that there must be a well-developed drainage system with conduits networks. Both α coefficients are lower than in Fuente Alta, so a deeper and attenuated flow is suspected because all the infiltrated water reaches the storage area in the aquifer system.

Acknowledgments

We gratefully thank to Antonio Muro, Victor Oliva and Mariano Palancar, technicians from the Basin Organism for their collaboration in the data provided by the control flow stations and especially to Raul Viedma, head of the Las Fuentes fish farm, whose collaboration and enthusiastic help has been essential for the realization of this work.

References

BONACCI, O. (1993) Karst springs hydrographs as indicators of karst aquifers. Hydrological Sciences Journal– Journal Des Sciences Hydrologiques, 38(1), 51–62.

FORD D., WILLIAMS P. (1989) Karst geomorphology and hydrology, Ed. Unwin Hyman Ltd. London, 601 p.

GONZÁLEZ RAMÓN A., CORTÉS CORTÉS M., LÓPEZ RAMÓN I., CARRA VÉLEZ R., ÁVILA ALBA J.B., SANTAELLA ALBA RODRÍGUEZ SAEZ A.D., CÁCERES A. (2016) Evolución del relieve y espeleogénesis. Las cavidades del Nacimiento del Río Guardal, Sierra Seca (Granada). Actas Espeleomeeting Ciudad de Villacarrillo, 39-44.

LUPIANI E., ROLDÁN F, VILLALOBOS M. 2007. Memoria y mapa geológico de España E: 1:50.000. Instituto Geológico y Minero de España.

MORAL MARTOS F. (2019) La altiplanicie kárstica de la Sierra de Segura: El mayor torcal de la Cordillera Bética. Boletín de la SEDECK 13, 34-46.

MORALES GONZÁLEZ A. L., MARTÍN RODRÍGUEZ J. F., MUDARRA M., BARBERÁ FORNELL J. A., ANDREO B., JIMÉNEZ ESPINOSA R., DURÁN VALSERO J. J.. (2019) Consideraciones preliminares sobre el seguimiento en continuo de las respuestas naturales de los acuíferos kársticos de las Sierras de Segura, Castril y Seca (provincias de Jaén y Granada). Congreso Nacional del Agua. Orihuela, 1313-132

The "Los Chorros del Río Mundo" cave (Albacete, Spain). Hydrogeological functionning and cave patterns

Antonio GONZÁLEZ-RAMÓN[(1)], José María CALAFORRA[(2)], Juan Leandro RONDA[(3)], Tomás RODRÍGUEZ-ESTRELLA & Juan MELERO[(3)]

(1) Geological and Mining Institute of Spain, Urb. Alcázar del Genil, 4 Edf. Zulema bajo, 18006 Granada, Spain, antonio.gonzalez@igme.es (correspondig author)
(2) Water Resources and Environmental Geology, University of Almería, 04120, Almería, Spain, jmcalaforra@ual.es
(3) Technician in industrial electronics, Camino de la Ermita-Moralet, 64 03699 Alicante, Spain, juanleronda@gmail.com
(4) Department of Mining, Geology, and Cartographic Engineering. Polytechnic University of Cartagena (Spain), tomasrestrrella@hotmail.com
(5) Coordinator of the Speleological Group "Extopocien", quibass@gmail.com

Abstract

The "Cueva de los Chorros del Río Mundo" is the most important cave system in the South Eastern part of the Iberian Peninsula. Currently, the surveyed network of cave passages, which is in the order of 30 km, can be divided in 3 well-differentiated main levels and a possible fourth higher level. It is an epigenic type cave characterized by sudden and heavy discharge episodes, locally as "reventones". Analysing the change in the evolution of the water level in the cave passages, monitored at different strategic nodes, allows us to understand how these extreme floods occur, which can reach level variations of up to 20 m in wide lakes (loops) located in areas near the main exit. The network of passages constitutes the main discharge route for an extensive karst platform (1500-1600 m a.s.l.) of erosive origin and with typical morphology of inverted relief, marked by soft folds with a generally synform arrangement. A preliminary study of the distribution pattern of the karst network, both fossil and active, is carried out, which reveals the existence of a complex network of passages with a marked looping cave pattern, characteristic of karst development controlled by irregular recharge.

1. Introduction

The way in which the passages in the caves are distributed and organized, has been used for their classification. Various studies have shown that caves are usually organized into a small number of patterns types that are related to the following: (1) position of the water table and how it changes over time, (2) type of recharge in the aquifer, (3) the density of fracturing and geological structures and finally, (4) to a lesser extent, porosity of the rock (WHITE, 1988; FORD & WILLIAMS, 2007; PALMER, 2007).

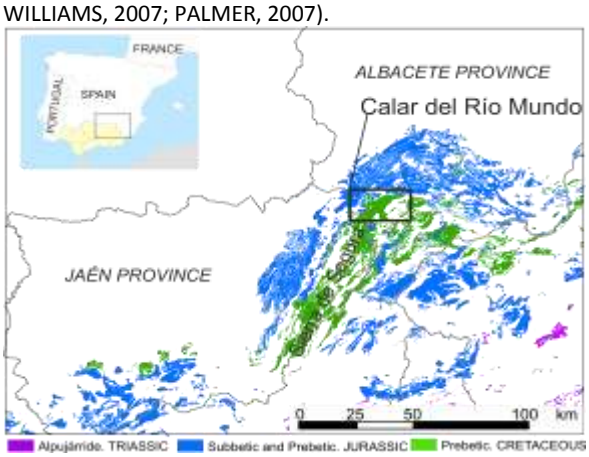

Figure 1: Location of Calar del Río Mundo in the context of carbonate outcrops in the Baetic Mountain Range.

Regarding epigenic caves, AUDRA & PALMER (2015) make a distinction between two types, depending on the defining patterns of their passages in the epiphreatic zone: *looping caves* and *water table caves*. *Looping caves* would be associated with irregular recharge. Their deeper passages are characterised by a wide epiphreatic zone with great variations in level and the existence of perennial springs and *trop plein* (overflow) with great variations in flow.

The aim of this work is to provide an initial overview of the study of the networks which the Cueva de los Chorros del Río Mundo forms part of, based on observations made in both the endokarst and the exokarst and to describe the conceptual model of hydrogeological functioning that best fits with the observations made.

El Calar del Río Mundo, where the cave is located, is part of an extensive karstic high plateau of erosive origin (MORAL, 2019) that extends from the Sierra de Segura (SE of Spain) towards the NE. These erosive high plains are the so-called "calares", that of the River Mundo being the most extensive (Fig. 1).

This calar is formed by Cretaceous limestones and dolomites slightly folded into anticlines and synclines. Its surface is sculpted into well stratified limestones of about 150 m in thickness and all the karstic levels which form the Cueva de los Chorros are found here. The base is made up of a dolomitic clayey formation more than 200 m thick, dating

from the Lower Cenomanian-Senonian. The dolomites show evidence of being more difficult to karstify, overall, when compared with the formation that overlaps them, and are also less permeable. This results in a hydrogeological rupture causing the emergence of the Cueva de los Chorros, leaving a semi-saturated level which occupies the Cañada de los Mojones syncline (Fig. 2).

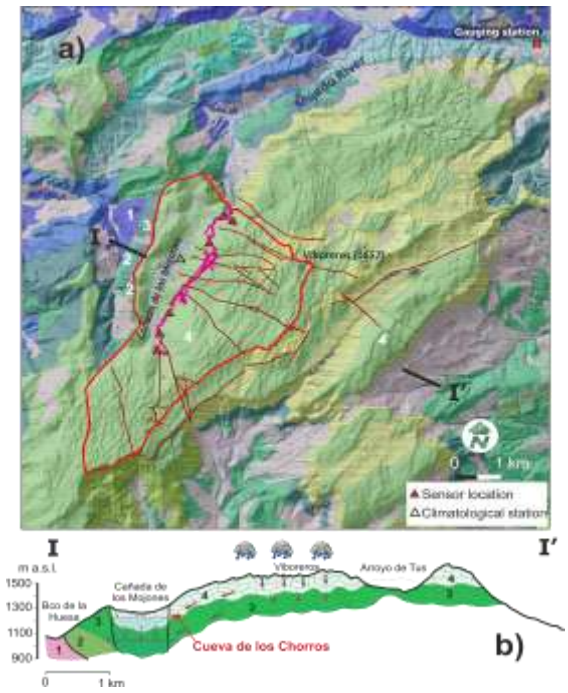

The exploration and documentation of the "Los Chorros del Río Mundo" cave began in the 1960s. During the course of this work, up to four sectors have been discovered, separated from each other by sumps, which have gradually been overcome. At present, some 28 km of underground galleries have been surveyed with a vertical diference of 162 m.

The area has a temperate Mediterranean type climate with an average annual temperature of 11-12°C and average rainfall of 1000-1100 mm (RODRÍGUEZ ESTRELLA & BALLESTA SÁNCHEZ, 1999) which is prevalent from autumn to spring with otherwise very dry conditions. The surface of the calar is characterized by a highly developed exokarst with a high density of dolines, especially in its higher areas such as Viboreros (1657 m a.s.l.). The plateau is slightly folded, forming a general syncline, but with anticlinal folds in its central area that affect the higher parts. The directions of the folding axes are NE-SW (RODRÍGUEZ ESTRELLA & BALLESTA SÁNCHEZ, 1999). The Cañada de los Mojones forms a syncline affected by normal faults on the edges, which give rise to a depressed area with a polje morphology, on whose SE side the cave has developed (fig. 2).

Figure 2 (on the left): a) a) The geological map of Calar del Río Mundo (www.igme.es) includes sets of main fractures observed in the orthophoto, polygonal of the passages surveyed in the cavity, and the proposed watershed slope to Cañada de los Mojones. b): Hydrogeological cross-section. 1 clays, silts and sandstones. Triassic. 2 Sands and clays. Inf. Cretaceous. 3 Microcrystalline dolomites and clayey dolomites. Upper Cretaceous. 4 Limestones. Late Cretaceous.

2. Materials and methods

Between 2017 and 2020, sensors have been installed in strategic locations throughout the cavity to monitor the swollen flow rate, which causes its emergence at the main entrance of the cave to increase abruptly from being practically dry to tens of m^3/s. This is known locally as a “reventón” (burst). At the same time, a thermo-pluviometric station was installed in the Cañada de los Mojones at a height of 1269 m. Both the sensors and the station were programmed for data collection at a fortnightly rate using Hobo® dataloggers. Between 2017 and 2020, sensors have been installed in strategic locations throughout the cavity to monitor the swollen flow rate, causing its emergence at the main entrance of the cave to increase abruptly from being practically dry to tens of m^3/s.

Since 2018, there has also been a gauging station on the Mundo River that monitors the water flowing out of the cave, also with a fortnightly rate of measurement. Fig. 2 shows the location of the monitored points and Fig. 4 shows the results obtained. In addition, a large part of Sector 2 of the cave is currently being reprogrammed, which has made it possible to review the morphology of the passages in the areas of greatest interest.

3. Results and discussion

The cave is spread out over three levels (N2, N3 and N4) which are in turn divided into several sub-levels and a possible fourth higher level (N1), which is incomplete and less extensive. The levels, like the syncline axis of the Cañada de los Mojones, appear inclined towards the NE in the order of 1°. From the frequency distribution graph showing the appearance of passages in terms of height, four main levels can be identified at the following height intervals (Fig. 3): Level 1 (1288-1292 m); Level 2 (1262-1272 m); Level 3 (1234-1256 m); Level 4 (1204-1220 m).

The changes in water level for the monitored points together with the flow data from the Mundo river and also the precipitations in the period Oct18/May20 are shown in Fig. 4. The hydrograph is characteristic of highly karstic aquifers with several short and sharp annual peaks. The flow rates during the control period range from 1-2 m^3/s to 74.3 m^3/s, recorded during December 2019. At all the points monitored inside the cave, the variations are synchronous, with the greatest floods occurring in the Lago del Brillo (Brillo Lake) and in the Sifón Mateo (Mateo sump), at the points just before where sumps and narrowing are present, both of which hinder the flow. These areas are considered to be loops.

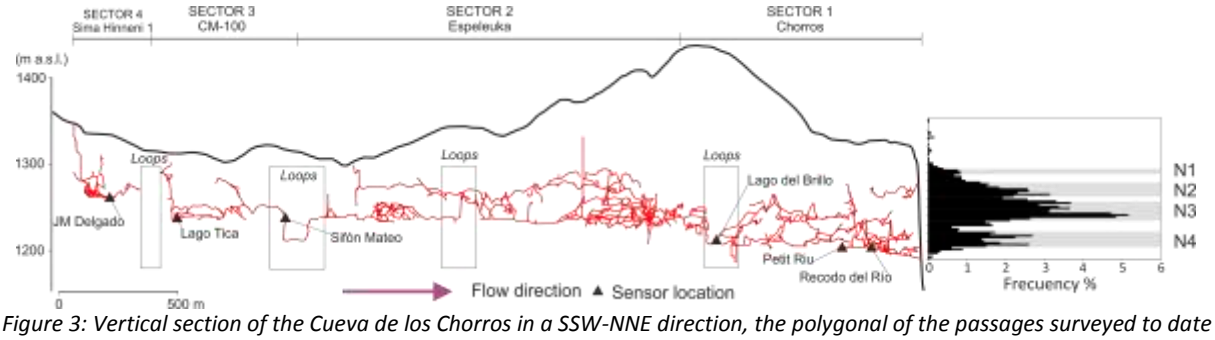

Figure 3: Vertical section of the Cueva de los Chorros in a SSW-NNE direction, the polygonal of the passages surveyed to date is included. The rectangles indicate the most significant distinguishable loops. The diagram shows the frequency of the distribution of passages vs the elevation. The different levels that can be discerned are inclined 1° towards the NNE.

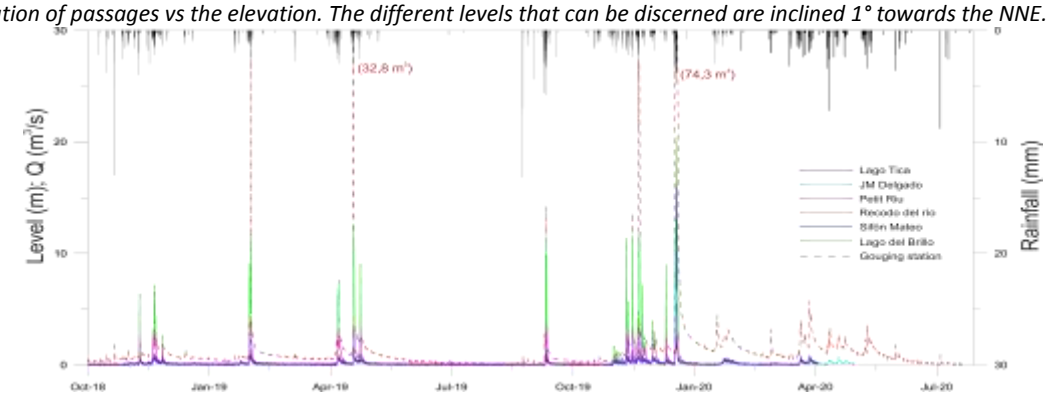

Figure 4: Flow is recorded at the Mundo River gauging station, rainfall at the Cañada de los Mojones station and levels measured by sensors installed in the Cueva de los Chorros. Period October 18/May 20.

The morphology of the cave is determined by several factors: geomorphological changes in the cliff, where its entrance is located (Fig. 5d); type of recharge which occurs in the limestone and finally the existence of a break in the permeability of the geological series due to the lithological change between the limestones and the dolomites.

Most of its passages have been formed in an epiphreatic/phreatic setting except, possibly, for the first phase of speleogenesis in which there may have been some semi-confined (Fig. 3, level N1). The cavity undergoes large and sudden variations in the piezometric level, due to a pronounced irregularity in the recharge, which is a consequence of the high permeability of the surface in the calcareous zone and the Mediterranean type climate, in which storms are concentrated over just a few days in autumn and spring. In this regard, the most common patterns found in the conduits are of the anastomotic maze type (AUDRA & PALMER, 2015; JOUDES et al., 2017), due to the existence of bottlenecks in the networks in the form of loops. The existence of loops causes temporary upstream storage, with diversification of the flow, which is what leads to the development of these special types of networks, in those particular areas (e.g. Fig. 5a).

Currently, the active levels run a few meters above the contact zone with the lower dolomitic formation, which is less permeable. The greatest storage of water occurs towards the west, in the trench which comprises the Cañada de los Mojones, formed by the nucleus of a syncline which has faulting around its edges (Fig. 2b). During times of low water, the phreatic level has a very low gradient, increasing greatly and rapidly during recharge episodes. A flood dome is created which drains quickly due to having an easier exit: the SE side of the la Cañada de los Mojones Polje. This has brought about greater concentration of karstification in this area, giving rise to the Cueva de los Chorros. The monitored points do not show a relationship between the level of the floods and the proximity of the water emergence via the upwelling. Quasi-synchronous floods are observed at all points. However, there are differences in the height of the level reached, which is greater near the loops (Fig. 5c).

When karstification advances thus generating galleries, in the most fractured areas (greater local permeability), there is a tendency for sloping conduits that generate *loops*. These conduits cause bottlenecks when there is an abrupt recharge, as they are not capable of draining the large volume of water. Consequently, they cause a rise in the phreatic zone upstream, generating new galleries, both horizontally and vertically, with labyrinthine morphologies of anastomosing conduits. These morphologies are best developed immediately upstream of the *loops*. An example can be seen at the beginning of Sector 2, upstream from the Sifón Vera and Lago del Brillo, which form one of these *loops*. The Sifón Mateo Martín is also considered to be a *loop* (Fig. 5a and b).

Fig. 5c shows the flood on 21 December 2019 in detail, which recorded flows of more than 70 m^3/s. The greatest level rises were recorded in Lago del Brillo and in the Sifón Mateo, and to a lesser extent in the Lago JM Delgado, the three points located upstream from important sumps that form *loops* (Fig. 3). Floods are lower at other points that are closer to the upwelling, such as the Recodo del Río or Petit Riu, or downstream from the *loops*, such as Lago Tica. The flooding in Lago del Brillo shows a plateau at 12 m which is adjacent to an upper gallery that acts as a *bypass* for the *loop*.

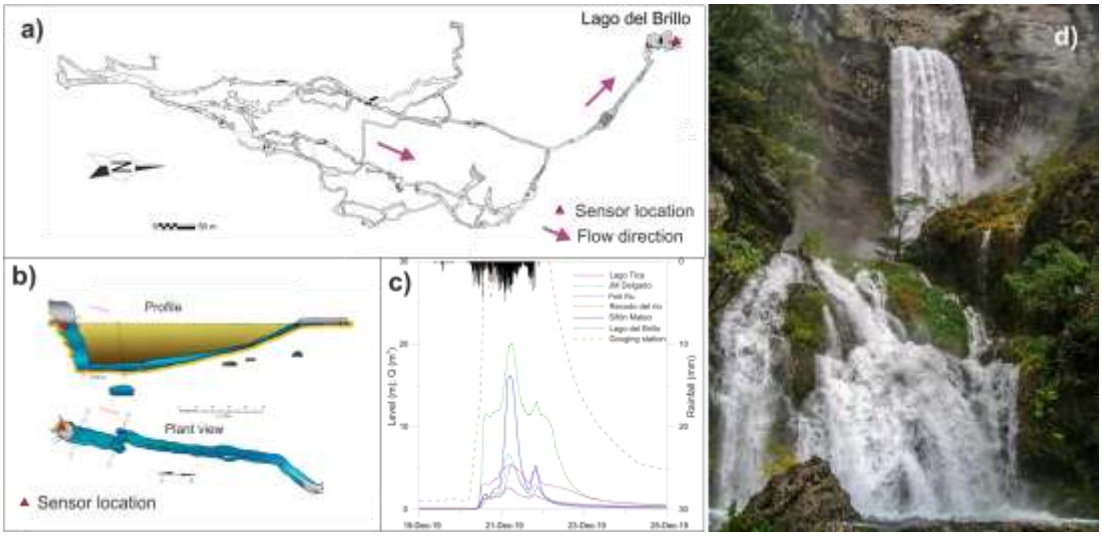

Figure 5: a) Distribution of galleries upstream from the point where the Lago del Brillo sensor is located. b) Profile and plan of the Sifón Mateo (modified from Llamusí et al., 2019). c) Change in levels at different points in the Cueva de los Chorros during the December 2019 flood. d) Entrance to the Cueva de los Chorros during a blowout.

5. Conclusion

The spring of the Cueva de los Chorros is characterized by abrupt overflows due to hard rainfall. The flow rates range from 1-2 m3/s to 74.3 m3/s during oct 2018/oct 2019. The morphology of the cave is determined by: the geomorphological evolution of the cliff, including the main entrance; the type of recharge and the existence of a break in the permeability of the geological series. The distribution patterns of fossil and active galleries show a looping-cave type. The cave is spread out over three levels and a possible fourth higher level. Currently, the active levels run a few meters above the contact with the lower dolomitic formation, less permeable. Monitored points do not show a relationship between the level of the floods and the proximity of the water emergence via the upwelling. Quasi-synchronous floods are observed at all points. However, there are differences in the maximum level reached in each gallery, which is greater at the points where loops exist.

Acknowledgments

The data included in this article have been obtained by the EXTOPOCIEN group, of which the authors are members. All the instruments inside the cave have been installed by the Research Group Water Resources and Environmental Geology of the University of Almería. Our thanks to the speleology groups that collaborate with EXTOPOCIEN and to all their members.

References

AUDRA P., PALMER A.N., (2015) Research frontiers in speleogenesis. Dominant processes, hydrogeological conditions and resulting cave patterns. Acta Carsologica, n° 44(3), 315-348.

FORD D. C., WILLIAMS P. W., (2007) Karst Hydrogeology and Geomorphology. Second edition. Ed. John Wiley & Sons, 562 p.

JOUVES J., VISEUR S., ARFIB B., BAUDEMENT C., CAMUS H., COLLON P., & GUGLIELMI Y. (2017) Speleogenesis, geometry, and topology of caves: A quantitative study of 3D karst conduits. Geomorphology, nº 298, 86-106.

LLAMUSÍ J.L., SÁNCHEZ J., ROS A., MARÍN A., BELTRÁN G., MARTÍNEZ J.A., PLA R. (2019) Exploraciones submarinas en la cueva de los Chorros del Río Mundo, Albacete, 2002-2018, n° 13, 59-70.

MORAL F. (2019) La altiplanicie kárstica de la Sierra de Segura: el mayor Torcal de la Cordillera Bética. Boletín de la Sociedad Española de Espeleología y Ciencias del Karst, n° 13, 34-46.

PALMER A.N. (2007) Cave Geology. Ed. Cave books, 454 p.

RODRÍGUEZ ESTRELLA T., BALLESTA SÁNCHEZ F. (1999) Estudio geohidroespeleologico del calar del mundo (provincias de Albacete y Jaén). Ed. Instituto de Estudios Albacetenses, 180 p.

WHITE W. B., (1988) Geomorphology and hydrology of karst terrains, Oxford University Press, New York.

Water balance and temperature regime in the bottom part of the Snezhnaya cave system (Western Caucasus)

Alexander GUSEV

Lomonosov Moscow State University, Sternberg Astronomical Institute, 13 Universitetsky pr., 119234 Moscow, Russia, gusev@sai.msu.ru

Abstract

Snezhnaya cave system, located in the alpine karst Khipsta massif, is the largest cavern in the Caucasus (total length 41 km, amplitude 1760 m, volume $2.7 \cdot 10^6$ m^3). The hydrological network of the cave includes two main separate rivers. We present the results of the analysis of monitoring data for water level and temperature and air temperature in 2015-2019 on both rivers in the bottom galleries of the cave system. Seasonal changes in water and temperature regimes in the cave are investigated. The correlations between air and water temperatures in both parts of the cave system were studied. The regimes of flashfloods are considered in detail. Based on the data of the 3D map of the cave and changes in water volume at the end of single flashfloods, a water balance model was reconstructed for both rivers in the approximation of Bernoulli's principle for a perfect fluid. The water discharges at the entrances to the bottom galleries of the cave system and at the exits from it was estimated. The results indicate the existence of two separate hydrological and climatic systems with significant differences in the morphology and catchment area of the two parts of the cave system.

Резюме

Водный баланс и температурный режим в донной части пещерной системы Снежная (Западный Кавказ). Пещерная система Снежная, расположенная на Хипстинском высокогорном карстовом массиве, является крупнейшей пещерой на Кавказе (общая длина 41 км, амплитуда 1760 м, объем $2.7 \cdot 10^6$ м^3). Гидрологическая сеть пещеры включает две основные независимые реки. Мы представляем результаты анализа данных мониторинга уровня и температуры воды и температуры воздуха в 2015-2019 годах на обеих реках в нижних галереях пещерной системы. Исследованы сезонные изменения водного и температурного режимов в пещере. Изучены корреляции между температурами воздуха и воды в обеих частях пещерной системы. Подробно рассмотрены режимы паводков. На основе данных трехмерной карты пещеры и изменений объема воды в конце одиночных паводков была восстановлена модель водного баланса обеих рек в приближении закона Бернулли для идеальной жидкости. Были оценены расходы воды на входах в нижние галереи пещерной системы и на выходах из них. Результаты указывают на существование двух отдельных гидрологических и климатических систем со значительными различиями в морфологии и площади водосбора двух частей пещерной системы.

1. Introduction

Snezhnaya cave system is located on the southern slope of the Caucasus (Khipsta massif of the Bzyb ridge). In terms of morphometric parameters, it is the longest karst cavity in the Caucasus (total length of passages 40840 m) and the fourth deepest cave in the world (amplitude 1760 m). Six known entrances to the system are located at the altitudes from 2389 m a.s.l. (Illyuzia) to 1318 m (Fantazia) (SHELEPIN *et al.* 2019). The three lower entrances are in the forest zone, the upper entrances are in the meadow zone.

The volume of the cave system is estimated at $2.7 \cdot 10^6$ m^3 (MAVLYUDOV 2016). Most of the volume falls on the bottom of the cave system, where the largest halls of the system are located (SHELEPIN *et al.* 2019).

The cave system has a well-developed hydrological network, which includes two main underground rivers and many smaller tributaries (GUSEV 2018; MAVLYUDOV 2016). The uniqueness of the cavity lies in the presence of two independent hydrological systems that have not yet been connected. The Guzhva cave river has been studied for 6.3 km ("old" part of the system). On the opposite side, under the same bottom blockage the same large Tatianina cave river flows, studied for more than 1 km ("new" part of the system). The deepest point of the system (−1760 m) is currently a siphon in the bottom of Morozov Lake, located on the Tatianina River (Fig. 1).

In recent years, a complex system of vertical passages and pits has been discovered at the bottom of the cave system. In several places it was possible to descend below the level of −1740 m. Under the blockage, it was possible to reach the Lebedinaya River (apparently, the continuation of the Guzhva River).

The cave system is formed in a southern wing of a large anticlinal fold in limestones and dolomites of the Upper Cretaceous (MAVLYUDOV 2016). Tracing tests indicated the

complex nature of the movement of groundwater in the karst massif. The cave has at least three water flow exits into the surface (GUSEV 2018).

Systematic monitoring measurements of the water level, water and air temperature in the bottom part of the cave system have not been previously carried out. The practical purpose of the study is to evaluate the parameters of unknown lower passages to search for possible extensions of the system and to analyze the flood regime for recommendations on the safety of caver expeditions.

2. Monitoring experiment, data reduction, and water balance estimation method

The monitoring used sensors produced by Solinst Canada Ltd. A pair of sensors consists of two devices: a barologger, which measures the air temperature, t_{air}, and compensation level (analogue of atmospheric air pressure), l_{comp}, and a levelogger, which measures the temperature, t_{water}, and pressure (level) of water, h_{exp}. Barologger is a sensor whose readings are used as a correction for atmospheric pressure. The parameters were measured with an interval of 1 hour.

The accuracies of loggers are 0.05% FS for the levels and 0.05˚C for the temperatures.

The first pair of sensors was installed in the area of Penelopa Hall (levelogger location at 645 m a.s.l.), the second pair was installed near Morozov Lake (635 m a.s.l.; Fig. 1).

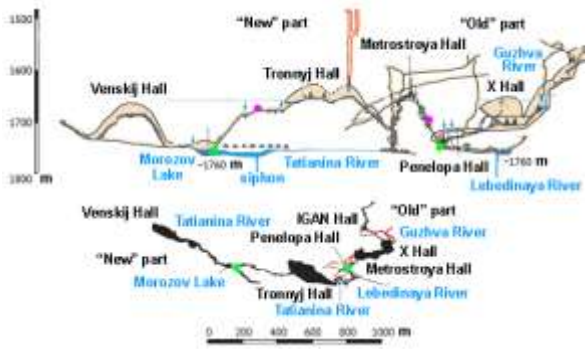

Figure 1: Profile and plan of the bottom part of the Snezhnaya cave system (from SHELEPIN et al. 2019) indicating the locations of the loggers. Places of leveloggers are marked by green circles, barologgers are by magenta circles (only on the profile).

At the first stage of data reduction, complete data series of t_{air}, l_{comp}, t_{water}, and h_{exp} were built for all four sensors. Both leveloggers have worked stable for 4.5 years, from January 2015 to July 2019. Both barologgers have work stable for only 12.5 months until early February 2016. The periods of unstable operation of the devices were excluded from further consideration.

At the second stage, the water levels were corrected for the level of compensation of the barologger. In cases where the values of the compensation level were measured, the correction was carried out according to the formula $h = h_{exp} - l_{comp}$, where h is the corrected water level.

We found the average compensation levels for the Penelopa Hall (l_{comp}=0.86±0.05 m) and Morozov Lake (l_{comp}=0.87±0.05 m). The analysis showed that the l_{comp} values are distributed according to the Gauss law, thus, their average values were used for cases when the values of the compensation level were not determined: $h = h_{exp} - 0.86$ for the Penelopa Hall and $h = h_{exp} - 0.87$ for the Morozov Lake. The corrected data series are shown in Fig. 2. A detailed description of the monitoring experiment and data reduction is given in GUSEV *et al.* (2020).

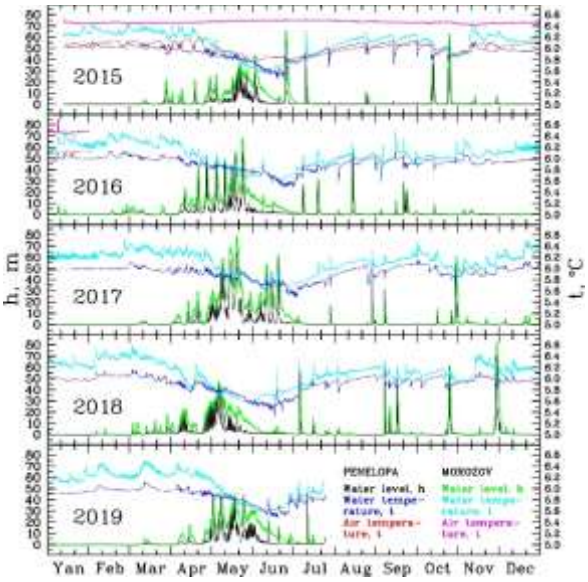

Figure 2: Profiles of the corrected water level (black and green curves), water (blue and cyan) and air temperature (red and magenta) in the Penelopa Hall (black, blue, red) and on the Morozov Lake (green, cyan, magenta curves).

Water balance was estimated based on the continuity equation for a liquid flow: $Q_1 - Q_2 - |Q_3| = 0$, where Q_1 is the inlet water discharge, Q_3 is the outlet water discharge, Q_2 is the change in water volume in the measured reservoir.

The water volume V_2 was calculated using a 3D map of the cave system. We estimated the areas of horizontal sections S_2 depending on the height h above the measurement sites for both the "old" (Penelopa Hall) and the "new" (Morozov Lake) parts with a step of 1 m by h and approximated $S_2(h)$ by a piecewise linear function. We estimate the error ΔS_2 at 20%. Received volume $V_2(h) = S_2(h)h$.

We assume that at the end of powerful summer single flashfloods (see Fig. 2), $Q_1 << |Q_2| \approx |Q_3|$. Knowing the morphology of the cave, we also adopt that $S_3 << S_2$, where S_3 is the area of outlet section for water flow. Thus, we can use Torricelli's law as a particular case of Bernoulli's principle for a perfect fluid: $v=(2gh)^{0.5}$, where v is the water velocity at an exit and g is the gravitational acceleration.

Note that we have previously found the absence of a hydrological connection between the "old" and "new" parts

of the cave system (see fig. 14 in GUSEV *et al.* 2020), i.e., both reservoirs can be considered separately. Another condition for the correct use of the Torricelli's law is the absence of numerous upper water outlets.

Thus, we use the final equation $|Q_2| = S_3(2g(h+y))^{0.5}$, where y is the difference in altitude between the levelogger and the outlet.

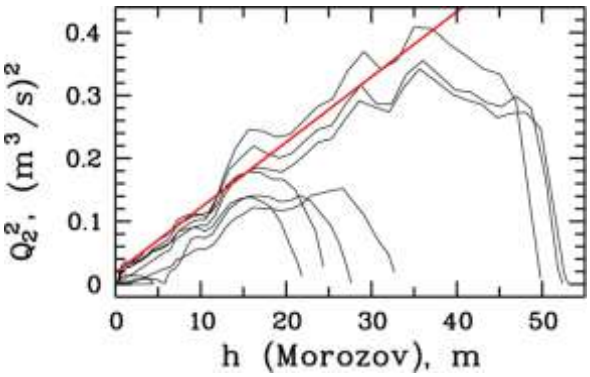

Figure 3: Q_2^2 vs. h diagram at the end of single summer flashfloods on the Morozov Lake (black curves). Red line shows the resulting linear regression.

Finding the linear regression coefficients in diagram Q_2^2 vs. h (see Fig. 3), we can obtain both S_3 and y: if $Q_2^2=Ah+B$, then $S_3=(A/2g)^{0.5}$ and $y=B/A$. In the absence of upper water outlets, S_3 and y are constants, so we can use formula $|Q_3|=S_3(2g(h+y))^{0.5}$ for any water regimes, including periods of low water. Such a situation is observed on the Morozov Lake, where there is one main gallery, and the water goes into a siphon (Fig. 1).

The "old" part of the cave is a complex 3D labyrinth with numerous blockages, vertical, horizontal and inclined passages. The analysis of the dependence Q_2^2 vs. h for the Penelopa Hall showed that the linear dependence $Q_2^2 \sim h$ persists up to the level $h \approx 5.7$ m, and the obtained $y=-5.3$ m, i.e., the water outlet is above the levelogger. For the low water level in the Penelopa Hall, Toricelli's law is not applicable. Therefore, we studied dependence ΔQ_2 on h for $h<5.7$ m in diagram log Q_2 vs. log h and obtained empirical correlation $Q_2 \sim h^{2.42}$, where the power 2.42 depends on the geometric shape of the extended outlet. We also took into account the lower water discharge of ≈200 l/s of the Guzhva River when calculating the minimal water discharges.

Knowing Q_2 and Q_3, we can find input water discharge $Q_1=Q_2+Q_3$. Correctness of the method used is supported by the fact that calculated $Q_1>0$ within errors in every case. Correctness of Torricelli's law using is confirmed by the linear dependence between experimental data in diagram Q_2^2 vs. h.

Here and below, we do not give formal errors for Q_n and regression coefficients due to the significant contribution of errors in determining the function $S_2(h)$. We estimate the error in measuring Q_n at 20%.

3. Main results and discussion

The seasonal features of the water and temperature regimes in the bottom of the system are clearly visible (Fig. 2). The winter low-water period is characterized by a complete absence of large floods and by relatively constant high temperatures of water and air. During spring flood period, the water temperature begins to decrease, and the air temperature reaches its minimum values (in the Penelopa Hall). The summer-autumn period is characterized by rare but powerful flashfloods. The temperature of water and air (in the "old" part of the cave) gradually increases.

The minimum values of air and water temperature in the bottom of the cave system are recorded in June, by the end of the spring flood. Hourly changes in water temperature on the Morozov Lake are systematically larger than in the Penelopa Hall, and reach values of ±0.1-0.15˚C during the winter low-water period. The maximum jumps in water temperature are recorded during powerful summer floods, when hourly temperature changes Δt_{water} reach of -0.30...+0.26˚C/hour in the Penelopa Hall and -0.27...+0.49˚C/hour on the Morozov Lake.

The average t_{water} in the Penelopa Hall is +5.92±0.13˚C and lies in the range from +5.32˚C to +6.16˚C, and on the Morozov Lake is +6,08±0,21˚C ranging from +5.56˚C to +6.60˚C.

The air temperature changes are much smaller. In the Penelopa Hall, t_{air} lies in the range from +5.77 to +6.16˚C with an average value of +6.00±0.10˚C, and hourly changes Δt_{air} only during flashfloods can reach -0.13...+0.06˚C/hour (see GUSEV *et al.* (2020) for more details). The air temperature on the Morozov Lake is 0.3-0.7˚C higher and does not change throughout the year, it is ranging from +6.41 to +6.53˚C with an average value of +6.47±0.02˚C (a small peak up to +6.70˚C in 4 p.m. on January 8, 2016 is apparently associated with anthropogenic impact).

Significant differences are observed between the values and nature of seasonal changes in both the water and air temperatures in the Penelopa Hall and on the Morozov Lake (see Fig. 2 and GUSEV *et al.* 2020).

During periods without flooding, the correlation between water temperature on the Morozov Lake, t_{water}(M) and in the Penelope Hall, t_{water}(P), is well described by a linear law $t_{water}(M) \sim 2t_{water}(P)$ with $t_{water}(M) > 2t_{water}(P)$. During floods, $t_{water}(M) \approx 2t_{water}(P)$.

Most of the large summer floods in the cave are not single, but have two, three and, occasionally, more maximums. Maximum water levels were 71.5 m in the Penelopa Hall and 81.4 m on the Morozov Lake during the flood of 28 November - 3 December 2018.

The rate of water rise in the cave is higher during single floods, and it is higher in the Penelope Hall than on the Morozov Lake. The highest rate of water rise Δh was 38.5 m/hour.

An important difference between the flood regime in the Penelopa Hall and on the Morozov Lake is the smoother nature of the flood flow in the latter. Equality of absolute water levels (above sea level) is achieved in the Penelopa Hall and on the Morozov Lake not simultaneously, but at those moments when the water in the Penelopa Hall begins

to subside, and on the Morozov Lake it continues to rise. The flood profiles show that the water reservoirs in the "old" and "new" parts of Snezhnaya system do not communicate with each other.

For a more detailed analysis of air and water temperatures, its correlations, and regimes of flashfloods, see GUSEV *et al.* (2020).

Water balance analysis showed an average water discharge of 1.0 m^3/s in the Penelopa Hall and 0.22 m^3/s on the Morozov Lake. Maximum discharges at the entrance to the Penelopa Hall and Morozov Lake are 69.2 and 5.04 m^3/s, respectively. Maximum discharges at the exit from the Penelopa Hall and Morozov Lake are, as expected, lower: 22.7 and 0.93 m^3/s, respectively. Maximum water volume in the cave system is $5.3 \cdot 10^5$ m^3, which is 20% of the total volume of Snezhnaya cave system. Obtained annual drainage is 0.04 km^3, close to estimates of 0.03 km^3 of MAVLYUDOV (2016), with 4/5 accounted for by the "old" part of the system.

Note that although 80% of the water flows through the Penelopa Hall, the average (6.6 versus 5.3 m^3) and maximum volumes ($4.1 \cdot 10^5$ versus $1.3 \cdot 10^5$ m^3) of water in the reservoir, V_2, are greater on the Morozov Lake. This is due to the lower capacity of the "new" part of the cave system.

One of the consequences of the analysis of the dependence of Q_2^2 on h is to find the maximum low-water discharge of 135 l/s on the Tatianina River. The second consequence is an estimate of the outlet area of 0.63 m^2 for the "old" part of the cave system.

Although the distance between the loggers in the Penelopa Hall and on the Morozov Lake does not exceed 800 m, the results obtained indicate the existence of two independent hydrological and climatic systems in the bottom of Snezhnaya cave system and can be interpreted by as a result of significant differences in the morphology of the "old" and "new" parts of the cave system.

The air temperature in the Penelopa Hall correlates with the water temperature, it reflects the temperature of air masses strongly cooled by water currents.

The discharge of the Tatianina River is estimated on average 4-5 times lower than the discharge of the Guzhva River. The catchment area of the hydrological system of the "new" part should also be approximately 4-5 times less.

Based on the study of catchment area of Snezhnaya cave system in GUSEV (2018) and the study of geology of massif in MAVLYUDOV (2016), the minimal and maximal catchment areas of cave rivers (Guzhva and Tatianina) are estimated at 15 and 18.5 km^2, respectively. Using these data and obtained annual drainage, we estimated the annual precipitation at 2100-2600 mm (without 500-800 mm of annual evaporation). Our estimates are close to the data of GIGINEJSHVILI (1979), who gave 2100-2300 mm taking into account the annual evaporation.

The catchment area of the Tatianina River is only 3 km^2 and it is apparently located entirely in the forest zone (see maps in GUSEV 2018).

4. Conclusion

Water and air temperatures as well as water levels were obtained and studied in the bottom galleries of "old" and "new" parts of Snezhnaya cave system based on monitoring data of 2015-2019. Such systematic monitoring measurements in this cave system have not been carried out before.

Water balance model was reconstructed for both cave rivers using the main hydrodynamic equations.

Obtained results indicate the existence of two separate hydrological and climatic systems with significant differences in the morphology and catchment area of the two parts of the cave system.

The developed water balance estimation method can be used for study the water balance in other caves with Snezhnaya-like morphology.

Acknowledgments

I would like to thank Anastasia YANINA, Gintautas ŠVEDAS, Tatiana NEMCHENKO, Victor SHADRIN, Aidas GUDAITIS, Bernardas PAUKŠTYS, Alexei SHELEPIN, Alexander DEGTYARYOV and Peter KOVESHNIKOV for the monitoring experiment and cave topographic data. I am grateful to the referees for constructive comments.

References

GIGINEJSHVILI G.N. (1979) *Karst water of the Greater Caucasus and the main problems of karst hydrology*. Tbilisi, 224 pp. [in Russian].

GUSEV A.S. (2018) Hydrology of underground water of Khipsta Massif (Abkhazia). *Problems of geography*, Moscow, V. 147, 107-133 [in Russian].

GUSEV A.S., ŠVEDAS G., NEMCHENKO T.A., SHADRIN V.O., YANINA A.A. (2020) Water and temperature conditions in the bottom part of Snezhnaya cave system (Western Caucasus, Abkhazia). *The Caves*, Perm, V. 43, 60-82 [in Russian].

MAVLYUDOV B.R. (2016) The Snezhnaya-Mezhennogo-Illyuziya cave system in the western Caucasus. *Boletín Geológico y Minero*, V. 127, n 1, 219-235.

SHELEPIN A.L., VAKHRUSHEV B.A., GUNKO A.A., GUSEV A.S., PROKHORENKO A.I., SAMOKHIN G.V., FILIPPOV A.G., TSURIKHIN E.A., eds. (2019) *Atlas of caves of Russia*, Moscow, 768 pp. [in Russian].

Discharge modelling of a highly dynamic flow regime in an Alpine vadose shaft (Hochschwab, Austria)

Eva KAMINSKY[(1)], Lukas PLAN[(1)], Barbara FUNK[(1)] & Thomas WAGNER[(2)]

(1) Natural History Museum Vienna, Burgring 7, 1010 Vienna, Austria; evakam@posteo.de (corresponding author)
(2) Institute for Earth Sciences, University of Graz, Heinrichstrasse 26, 8010 Graz, Austria

Abstract

A brook in a 713 m-deep cave (Furtowischacht) in the Hochschwab Massif enables the characterisation of the recharge processes and water flow in the vadose zone. A Thomson weir was installed in a canyon stream 100 m below the entrance and logged the water level at least every 10 minutes for four years. The discharge shows extreme fluctuations between 0.002 and 19 l/s. The analysis of recession curves allows the distinction of quick, intermediate and slow components with α-values of 4, 1.4, and 0.4 1/d, respectively. A rainfall-runoff model reproduces the highly dynamic flow regime, using discharge simulations of two different precipitation measurements. The water storage component is quite low and very quick responses after rainfall show the danger of water increase within the vadose shaft for cavers.

1. Introduction

Percolation through the vadose zone has a major effect on the groundwater recharge of a karst aquifer. Large fractures or conduits provide quick water flow paths whereas the matrix within the carbonate rock may provide a storage component. Flooding events and their intensity within the cave and shaft system are of interest for speleologists as flood events can be very risky during caving. The storage component is of interest due to the water self-purification over time. Therefore, the characterization of the hydrological behavior depending on the recharge is of interest.

In many conceptual karst hydrological models, a dual-porosity system is used to describe the flow characteristics within conduits and the matrix. The quick responses are caused by hydrologic events, where water rapidly moves through tubes, conduits, or large fractures. Various karst models have been developed as quantitative approaches to provide a deeper understanding of karst aquifer systems (e.g., HARTMANN et al., 2014). However, modelling these systems is challenging due to the extreme heterogeneity of their hydraulic parameters. Global numerical models, like rainfall-runoff models can be used to reproduce the water flow dynamics highlighted by experimental approaches (e.g., MAZZILLI et al., 2019). Only meteorological data and discharge (Q) are needed as input parameters for lumped rainfall-runoff models and the output parameter provide information about the physical properties (e.g., HARTMANN et al., 2014).

The Hochschwab, with its 2277 m high summit and its 650 km² areal extent is one of the extensive karst plateaus of the Northern Calcareous Alps, 80 km southwest of Vienna. Up to date 1204 caves have been registered at the Hochschwab, predominantly vadose canyon shaft systems, with Furtowischacht being the second deepest cave (-713 m). The entrance opens at 1785 m a.s.l. (UTM 33N: 5,271,884 N / 502,845 E) in a 25° steep west facing slope of the so-called Polsterkar. The Polsterkar is a glacially formed cirque, currently above the timberline and shows a fragmentary grassy vegetation. Near the cave, the soil cover consists mainly of humus and reaches a thickness of 0.3 m, but bare rocks with karren, small dolines and shaft entrances are common in this area.

A Thomson weir has been installed in a stream of a vadose canyon 100 m below the entrance of Furtowischacht (Fig. 1 and 2).

The study of KAMINSKY et al. (2021) focuses on a hydrologic characterisation of the upper vadose zone by applying experimental methods on this stream in Furtowischacht. The runoff at the weir in Furtowischacht is 0.28 l/s on average and extremely dynamic (0.002 to 19 l/s) with a variability degree (Qmax/Qmin) of 9500. Hydrograph recession analysis distinguishes a quick, intermediate and slow component with α-values of 4, 1.4, and 0.4 1/d, respectively. Calculating the storage volume according to average baseflow recessions and their initial Q resulted in only 22 m³ (or 5 mm for the catchment of 4500 m²), which may be contained within the partial soil cover. Repeated tracer tests show that the transit velocities differ by three orders of magnitude between base flow and high flow conditions.

To reflect the hydrological dynamic of the system, the GR4J+ Model (rainfall-runoff model extended with a snow module from WAGNER et al., 2016) was applied with daily values for the time period 12/2016 to 10/2020. The general trend is quite well simulated but for quick responses especially after a rainfall event the temporal resolution of one day is not sufficient. Further, input parameters are of high uncertainty due to the fact that the meteorological station is a bit far from the entrance (Fig. 1). Hence, a rain gauge was installed for two summer periods to measure the precipitation (P) directly within the catchment aiming to characterise the flow dynamics and storage potential in the upper vadose zone.

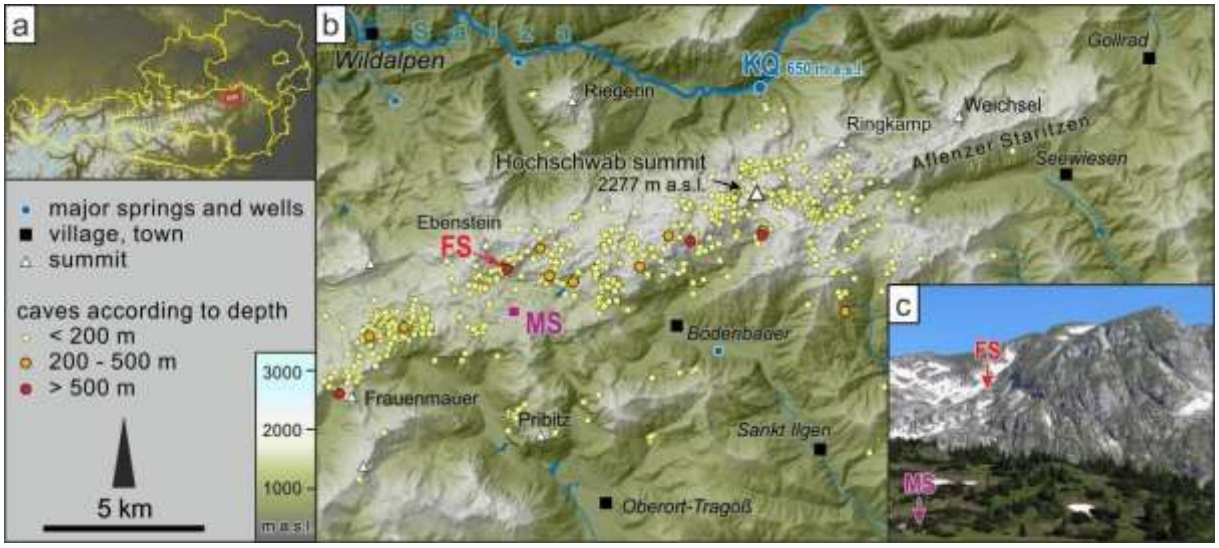

Figure 1 (a): Location of the Hochschwab massif within the Austrian eastern Alps.
(b): The central and eastern Hochschwab massif with its caves, the location of Furtowischacht (FS), the meteorological station at Sonnschienalm (MS), and Kläfferquellen (KQ; see KAMINSKY et al., 2021).

In this study, the established rainfall-runoff model KarstMod (MAZZILLI et al., 2019) was selected as different model setups can be tested with a resolution of one hour (this is a higher resolution than the daily GR4J+ Model used in KAMINSKY et al., 2021). It was used to simulate the discharge from two rain measurement stations to assess the dynamic of rainfall events on the stream within the cave. Further, the timespan of the reaction between a rain event and discharge maximum at the stream at 100 m below the surface was analysed.

2. Materials and methods

Water leaks from various parts of the cave, but a short horizontal canyon enabled the installation of a Thomson v-notch (weir) 100 m below the entrance of Furtowischacht in 2016 (PLAN & OBERENDER, 2018; Fig. 2). Since 16/12/2016 a SEBA PTEC logs the water level, water temperature, and electrical conductivity with a time interval of 10 minutes. Manual water level and discharge measurements at a large range of different flow events during field work enable the setup of a rating curve for discharge conversion (KAMINSKY et al., 2021).

Meteorological data with 10 minutes interval of air temperature [°C], precipitation (P-Sonn) [mm] and global radiation [Wm²] were provided by the MA 31 Vienna Water and measured at the meteorological station "Hochschwab Sonnschienalm" at 1524 m a.s.l.. The station is located 1.5 km south and 260 m below the entrance of the Furtowischacht (Fig. 1). Since the measurements are not made directly in the catchment area, uncertainties in the meteorological data must be considered. To estimate local differences of P, a rain logger "EML ARG 100 Aerodynamic Rain Gauge" with a 10-minute interval (P-Furt) was installed during snow free periods: from 04/08/2019 to 30/10/2019 (r2019) and 13/07/2020 to 09/10/2020 (r2020). The position of the rain gauge was 60 m north of the cave entrance where a direct connection to the stream has been verified by a tracing experiment. Due to the altitude difference between the cave entrance and the meteorological station at the Sonnschienalm, the air temperature was adjusted with -1.3 °C (KAMINSKY et al., 2021). Potential evapotranspiration (ETp) was computed hourly using a simplified approach from OUDIN et al. (2005) and is used in the rainfall-runoff model.

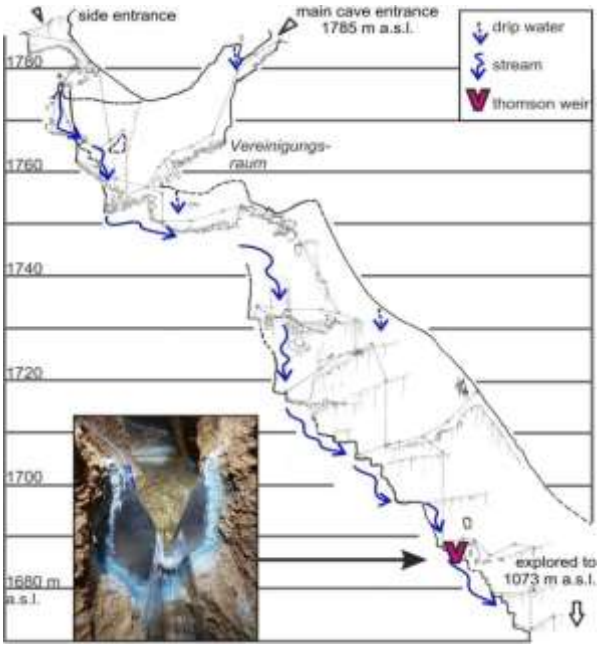

Figure 2: Profile view of Furtowischacht down to -120 m (modified after E. HERMANN 1996 – 2003; archive of the Speleologic Society of Vienna and Lower Austria); picture of the weir at -100 m (18/11/2019 14:00; 0.8 l/s; photo: Lukas PLAN).

KarstMod can be used as a physical based approach for rainfall-discharge simulations (MAZZILLI et al., 2019). Different model setups can be chosen, which simulate the runoff based on physical structures and formulars. It can reproduce the structure of most conceptual lumped models of the karst system and is commonly used (MAZZILLI et al., 2019). Its structure and graphical interface (Fig. 3) are defined on the conceptual model and outcomes from KAMINSKY et al. (2021) with an hourly time step. Input parameters (P, ET) are described above, and measured Q is used for the calibration and validation. The reservoir (E) represents the soil/epikarst, receives P as an input and ET is active as long as the reservoir is filled. The model distinguishes between diffuse (k_{EC}, k_{CS}) and quick (k_{hy}) flow. The diffuse flow percolated with the threshold (E_{min}) into the reservoir C. The quick flux is a hysteretic discharge law for a preferential flow path that is deactivated by the threshold (E_{hy}) and split (x) into direct simulated discharge and inflow into the reservoir C. The simulated Q (Qsim) is composed from the diffuse flow out of reservoir C (k_{CS}) and quick flow. By applying the model, time series r2019 and r2020 are combined into a continuous one, to use both within one model procedure (r2019 mainly for calibration and r2020 mainly for validation). Following periods are used: (1) warm-up, (2) calibration: 50 days, and (3) validation: 100 days. Calibration efficiency was tested by using the classical Nash-Sutcliffe efficiency (NSE Q, which weighs on high flows) or square-root-transformed NSE (NSE √Q, weighting on low flow simulations). A NSE of 100 % reflects a perfect match between the Q and Qsim. Sobol sequences or quasi-Monte Carlo simulations are used as calibration steps (10.000 steps with a NSE √Q > 0.6) and sensitivity analysis was carried out after the simulation. A further performance criterion is the water balance error (wb) where a value below 100 % means that the total Qsim is underestimated compared to the observed Q.

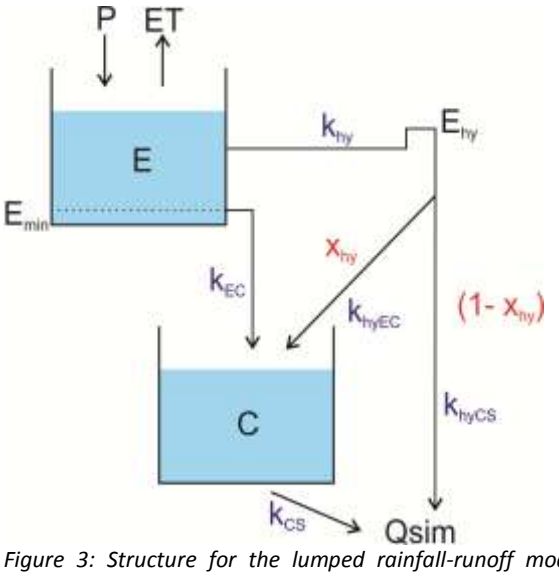

Figure 3: Structure for the lumped rainfall-runoff model (KarstMod, MAZZILLI et al., 2019).

3. Results

The measured P from both stations, discharge values from the cave stream, and simulated discharges are shown in Fig. 5. For both periods the sums of P are almost twice as high at Furtowischacht compared to Sonnschienalm (r2019: 605 vs. 300 mm, r2020: 1133 vs. 628 mm). The general dynamics are similar, but absolute values are very different; in particular, heavy rain events are much higher for P-Furt.

Simulations with the rainfall-runoff model are carried out hourly with a NSE √Q between both stations (Fig.4), whereby the calibrated catchment size is different. Different model setups are tested and neither a distinction in quick, intermediate, and baseflow, nor the variation of the free parameters improves the results. Therefore, only a fast and diffuse flow component, as in a dual-porosity model, was used. Further calibrations and validations of the model were tested with Q of NSE and √Q of NSE. Since √Q focuses more on low discharges, better results could be gained. A sensitivity analysis showed that the catchment size, k_{EC}, and E_{hy} are the most sensitive parameters. Only heavy P events with more than 4 mm/h at P-Sonn or 10 mm/h at P-Furt resulted in a discharge >1 l/s (Fig. 5). For both stations, a rise in Q was observed within a measuring interval of 10 minutes after intense rainfall event.

Value	P-Sonn	P-Furt
Catchment [m²]	2770	1090
Ehy [mm]	13	49
Emin [mm]	6	5
khy [mm/h]	0.21	0.15
kEC [mm/h]	0.001	0.001
kCS [mm/h]	0.031	0.045
x [%]	0.36	0.23
NSE Q [cal %]	64	58
NSE Q [val %]	56	35
NSE √Q [cal %]	81	78
NSE √Q [val %]	71	65
Water balance error √Q [val %]	99	99
Water balance error √Q [cal %]	99	86

Figure 4: Results of the parameters simulation with KarstMod.

4. Discussion

A highly dynamic water flow is represented with a small storage volume (6 and 5 mm) which can be interpreted as very thin or missing epikarst. This is in accordance with the results of an insignificant epikarst layer of Kaminsky et al., submitted. Although POULAIN et al. (2018) simulated with KarstMod threshold values of 2.3 and 5.8 mm for the soil-epikarst reservoir of a 20 to 30 m thick vadose zone in the Rochefort Cave in Belgium.

Already the difference between P-Sonn and P-Furt with a factor of 2 shows how local and variable P occurs. The

models estimated for both a smaller catchment than assumed with 4500 m² by KAMINSKY et al. (2021). The catchment size plays a major role for the water budget. Here these discrepancies can be explained by e.g., orographic effects or an outflow of the catchment during high flood events. Very high quick flow components are confirmed with both simulations (k_{hy}= 3.6 and 5.0 mm/d) and are in the same range as the α-value of 4 1/d from the hydrograph recession analysis of KAMINSKY et al. (2021). The general dynamic of the discharge at the weir can be simulated, but the maximum values of Q measured in the cave cannot be reached. As a result, both P measurements cannot be seen as fully representative for the actual catchment, although P-Sonn was found to be more suitable.

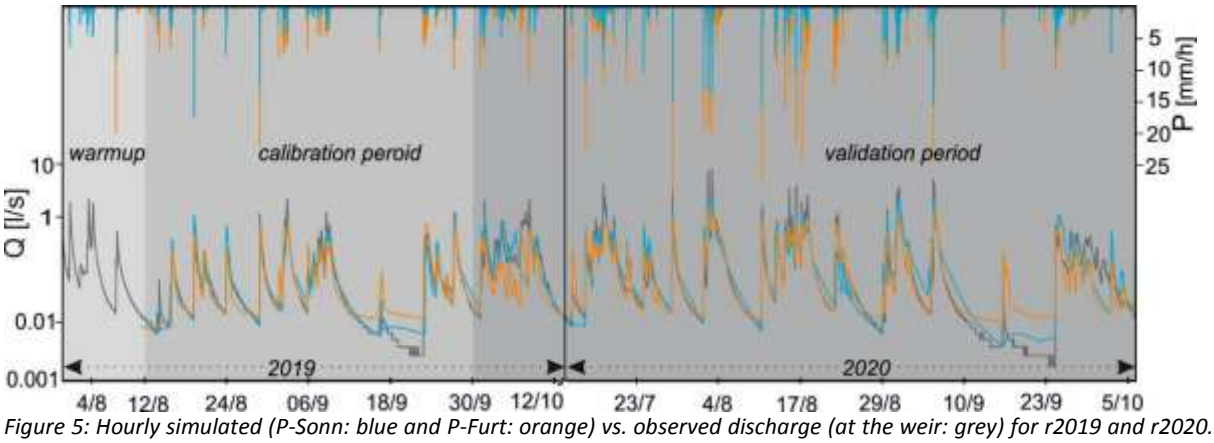

Figure 5: Hourly simulated (P-Sonn: blue and P-Furt: orange) vs. observed discharge (at the weir: grey) for r2019 and r2020. Warm-up, calibration, and validation period is marked in grey. Two rain measurements are shown (P-Sonn: blue and P-Furt: orange).

5. Conclusion

The aim of this investigation was to test whether a rain gauge directly at the cave entrance or the measurements of the distant meteorological can be used to simulate the flow dynamic in a vadose canyon system 100 m below the cave entrance. Both simulations give acceptable results concerning flow dynamics, however the catchment size differs due to significant differences in the amount of P at both measurement sites. It is shown that heavy P events with a minimum of 4 mm/h and maximum of 25 mm/h can increase the discharge at the weir so that it can be dangerous to climb in the shafts. A discharge decrease under the level of 0.1 l/s depends on the rain event but varies between 10 minutes and 11 hours. Nevertheless, previous discharge conditions must be considered.

Acknowledgments

We would like to thank Vienna Water (especially Christian Böck, Gerhard Kuschnig, and Christoph Riegler) and the Austria Research Promotion Agency (FFG) for their financial support. Thanks to our caving friends for the support of the fieldwork.

References

HARTMANN, A., GOLDSCHEIDER, N., WAGENER, T., LANGE, J., WEILER, M. (2014) Karst water resources in a changing world: Review of hydrological modeling approaches. Reviews of Geophysics, 52, 218–242.

MAZZILLI, N., GUINOT, V., JOURDE, H., LECOQ, N., LABAT, D., ARFIB, B., BAUDEMENT, C., DANQUIGNY, C., DAL SOGLIO, L., BERTIN, D. (2019). KarstMod: A modelling platform for rainfall - discharge analysis and modelling dedicated to karst systems. Environmental Modelling and Software, 122, 1–7.

OUDIN, L., HERVIEU, F., MICHEL, C., PERRIN, C., ANDREASSIAN, V., ANCTIL, F., LOUMAGNE, C. (2005). Which potential evapotranspiration input for a lumped rainfall-runoff model? Part 2 - Towards a simple and efficient potential evapotranspiration model for rainfall-runoff modelling. Journal of Hydrology, 303, 290–306.

KAMINSKY, E., PLAN, L., WAGNER, T., FUNK, B., OBERENDER, P. (2021). Flow dynamics in a vadose shaft – a case study from the Hochschwab karst massif (Northern Calcareous Alps, Austria). Int. Journal of Speleology.

POULAIN, A. WATLET, A., KAUFMANN, O., VAN CAMP, M., JOURDE, H., MAZZILLI, N., ROCHEZ, G., DELEU, R., QUINIF, Y., HALLET, V. (2018). Assessment of groundwater recharge through karst vadose zone by cave percolation monitoring. Hydrological Processes, 32, 2069-2083.

WAGNER, T., PAURITSCH, M., WINKLER, G. (2016). Impact of relict rock glaciers on spring and stream flow of alpine watersheds: Examples of the Niedere Tauern Range, Eastern Alps (Austria). Austrian Journal of Earth Sciences, 109/1, 84-98.

Inferring karst conduits organization from the use of hydraulic models; application to the Beuchire-Creugenat flow-system (JU, Switzerland)

Arnauld MALARD, Pierre-Yves JEANNIN

Swiss Institute for Speleology and Karst Studies, 2300 La Chaux-de-Fonds, www.isska.ch, arnauld.malard@isska.ch

Abstract

The Beuchire-Creugenat karst flow-system is one of the largest in the region of the tabular Jura. The catchment area extends over approx. 57 km^2. The Beuchire (423 m a.s.l.) is a perennial spring; its annual mean discharge is about 800 L/s and it may discharge up to 3.5 m^3/s. The Creugenat (451 m a.s.l.) is a temporary spring located 4.3 km upstream of the Beuchire. It may overflow more than 10 times per year and the recorded discharge may exceed 20 m^3/s. Hydraulic relations (comparison of hydraulic heads vs. discharge, discharge vs. discharge and hydraulic heads vs. hydraulic heads) in different points of the karst network have been analysed in order to understand mechanisms of flooding. Finally, a pipe-flow model of the main supposed conduits has been designed to reproduce the observed relations. Results of the calibration suggest that a large by-pass conduits (> 2 m in diameter) must exist in the epiphreatic zone between Creugenat and Beuchire springs at an elevation of 443 m. These results open new perspectives for speleological prospecting or for the prevention of flood risks.

1. Introduction

One of the main issues in karst hydrology deals with the development of conduits and the organization in flow networks. A few authors offer methods and tools for generating conduits networks: HENRION (2011), BORGHI (2013), etc., most of them being based on stochastic approaches and usually developed on a specific site and for specific issues. The main limitations of these tools concern the validation of the results as no direct or indirect investigations / measurements do really exist to attest the accuracy of the proposed methods.

The application of a karst-conduits generation model on the Beuchire-Creugenat karst system has been coupled to a hydraulic flow simulation model in order to test the consistency of the generated network (branching, elevation, conduits diameter, etc.). Indeed, flow and head measurements at permanent springs, within caves, drillholes, or at overflow outlets may bring a valuable information on the way the conduits are organized (Fig. 1). This information must be considered when looking for the organization of the conduits, ex: JEANNIN (2001).

In the following sections, the proposed model of the conduits network for a well-known site in the Jura Mountain has been tested with a hydraulic flow model. Objectives of the model are: (i) to validate the geometry and the organization of the supposed conduit network, (ii) to assess the evolution of the hydraulic gradient in the conduit-network along a flood event, and (iii) to assess respective discharge rates of permanent and overflow springs.

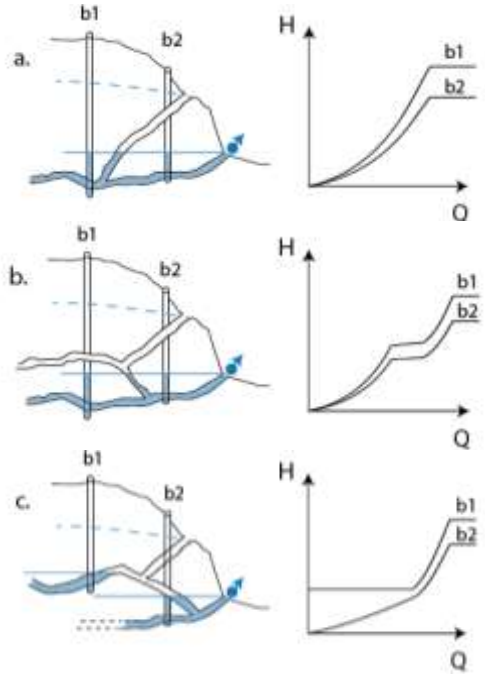

*Figure 1: Hydraulic functioning for high-flow conditions for three types of situations: **a.** Simple functioning, **b.** By-pass functioning, **c.** Threshold functioning. The type of the conduit network may thus be inferred from the relationship between hydraulic heads (H) measured at different locations of the karst system and the discharge rates (Q) measured at the spring. Such relations provide indications on the conduit organization and on the existence of several conduit levels (MALARD 2018).*

2. Test site and data

The Beuchire-Creugenat karst aquifer is located in north-western Switzerland and belongs to the tabular part of the Jura Mountains (Fig. 2). Geology and hydrogeological aspects of the site have been studied by SCHWEIZER (1970), MALARD et al. (2015), MALARD (2018). The site is mainly composed of low-elevated plateaus (~500 m a.s.l) formed by Jurassic limestone and crossed by numerous dendritic valleys.

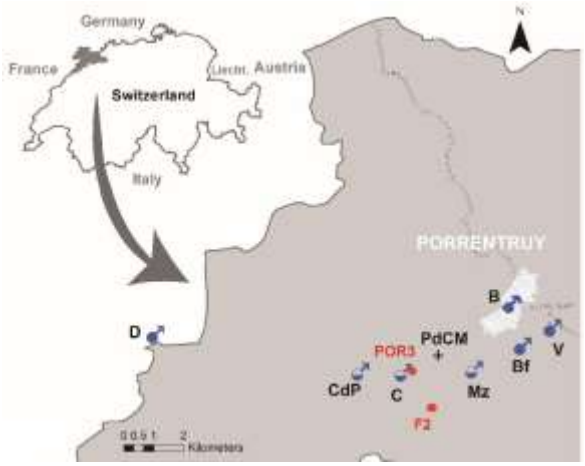

Figure 2 : Location of the studied area and of the main permanent / overflow springs (B: Beuchire, C: Creugenat, CdP: Creux-des-Prés). V, Bf, Mz and PdCM refer to other springs which are not considered here. POR3 and F2 are drillholes.

The main aquifer develops in the Jurassic limestone which is frequently interbedded by thin layers of marls. The basement of the aquifer is formed by the Astartes marls which thickness approaches 30 m. Beuchire (B) is the main permanent spring emerging in the city of Porrentruy (elevation 423 m a.s.l.). It is considered as the baseflow spring of the karst aquifer. Its annual mean discharge is about 800 L/s and it may discharge up to 3.5 m^3/s. The Creugenat overflow spring (C) lies upstream of the city (elevation 451 m a.s.l.) and activates only for high flows (13 times/year on average between 2002 and 2010). It usually discharges ~10 m^3/s, but it may exceed 30 m^3/s for an extreme event. Upstream from Creugenat, the Creux-des-Prés (CdP) is a second overflow spring located at 465 m a.s.l. This may discharge ~1-4 m^3/s every ~30 years on average.

Available measurements are: (i) discharge rates at the Beuchire spring (from 2002 to 2004 and 2009 to 2013), (ii) hydraulic heads in the entrance shaft of the Creugenat overflow spring (from 2001 to 2012) and in the POR3 borehole (from 2001 to 2004 and 2012).

Dimensions of the catchment area have been assessed by MALARD et al. (2015) by applying the KARSYS approach (JEANNIN et al. (2013)) see Fig. 3. The catchment extends over 57 km^2 (autogenic/allogenic parts, resp: 50.5 and 6.5 km^2).

Figure 3: Delineation of the catchment area for the Beuchire-Creugenat karst system. Orange areas refer to allogenic parts and "GW" to the extension of the phreatic zone.

The same authors also proposed a model for the karst conduit network based on the application of KARSYS for low flow conditions (i.e. "steady-state conditions"). This conduits network is displayed on Fig. 4.

(black lines refer to generated vadose conduits while red lines refer to generated phreatic conduits). The model assumes that a vertical vadose conduit does exist for each autogenic parcel of 0.25 km^2 (i.e., 500 x 500 m). Vadose vertically-controlled conduits (Vcc) extend vertically until they reach the top of the impervious units (i.e. the Astartes marls). Conduits then develop by following the topography of the aquifer basement until they penetrate the phreatic zone ("basement-controlled conduits", Bcc). In the phreatic zone, conduits develop according to the orientation of the hydraulic gradient. Starting from the downstream ends of vadose conduits (vertically- or basement-controlled), phreatic conduits organize along the "least hydraulic resistance" way toward the main permanent spring (Beuchire). In this zone, conduits may develop primarily along existing weaknesses (so-called "inception horizons") as faults or specific bedding planes.

Models of conduits network are difficult to validate as little data or information on the existing caves network do exist. The proposed model has been compared to existing dye-tracing tests and to the cave map of the Creugenat (C. MEYER, not published).

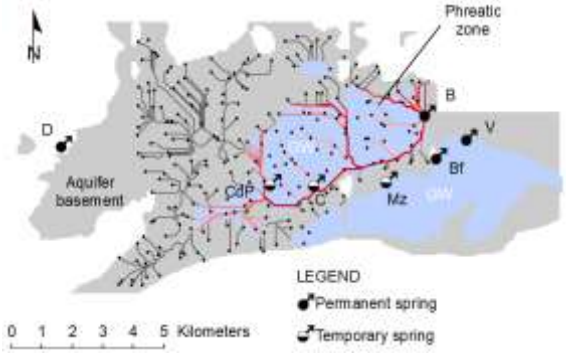

Figure 4: Generated conduits network for the Beuchire-Creugenat karst system.

3. Set up, calibration and simulations of the hydraulic flow model

The model of the conduit network has been transferred into a pipe-flow simulation software (SWMM© 5.0). SWMM is a dynamic rainfall-runoff simulation model used for single event or long-term (continuous) simulation of runoff, drainage and sewers water quantity and quality. Applications of SWMM to reproduce karst hydraulic processes have been already tested in JEANNIN et al. (2015). The conduit network has been adapted according to changes observed for high-flow conditions in the hydraulic relationship between Beuchire and Creugenat (see Fig. 5) with regards to situations depicted in Fig. 1. It has been finally simplified in order to optimize computation time. The final model is displayed in Fig. 6.

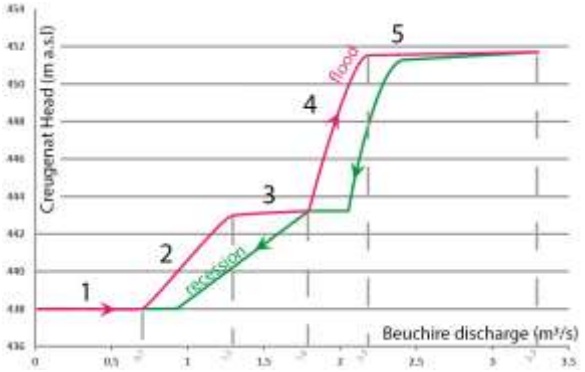

Figure 5: 1) As long as the Beuchire spring discharge rate remains lower than 700 L/s, the water level at Creugenat does not react (~438 m a.s.l): both emergences are disconnected by a threshold. 2) As the Beuchire discharge rate exceeds 700 L/s the hydraulic head in Creugenat progressively rises up until reaching a threshold at 443 m a.s.l. This threshold may correspond to a by-pass conduit diverting the flow to the Beuchire spring, 3) as the discharge rate of the Beuchire spring increases from 1'300 L/s to 1'800 L/s the water level in Creugenat does not change (~443 m). 4) As the discharge rate exceeds 1'800 L/s the water level in Creugenat rises up again until reaching the outlet elevation at 451 m a.s.l. 5) As the discharge rate exceeds 2'200 L/s, the Creugenat spring starts overflowing.

Conduits diameters linearly increases from the upstream part of the network (1 m) to the downstream sections (4 m max. according to the observations in the Creugenat and the Creux-des-Près caves. Observed changes in heads and discharge rates suggest modifying or adding hydraulic features to the conduit network:

- A threshold has been positioned at an elevation of 438 m a.s.l., which disconnects the Creugenat from the Beuchire stream at low flow. This threshold becomes flooded once the Beuchire discharges 0.7 m^3/s.
- The narrow conduits linking the Creugenat to the POR3 borehole does not exceed 0.8 m in diameter.
- A perched by-pass conduit between the Creugenat and the Beuchire springs has been implemented in the epiphreatic zone to explain the observed plateau at 443 m a.s.l. The diameter of the conduit is ~1.3 m.

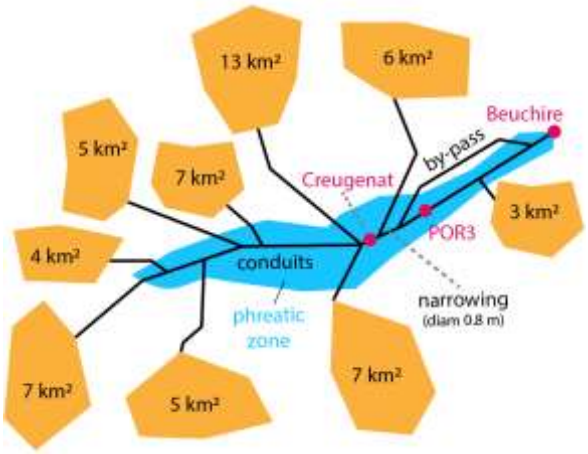

Figure 6: Simplified hydraulic model of the Beuchire-Creugenat. The catchment area has been divided into 9 sub-catchments that correspond to the main expected conduit inputs.

A groundwater recharge model (KRM_1) has been applied on the catchment area for the year 2004 in order to assess the flow rate of the whole system (i.e., Beuchire + Creugenat) at hourly time-step. The workflow is not discussed here but details can be consulted in MALARD (2018). The simulated recharge has been used as input over the 9 sub-catchments. The hydraulic model has been run over the years 2002-2004 at hourly time step.

4. Results

Results of hydraulic simulations for the year 2004 are presented in Figs. 7 and 8.

Simulations well reproduce the observed stages (1 to 5, Fig. 5). These confirm the existence / role of the threshold at 438 m, the narrowing and the by-pass conduits at 443 m in the hydraulic functioning for high-flow conditions. Finally, hydraulic heads and discharge rate fluctuations for Beuchire, Creugenat and POR3 can be simulated for the whole year 2004 and compared to measurements (Fig. 8).

Even if misfits may be observed, especially for low-flow conditions (recession), simulations are quite close to the measurements. As the focus was put on flooding processes, less attention has been paid to low-flow processes (i.e., storage, release from the Low Permeability Volumes, epikarst, etc.). It should be mentioned that misfits may result from the meteorological measurements, from uncertainties of the KRM_1 recharge model and of course from the SWMM hydraulic model.

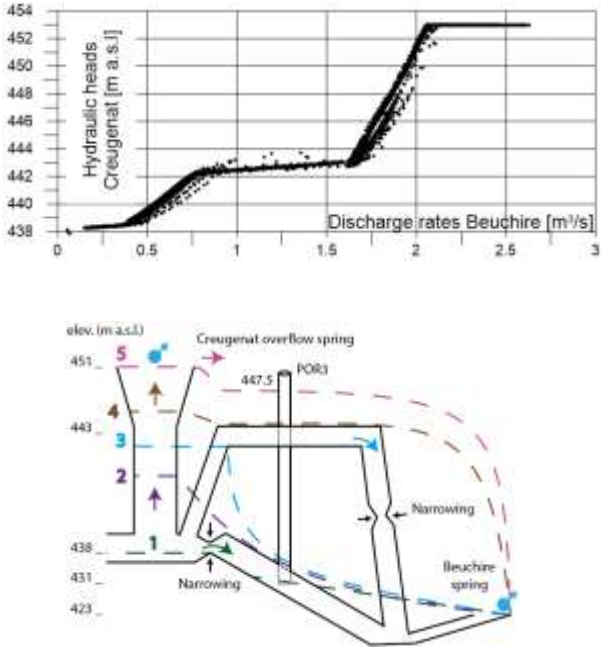

Figure 7: Simulated hydraulic relations using SWMM© and interpreted functioning on a hydraulic profile.

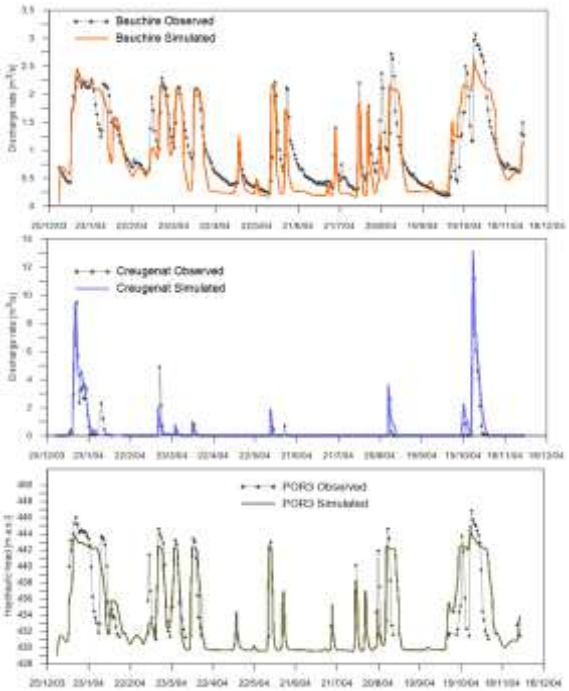

Figure 8: Results of the hydraulic simulation models for the different stations over the year 2004 (daily time-step)

.

5. Discussion / conclusion

This work shows that hydraulic "obstacles" like thresholds, narrow passages and by-passes might be identified from the hydraulic relations between the different measurement points in the conduit network and at the different permanent / overflow springs. These obstacles may be implemented in a simple hydraulic model (pipe-flow) in order to infer interesting information on the organization of the conduit network, especially in the phreatic and epiphreatic zone. Main difficulties always are: (i) this requires heads and discharge data at different locations of the conduit network (even a short measurement period may be enough), (ii) to find a method to validate the expected organization / geometry of the conduit network. The use of a recharge model is a plus, but other datasets can be used as input, the aim being to reproduce hydraulic relations which do not depend on climatic conditions but on the conduit network itself. In the vadose zone, conduit hydraulics play a weaker role and less information can be inferred. This is the reason why conduits can be oversimplified in the vadose zone. As observed in the results, low-flow processes are not well reproduced (storage and release from the epikarst or from the Low Permeability Volume). These do not strictly depend on the hydraulics but mainly on the recharge processes and the use of SWMM in such case may not be very useful.

References

BORGHI A. (2013) 3D stochastic modeling of karst aquifers using a pseudo-genetic methodology. CHYN, UNINE, PhD dissertation. 207 p.

HENRION V. (2011) Approche pseudo-génétique pour la simulation stochastique de la géométrie 3D de réseaux fracturés et karstiques. Institut National Polytechnique de Lorraine (Nancy-Université), PhD dissertation. 160 p.

JEANNIN P.Y. (2001) Modeling flow in phreatic and epiphreatic karst conduits in the Hoelloch cave (Muotatal, Switzerland). Water Resources Research, 37(2): 191-200 p.

JEANNIN P.Y, EICHENBERGER U., SINREICH M., VOUILLAMOZ J., MALARD A. et al. (2013) KARSYS: a pragmatic approach to karst hydrogeological system conceptualization. Assessment of groundwater reserves and resources in Switzerland. Environmental Earth Sciences, 69(3): 999-1013 p.

JEANNIN P.Y., MALARD A., RICKERL D., WEBER E. (2015) Assessing karst-hydraulic hazards in tunneling - the Brunnmühle spring system - Bernese Jura, Switzerland. Environmental Earth Sciences, 74(12): 7655-7670 p.

MALARD A. (2018) Hydrogeological characterization of karst aquifers in Switzerland using a pragmatic approach. CHYN, UNINE, PhD dissertation. 253 p.

MALARD A., JEANNIN P.Y., VOUILLAMOZ J., WEBER E. (2015) An integrated approach for catchment delineation and conduit-network modeling in karst aquifers: application to a site in the Swiss tabular Jura. Hydrogeology Journal, 23(7): 1341-1357 p.

SCHWEIZER H.U. (1970) Beiträge zur Hydrologie der Ajoie (Berner Jura). Beiträge zur Geologie der Schweiz 17: 223 p

Variation de la température de la rivière souterraine de Cauvel (Gard) : comment en tirer des enseignements sur le fonctionnement de ce karst ?

Philippe MARTIN

Université d'Avignon, UMR ESPACE, 74 rue L. Pasteur, 84000 Avignon, France, philippe.martin@univ-avignon.fr

Résumé

En Basse Cévenne Carbonatée, un réseau de mesure hydrologique est installé depuis 2011. Celui-ci permet de mieux caractériser le fonctionnement d'un karst barré qui est drainé par la rivière souterraine pérenne de Cauvel. Les sondes installées produisent des mesures thermiques. Une question est donc de savoir comment traiter ces données et quels enseignements nous pouvons en retirer ? Ces chroniques à haute résolution sont structurellement semblables à toutes les séries affines. Les nombreuses phases de variation de la température, à l'issue d'une crue, pourraient être décrites avec des modèles empiriques, comme avec des débits. Toutefois, ces fonctionnements répétitifs font apparaître deux situations thermiques particulières : -1- un apport de chaleur à l'eau de l'aquifère lors des premières pluies de fin d'été ou d'automne et -2- une chute de température lors des pluies plus froides d'hiver. Nous proposons quelques réflexions sur ces variations. De même, des boucles d'hystérésis, morphologiquement semblables, de variation de la température, mais décalées thermiquement (crue après crue), sont identifiables. Elles semblent constituer un invariant de ce karst traduisant une grande stabilité structurelle de son fonctionnement. Il est donc possible, au moins conceptuellement, d'envisager un processus inverse, une remontée de ces conséquences thermiques à leurs causes hydrologiques et morphologiques.

Abstract

Variation of the temperature of the underground river of Cauvel (Gard): how to draw lessons on the functioning of this karst? A hydrological measurement network has been installed in the Lower Carbonated Cévennes since 2011. It allows to better characterising the functioning of a barred karst which is drained by the perennial underground river of Cauvel. The installed sensors produce thermic measurements. One question is how to process these data and what lessons can we learn from them? These high resolution chronicles are structurally similar to all the affine series. The numerous phases of temperature variation, after a flood, could be described with empirical models, as for the flow. However, these repetitive processes reveal two thermal situations: -1- a supply of heat to the aquifer water during the first rains at the end of summer or autumn and -2- a drop in temperature during the colder winter rains. We propose a statistical method to study these variations. Similarly, morphologically similar hysteresis loops of temperature variation, but thermally shifted (flood after flood), can be identified. They seem to be an invariant of this karst, reflecting the great structural stability of its functioning. It is therefore possible, at least conceptually, to envisage an inverse process, a rise from these thermal consequences to their hydrological and morphological causes.

1. Introduction

Les bassins versants des rivières cévenoles (Ardèche, Cèze et Gardon), appuyés sur le rebord sud-est du Massif central, sont connus par leurs rivières qui recoupent, en gorges, de vastes plateaux urgoniens (des Garrigues, des Gras…). Sur le piémont des Cévennes, les termes inférieurs de la série secondaire recouvrent la surface d'aplanissement anté triasique – dont des formations carbonées primaires – et forment de petits karsts (Basse Cévenne Carbonatée - BCC) marqués par des pendages assez forts, une fracturation notable et des minéralisations souvent non négligeables. En raison de ces conditions géologiques particulières, mais aussi de l'importance des précipitations alimentant ces systèmes karstiques aux amonts souvent non karstifiables (socle), le cavernement y est très développé. Dans le Gardon, au droit de la ville d'Alès s'est développé ainsi un petit karst barré (par des formations marneuses valanginiennes) drainé pour partie vers le Grabieux (source des Fonts, affluent du Gardon d'Alès), vers l'Auzonnet (source des Peyrouses, affluent de la Cèze) et qui recoupe le bassin versant topographique de l'Avène (affluent du Gardon d'Alès). Les explorations spéléologiques conduites depuis plusieurs dizaines d'années (MARTIN, 1980, 1981, 1982, 1983.a et b, 1986, 1988, 1993.a, b et c, MARTIN et *al.*, 2017) y ont mis en évidence des cavités importantes comportant des zones noyées parfois très profondes (Boulidou Franco ≈ 50 m sous le niveau d'étiage, ≈ 25m sous la surface) et une circulation pérenne (rivière de Cauvel ≈ 10 l/s à l'étiage, mais où s'observent des mises en charge

majeures). Ce karst s'est donc établi sur un temps long en particulier en raison d'une fracturation majeure et de formations minérales particulières (pyrite, galène…) anciennement exploitées. Ces aspects ne seront pas abordés ici au-delà d'un cadrage général. Les observations réalisées montrent un fonctionnement dual avec un écoulement permanent vraisemblablement lié aux dolomies hettangiennes sises à l'amont et portées, par la tectonique, en position haute, et des mises en charge majeures pouvant atteindre une trentaine de mètres, lors d'épisodes cévenols (Fig. 1).

En raison d'une situation de tension, certains étés, sur la ressource en eau dans le bassin de l'Avène et dans l'agglomération d'Alès, l'aspect capacitif de ce petit karst doit être exploré. De même, son rôle lors des épisodes cévenols doit être mieux compris. La diffluence karstique (Gardon *vs* Cèze) sur les flux drainés doit aussi être précisée. Les stockages temporaires lors des crues doivent être évalués. On peut ainsi espérer identifier un apport complémentaire pour l'AEP, quitte à sur-pomper l'aquifère en période de tension estivale. On peut aussi attendre un écrêtement et un amortissement des crues lors du remplissage de ce karst, et cela d'autant plus que le niveau piézométrique aurait été fortement déprimé. Une telle utilisation de cet hydrosystème pourrait contribuer à protéger des inondations récurrentes la plaine de Saint-Julien-les-Rosiers qui constitue un des espaces d'expansion assez aisée de la ville d'Alès.

Dans la perspective de tester ces hypothèses, ce karst a été progressivement équipé, à partir de 2011, de stations piézométriques (sondes à deux : hauteur d'eau et température, ou à trois voies : h, t et conductivité) endo karstiques (Roberts, Fiagoux, Courlas, Franco), de trois stations sur des sources (Carabiole, Rascasse et Peyrouses) et de quatre stations limnigraphiques (Avène amont, médiane et aval, et ruisseau de Gravelongue), stations qui pourraient être complétées par une station sur le Grabieux aval (en amont de la confluence avec le Gardon). Les entrées sont enregistrées par un pluviographe et un thermomètre situés au mas des Mathieux. Les mesures ont été faites à haute résolution (30 min ou moins) même si elle a pu varier entre 2011 et 2020. Ces données hydrologiques restent à analyser, mais il apparaît déjà que les signaux thermiques, systématiquement acquis avec les sondes de pression, se révèlent très riches. Cette information complète donc celle basée sur les hauteurs d'eau, ou les débits, voire les mesures de conductivité, mais à condition de déployer une méthodologie *ad hoc*.

2. Fonctionnements thermiques de début de cycle

Les moyens de mesurer la température de l'eau des rivières souterraines, avec une bonne précision et à haute résolution, se multiplient. Cette mesure peut être faite aujourd'hui à des prix abordables ou quasiment nuls quand la mesure est conjointe à une mesure de hauteur d'eau.

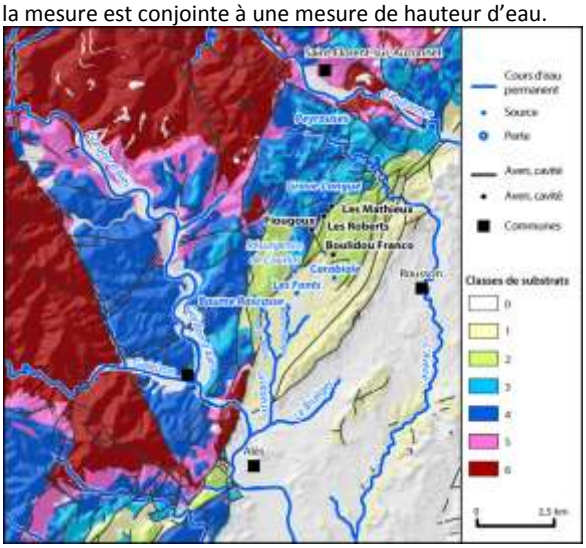

Figure 1 : Carte lithostratigraphique de la BCC : 0 - Quaternaire (alluvion et dépôt anthropique) 1 – Jurassique sup. & Crétacé inf. (niveau imperméable) 2 – Jurassique sup. (calcaire) 3 – Jurassique moyen (calcaréo gréseux & calcaire) 4 – Jurassique inf. (calcaire & dolomie) 5 – Trias 6 – Houiller & roche métamorphique.

Ces données sont rarement exploitées ce qui est à la fois regrettable, car elles sont acquises après bien des efforts et fort dommageable, car il y a là des enseignements à tirer. Dans les travaux présentés ici, nous nous sommes attaché à analyser certains éléments des signaux thermiques enregistrés. Ceux-ci font apparaître des réponses lors d'épisodes pluvieux tout à fait remarquables (Fig. 2, 3, 4). Globalement la température baisse lors des crues (Fig. 5), puis remonte selon une loi de relaxation. Dans le détail, les fonctionnements sont plus compliqués. À l'automne 2014, on a observé trois crues majeures de durée différente, mais avec des hauteurs d'eau semblables (25 – 30 m) dans le Franco (Fig. 2) qui est un conduit de type vauclusien, rarement émissif. La réponse thermique est différente entre la crue de septembre et celle d'octobre (Fig.3). En septembre, les deux crues portent la température de ≈ 14°C à ≈ 18 °C. Ce phénomène ne se reproduit pas en octobre. L'hypothèse la plus vraisemblable est que l'eau de pluie, pas nécessairement froide, lessive les calories emmagasinées dans l'épikarst pendant l'été. Des crues thermiques complexes apparaissent si on zoome sur les signatures thermiques de septembre (Fig. 4).

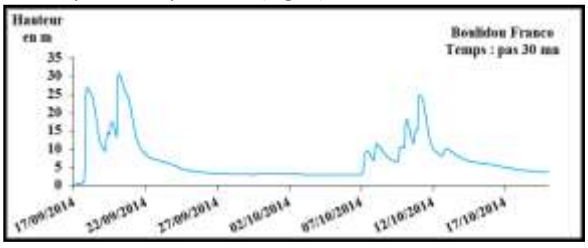

Figure 2 : Variation de la hauteur d'eau dans le Franco lors de deux crues successives (sept et oct.)

À la suite d'un pic se produit une fluctuation de plus faible ampleur. La répétitivité et la stabilité de la forme de ce signal soulèvent des questions. Le pic pourrait être lié à un réchauffement rapide et local, la fluctuation qui suit pouvant être déterminée par un réchauffement plus général, mais plus limité de la masse d'eau. Il pourrait donc

exister deux modes de circulation déphasés de ces flux thermiques, l'un rapide et local, l'autre plus lent.

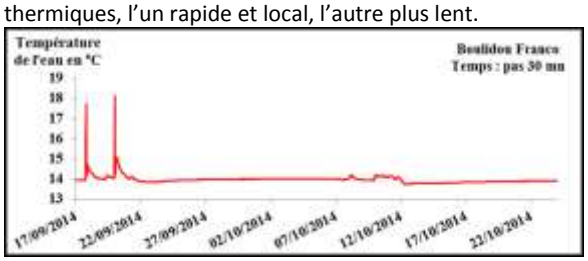

Figure 3 : Variation de la température de l'eau dans le Franco lors de deux crues successives (sept et oct.)

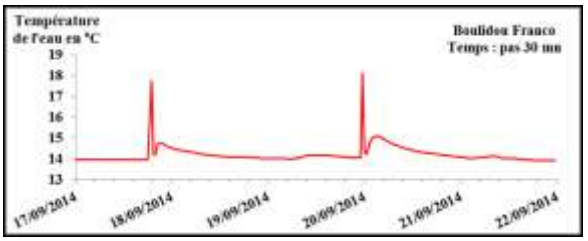

Figure 4 : Variation de la température de l'eau dans le Franco lors de deux crues successives (18 et 20 sept)

3. Fluctuations conjointes des niveaux d'eau et de la température lors de cycles

Cette fluctuation conjointe des hauteurs d'eau (en m) et de la température (en °C) se retrouve systématiquement lors des cycles : 2011-12, 2012-13 et 2013-14 (Fig. 5), pris pour exemple. Les températures ont alors varié (avec un pas de 30 min) entre 12,7 et 14,3 °C dans la rivière de Cauvel.

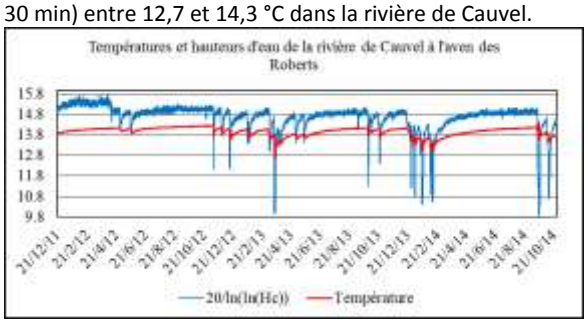

Figure 5 : Co-variation de la température et des hauteurs d'eau dans la rivière de Cauvel ; indices : voir texte

Pour faciliter la comparaison des deux informations (superposition), une anamorphose [20/ln(ln(H))] a été appliquée aux hauteurs d'eau qui sont bruitées, contrairement aux températures. Les mises en charge peuvent atteindre, voire dépasser, 20 m aux Roberts.

Lors d'une crue, on observe une chute rapide de la température, qui peut s'expliquer par des circulations rapides dans de gros drains en partie spéléologiquement connus, qui est suivie par une remontée lente qui peut traduire l'effet d'un transit lent et de plus en plus lent, après la décrue, lors de phases de tarissement, de l'eau. Il s'agirait là de phases de relaxations thermiques du système karstique qui retrouverait progressivement sa température maximale limite, un état donc stationnaire après une perturbation.

4. Boucles successives d'hystérésis

Le graphique n°6 croise la hauteur d'eau en fonction de la température, après que la hauteur d'eau ait été mise sous la forme d'un double logarithme inversé (20 est une constante de calage). Il apparaît alors clairement trois situations génériques. D'une part, une relation linéarisée (Ellipse verte) qui traduit une augmentation tendancielle de la température de l'eau, de 13 °C environ à 15 °C environ lorsque les hauteurs d'eau sont très faibles (situation de bas débits, d'étiage). Il y a toutefois un ensemble de points (Ellipse noire) qui correspond à des températures de 13,9 °C à 14,2 °C qui ne s'intègrent pas, ou mal, dans la relation principale. Il semblerait donc que sous certaines conditions de vidange (très bas débits), il y ait des eaux plus chaudes (certes de peu) qui soient mobilisées, donc des eaux venant probablement des parties les plus internes de la matrice du karst, possiblement hettangiennes (?).

Cela étant, ce qui structure le graphique dans son extension ce sont de très belles boucles. À cette fin, nous en avons isolé deux (Fig.7) : l'une du 03/01/2014 à 14 h 30 au 13/01/2014 à 6 h 30 (point A – B – C) et l'autre du 13/01/2014 à 8 h 30 au 01/02/2014 à 20 h 30 (points D – E – F). Ces boucles d'hystérésis s'enchaînent donc dans le temps en fonction des crues et des décrues. La seconde boucle fait apparaître une température minimale inférieure (13,27 °C pour 13,09 °C).

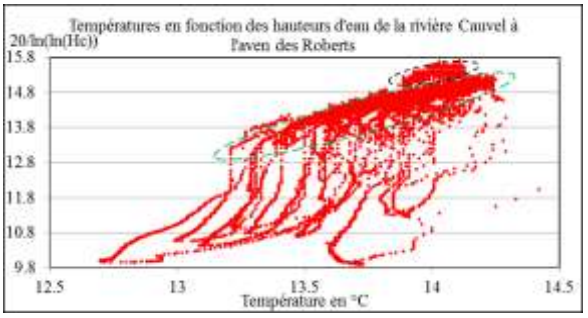

Figure 6 : Relations entre les hauteurs d'eau et la température dans la rivière de Cauvel à l'aven des Roberts

On voit aussi que, tant les phases initiales de variation de débit, que les phases presque finales (avant l'évolution très graduelle) s'accompagnent d'une variation du débit sans que la température ne fluctue (alignements verticaux des points). De même, les périodes de décroissance du débit qui conduisent au minimum de température, sont de même forme. Il en est ensuite de même pour les remontées qui apparaissent toutefois beaucoup plus linéaires. La figure 7 montre en outre que les phases finales des boucles correspondent à une remontée très graduelle de la température, ce qui correspond à l'ellipse verte de la

figure 6. De même on constate qu'une partie non linéaire, en forme de corne correspondant pour la courbe « droite » du cône à une diminution de la température et une augmentation de la hauteur d'eau, et pour la partie « gauche » à une augmentation de la température et une diminution de la hauteur d'eau. La multiplicité des boucles enregistrées montre que l'on doit pouvoir arriver à une description analytique très fine des phases hydrologiques en fonction des moments du cycle.
Ces boucles d'hystérésis traduisent donc des conditions changeantes dans les modalités de mélange d'eaux issues des précipitations et de la matrice du karst, très vraisemblablement des dolomies hettangiennes.

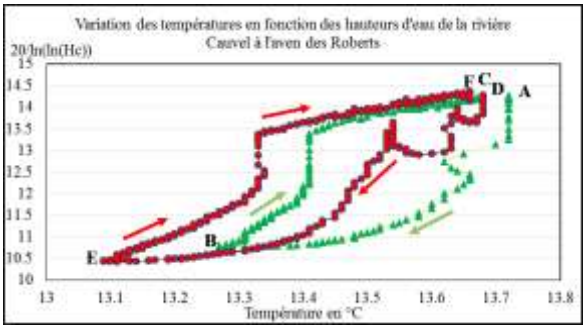

Figure 7 : Exemples de boucles d'hystérésis dans la rivière de Cauvel à l'aven des Roberts

5. Conclusions

Cette première analyse des données thermiques du karst barré de Saint-Julien-les-Rosiers (BCC) fait apparaître une relation complexe entre les débits (ou les variations de hauteurs d'eau) et les températures qui est probablement contrôlée par : -1- la chaleur emmagasinée dans l'épikarst en été, -2- par le niveau de cavernement en particulier dans les faciès du Jurassique supérieur, mais pas seulement, -3- par l'apport de l'aquifère dolomitique hettangien, et -4- par un flux géothermique pérenne, difficile à préciser, mais connu des mineurs de charbon.

Nous sommes donc face à un karst polyphasé au fonctionnement complexe, bien que de petite extension. Un tel cavernement même en prenant en compte les minéralisations de pyrite et de galène, est surprenant. Ces premières analyses montrent que nous aurons besoin de toutes les informations disponibles, y compris donc thermiques, pour rendre compte de ce beau potentiel hydrologique.

Remerciements

Mes remerciements au Spéléo Club Lasallien (SCL) et plus largement aux spéléologues d'Alès et du Gard pour l'aide apportée pour l'installation et la gestion de ce réseau. Certaines sondes ayant même dû être relevées par des plongeurs…

Références spéléologiques

MARTIN Ph. (1980) Étude d'un karst barré de la couverture sédimentaire sous cévenique en pays alesan, *Bulletin du CDS du Gard*, n° 21, p. 79-85.

MARTIN Ph. (1981) Réseau des Fonts, aven du Fiagoux, résurgence de Courlas, *Bulletin du CDS Gard*, n° 22, p. 134-138.

MARTIN Ph. (1982) Pompage du 15 août 1980 à la Baume Rascasse, *Bulletin du CDS du Gard*, n° 23, p. 98-102.

MARTIN Ph. (1983.a) Contribution à l'étude d'un karst barré en pays alesan, Inventaire des cavités, sources et pertes du pays jurassique d'Ales à l'Avène, *Bulletin du SCL* n° 11-12, p. 31-90.

MARTIN Ph. (1983.b) *La basse Cévenne calcaire, Étude géomorphologique*, Mémoire de Maîtrise de Géographie, U. Montpellier, 135 p.

MARTIN Ph. (1986) L'aven des Roberts (Gard), *Bulletin du SCL*, n° 13, p. 83-87.

MARTIN Ph. (1988) Le karst du compartiment oriental de la Basse Cévenne carbonatée (Gard), *Karstologia*, n° 11-12, p. 25-36.

MARTIN Ph. (1993.a) Importance des réserves en eau sous la plaine de St-Julien-les-Rosiers (Gard) révélées par explorations en scaphandre autonome, *Spelunca*, n° 49, p. 33-38.

MARTIN Ph. (1993.b) Étude du karst des Cévennes gardoises : Les pertes de Gravelongue. *Baumes et Abîmes : bulletin du SCL*, n° 14, 2e édition, p. 13.

MARTIN Ph. (1993.c) Étude du karst des Cévennes gardoises : Compte rendu du pompage de la source de Carabiole (Gard, France). *Baumes et Abîmes : bulletin du SCL*, n° 14, 2e édition, p. 14-19.

MARTIN Ph. et DOMERGUE J.-M. (2017) Variation de la température mesurée à haute résolution et fonctionnements karstiques. Workshop AFK, AFS, IM2E, Terinov, Total et IMT Mines Alès organisateurs, *Livre des résumés*, p. 53.

MARTIN Ph., AYRAL P.-A., DIDON-LESCOT J.-F., DOMERGUE J.-M. et GRARD N. (2017) Suivi à hautes résolutions spatiale et temporelle du système karstique des Fonts (Gard, France), Collection Edytem, n° 19, *Monitoring en milieux naturels*, p. 169-176.

The hydrology of Riesending cave in Untersberg

Ulrich MEYER(1), Georg ZAGLER(2) & Giorgio HÖFER-ÖLLINGER(3)

(1) Schlossmatte 17, 3110 Münsingen, Switzerland, ulrich.meyer@aiub.unibe.ch (corresponding author)
(2) König-Ludwig-Str. 20, 5020 Salzburg, Austria, gzagler@yahoo.de
(3) Geoconsult ZT GmbH, Hölzlstr. 5, 5071 Wals bei Salzburg, Austria, giorgio.hoefer-oellinger@geoconsult.eu

Abstract

Untersberg mountain in the Northern Calcareous Alps near the cities of Berchtesgaden and Salzburg is an isolated monadnock with a limestone plateau of 15 km^2. The whole plateau drains to the single huge karst spring of Fürstenbrunn with a mean flow of about 750 L/s and peak flow of more than 30 m^3/s. While response to precipitation is very fast, the hydraulic retention time reaches 157 days for the more remote parts of the plateau, which was also confirmed by Isotope analyses. Several caves provide access to the karst water table within the mountain, the furthest of which is Riesending, at almost 3 km distance from the resurgence, where the final sump is reached at 1149 m depth. Water levels, temperature and flow were measured at several locations in Riesending, in Kolowrathöhle and in the resurgence cave for several years. The observations indicate a continuous karst water body with a volume of approx. 10^7 m^3 connecting all three caves.

Résumé

Hydrologie de la grotte du Riesending à Untersberg. L'Untersberg, situé à proximité des villes de Berchtesgaden et Salzburg, est une montagne calcaire isolée avec une surface de 15 km^2. Tout le plateau est drainé par la source de Fürstenbrunn, avec un débit de 750 L/s en moyenne et un de plus de 30 m^3/s en crue. Bien que la réponse aux précipitations soit rapide, le temps de résidence monte à 157 jours pour les parties éloignées, cela est confirmé par des analyses isotopiques. Plusieurs grottes atteignent l'aquifère, dont le Riesending situé à 3 km de la source. Là, le siphon final se trouve à une profondeur de 1149 m. Le niveau d'eau, la température et le débit ont été mesurés à plusieurs endroits dans le Riesending, la Kolowrathöhle et dans la source durant plusieurs années. Les observations nous indiquent une nappe contiguë avec un volume d'approximativement 10^7 m^3 connecté à toutes les cavités.

1. Introduction

Riesending Cave is located on Untersberg, an isolated mountain to the southwest of Salzburg, which belongs to the Northern Calcerous Alps. The main characteristic of Untersberg is its large karst plateau at altitudes between 1500 m and 1900 m, which in general slightly dips to the South-West. The plateau culminates in peaks of little prominence along its Eastern border, the highest of which is Berchtesgadener Hochthorn (1975 m). Towards the valley of Berchtesgadener Ache in the East these peaks tower with impressive 300 m high limestone cliffs above steep dolomitic slopes. The geologic layers gently dip to the North-West. While the top limestone layer reaches down to the foot of Untersberg along its Northern slopes, the underlying dolomite is exposed along the South-Western edge of the plateau at the alpine pasture of Zehnkaser.

The limestone plateau is intensely karstified, while the dolomite flanks are drained by surface streams, which have excavated steep trenches. The main resurgence of the water sinking on the plateau is located at the Northern slope of Untersberg near the village of Fürstenbrunn. The water surfaces about 150 m above the gravel plain through Fürstenbrunner Quellhöhle (1339/10) at an altitude of 600 m. While the mean flow of the resurgence is about 750 L/s, the peak flow can reach more than 30 m^3/s (HÖFER-ÖLLINGER et al., 2016). Dye tracing confirmed the dominant role of Fürstenbrunner Quelle (Fig. 1). The retention time reaches 157 days for the westernmost infeed point (HASEKE-KNAPZYK, 1989). Recent explorations in Kolowrat Cave (1339/1) and Riesending (1339/336) indicate a continuous karst water body within Untersberg.

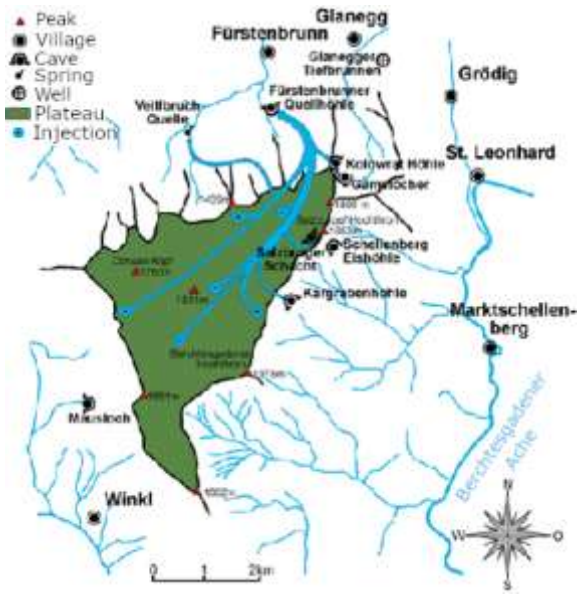

Figure 1: Dye tracing at Untersberg.

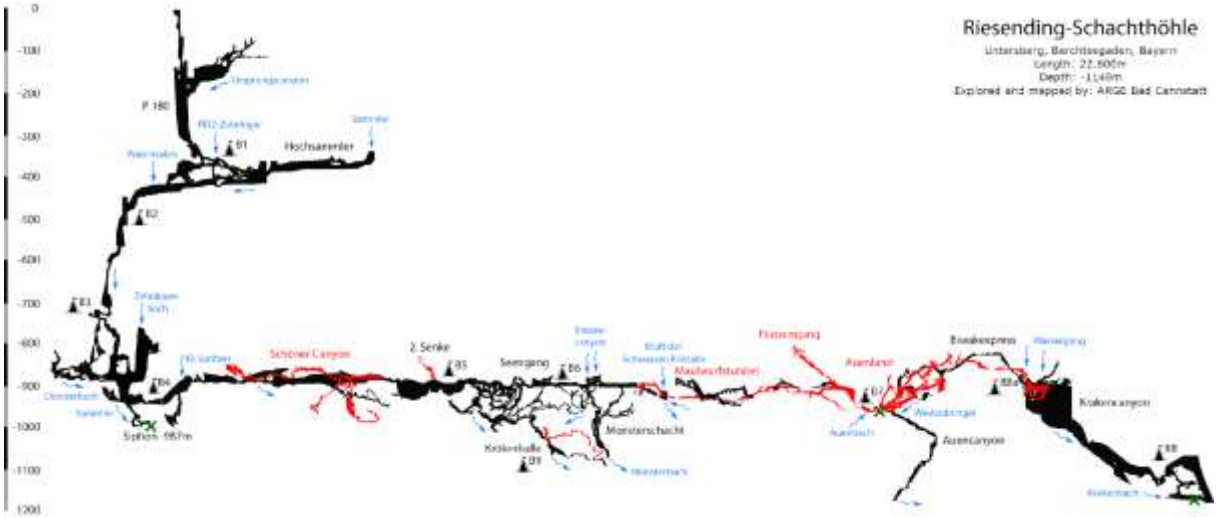

Figure 2: Vertical section of Riesending, with major waterways (blue) and the location of water pressure gauges (green).

2. Materials and methods

Within recent years, cavers from Salzburg found large extensions to Kolowrat Cave, where three active streams were explored down to large sumps, all at comparable altitude. At the same time, Riesending (Fig. 2) was explored by cavers from Bad Cannstatt (MEYER, 2022). In 2006, a first sump was found at the depth of -987 m, in 2013 a new deep point was reached in the stream of *Krakencanyon* (-1148 m), which in 2016 was confirmed to terminate at a sump just 1 m below (MEYER et al., 2017). Just one year later a sump at the same depth was reached at the end of *Auencanyon*.

With so many new windows to the karst water body and with the availability of cave-proof pressure gauges from the Swiss engineer Felix Ziegler, the idea of a karst water monitoring programme was born. First pressure gauges were positioned in 2009 at the first sump (-987 m) within Riesending and in the resurgence cave above Fürstenbrunn. Data loggers recording water or air pressure and temperature at further locations in Fürstenbrunner Quellhöhle (FBQ), Kolowrat cave (KW), Riesending (RD) and in the small resurgence cave Mausloch in the western flank of Untersberg soon followed (Fig. 3). The sampling interval of the pressure and temperature observations is 15 minutes, and the precision of the pressure measurements is at the level of 10 mBar.

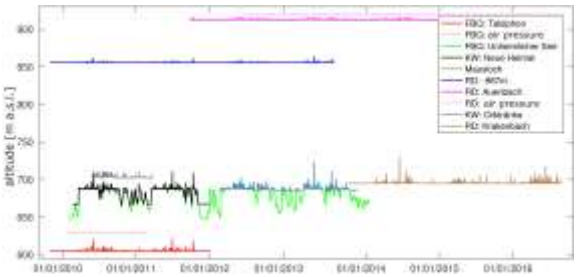

Figure 4: Altitude and observation period of pressure and temperature loggers in Untersberg (mod. from MEYER et al., 2017).

The water pressure recordings are transformed into water-level changes and are corrected for air pressure variations. The altitude above sea level of the different pressure gauges (Fig. 4) was determined by classical cave surveying techniques and is accurate at the meter or even decameter-level. Consequently, only relative pressure changes are evaluated. The pressure observations are augmented by discharge measurements based on the salt dilution method at the resurgence and at individual cave streams in Riesending and Kolowrat cave. Outside the caves, isotope-analyses were performed by REISCHER et al. (2015).

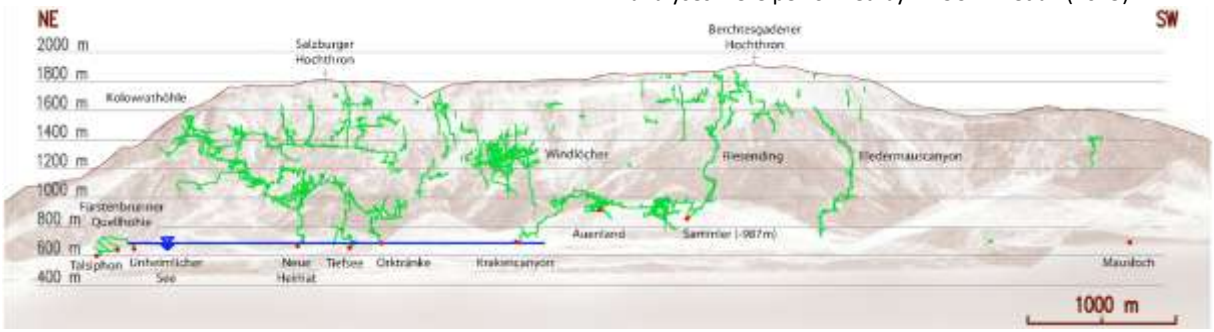

Figure 3: Cross section through Untersberg with major caves, logger positions are indicated by red dots (mod. from Zagler, 2016), the saturated zone by a blue line. Water level of the saturated zone may vary by 40 m at Unheimlicher See.

3. Results

We first focus on the comparison of the two streams of *Auenbach* and *Krakenbach* in Riesending (Fig. 2). The pressure gauge at *Auenbach* is located at a depth of -940 m (altitude 903 m) close to bivouac 7. *Auenbach* emerges from a small sump and meanders quietly through *Auenland*, before it tumbles into *Auencanyon* and sumps again at -1148 m. *Krakenbach* on the contrary rushes steeply down *Krakencanyon*. The pressure gauge is located at -1148 m (altitude 695 m) shortly before the final sump is reached (not yet known at the time the pressure gauge was installed).

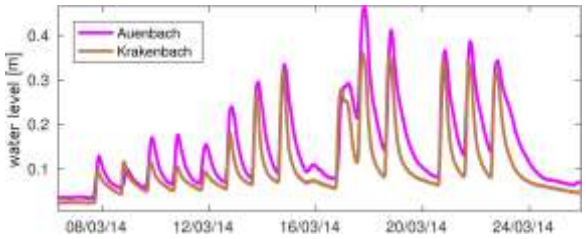

Figure 5 : Water-levels of Auenbach and Krakenbach during snow melt in March 2014 (mod. from MEYER et al., 2017).

An example of daily water level variations due to snow melt in the month of March 2014 is provided in Figure 5. Both streams react in a very comparable way, the inset of the daily flood peak being slightly earlier at *Krakenbach* (barely visible in Fig. 5), probably due to the steep course of *Krakencanyon*. The daily flood pulse is accompanied by a drop in water temperature (not shown). A water level of 0.2 m at *Auenbach* corresponds to a discharge of approx. 50 L/s. At *Krakenbach* no discharge measurements were performed.

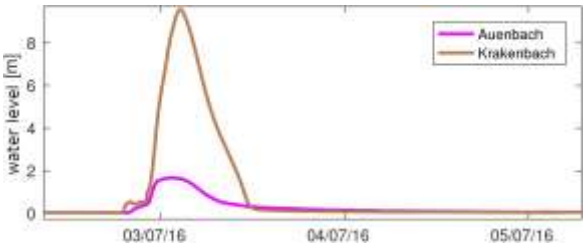

Figure 6: Water-levels of Auenbach and Krakenbach during a flood pulse in July 2016 (mod. from MEYER et al., 2017).

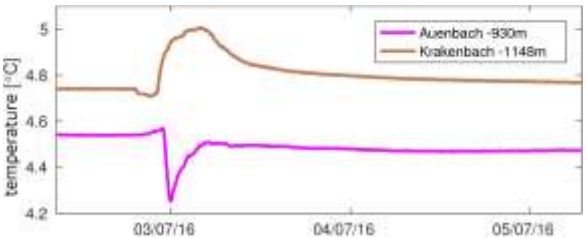

Figure 7: Water temperatures of Auenbach and Krakenbach (mod. from MEYER et al., 2017).

We now compare to a flood pulse caused by heavy rain during the 2nd/3rd night of July 2016 (Fig. 6). The flood peak at *Auenbach* is cut just below 2 m due to an important increase in passage width at this height. The water temperature, after a minor rise due to the water of the upstream sump being replaced, shows the expected drop as soon as the surface water reaches the sensor (Fig. 7). In contrast the flood peak at *Krakenbach* is not truncated, despite a drastic enlargement of the cave passage at height, and the water temperature, after a slight decrease due to the arrival of cold surface water, rises quite significantly.

While from the cave survey we can guess that the pressure gauge in *Krakenbach* is located close to the karst water table, we unfortunately cannot prove this by direct comparison with the logger at *Unheimlicher See* in FBQ (which was recovered in January 2014). But simultaneous observations exist from *Unheimlicher See* in FBQ and *Orktränke* in KW. At both locations the sensors are located in sump pools at the karst water table that are either fed (*Orktränke*) or drained (*Unheimlicher See*) by active streams. Instead of comparing individual flood peaks we provide a statistical evaluation of simultaneously observed water levels (Fig. 8).

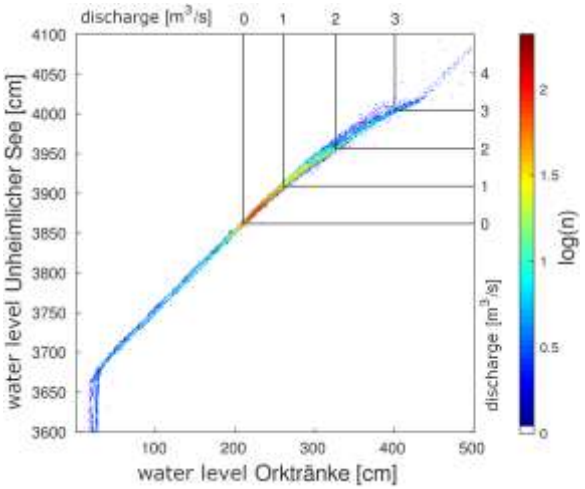

Figure 8: Water levels measured simultaneously at Unheimlicher See and Orktränke, colour-coded the frequency of occurrence; discharge refers to Unheimlicher See (mod. from MEYER et al., 2017).

The water level at *Unheimlicher See* can vary by more than 40 m, the sensor was installed during extremely dry conditions in winter. Normal water level is reached just below 39 m, where the summer overflow of the sump pool is reached (altitude 688 m). This corresponds to a water level of about 2.5 m at *Orktränke*. Below a water level of 37 m at *Unheimlicher See* the sensor at *Orktränke* falls dry. In between we see an almost perfect correlation between water levels. Above the summer overflow the flood peaks tend to be higher at *Orktränke*. This can be explained by an increase of passage size in FBQ above the summer overflow and restrictions in the submerged passage between *Unheimlicher See* and *Orktränke* that cause friction and turbulent flow. From FBQ we moreover have discharge measurements that are also provided in Fig. 8.

4. Discussion and Conclusions

REISCHER et al. (2015) conclude from their isotope analysis that the catchment area of Fürstenbrunner Quelle is at a mean altitude of 1650-1700 m, which corresponds to the karst plateau of Untersberg. They calculate the retention time of the water discharged by the resurgence to be 4-5 months. This is in agreement with dye tracing times of up to 157 days observed by G. Völkl (HASEKE-KNAPCZYK, 1989). Based on a mean flow of 750 L/s one can calculate the volume of the karst water body drained by Fürstenbrunner Quelle to be approx. 10^7 m^3.

Several recently discovered sumps in the deep caves of Untersberg plateau allow the direct observation of this karst water body. A continuous karst water table reaching from the resurgence to *Orktränke* in Kolowrat cave (at 2 km distance) could be verified by simultaneous observation.

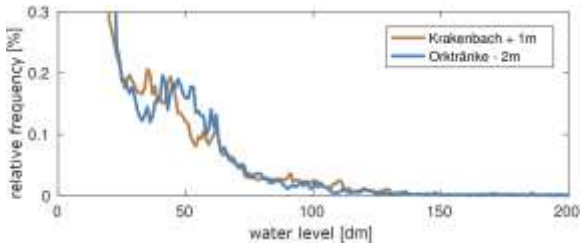

Figure 9: Statistical evaluation of water levels at Krakenbach and Orktränke. The best fit is reached applying a relative shift in elevation of 3 m, e.g., -2 m at Orktränke and +1 m at Krakenbach to show water levels relative to summer overflow at FBQ (mod. from MEYER et al., 2017).

An even farther window to this continuous karst water table exists in *Krakencanyon* of Riesending cave (distance 2.8 km). While no simultaneous observations exist, a statistical evaluation of how frequent certain water levels occur at *Orktränke* or *Krakenkanyon* (Fig. 9) indicates a geometrically similar karst water body, which most probably is explained by a common karst water table reaching from the Fürstenbrunner Quellhöhle all the way to Riesending. The surveyed depth of Riesending at the final sump, more than 5 km from the entrance, differs only 6 m from the altitude of the common water table as indicated by the water level measurements. This is a remarkable accuracy, considering the harsh surveying conditions in the cave.

The anomalous temperature behaviour at *Krakenbach*, exemplified by a flood event in July 2016 (Fig. 7), can be explained by the proximity to the karst water table. While cold surface water reaches the sensor first, it is followed by a dramatic rise of the karst water table due to the heavy rain. The comparably warmer water rises from the sump pool and floods the whole passage (Fig. 10). During the three years observation period a maximum water level of 35 m above normal (e.g., above the summer overflow of *Unheimlicher See* in Fürstenbrunner Quellhöhle) could be observed.

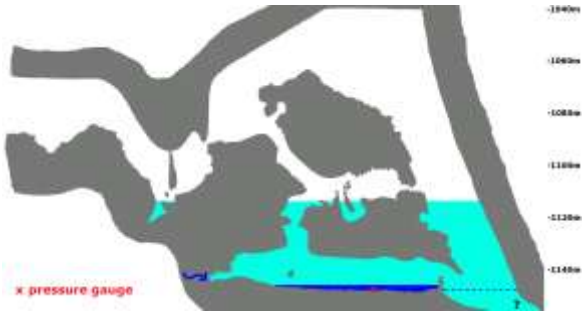

Figure 10: Cross section of Krakencanyon near the final sump. Warm water (light blue) rising from the sump floods the passage up to 35 m above normal water level (mod. from MEYER et al., 2017).

Acknowledgments

We gratefully thank all the enthusiastic cavers who installed and recovered numerous sensors, prepared salty solutions for discharge measurements (often in the middle of the night) or carefully observed survey leg after survey leg, soaked to the bone, during week-long expeditions into the dark heart of Untersberg.

References

HASEKE-KNAPCZYK H. (1989) Der Untersberg bei Salzburg, 4. Hydrogeologische Verhältnisse. Universitätsverlag Wagner Innsbruck, 44-62.

HÖFER-ÖLLINGER G., GADERMAYR W., ZAGLER G., BUTSCHEK M. (2016) Der Einfluss der Einzugsgebiets-höhe auf das Abflussverhalten beim Hochwasser vom Juni 2013, aufgezeichnet in Höhlen und Karstquellen im Land Salzburg. Die Höhle, n°67, 49-67.

MEYER U., ZAGLER G., HÖFER-ÖLLINGER G. (2017) Hydrologie der Riesending-Schachthöhle. Die Höhle, n°68, 79-99.

MEYER U. (2022) The exploration of Riesending. In Proceedings of the 18th International Congress of Speleology, Chambéry, France.

REISCHER M., BICHLER B., SPÖTL C., HÖFER-ÖLLINGER G., WYHLIDAL S. (2015) Karst hydrogeology of the Untersberg massif and its interaction with the porous aquifer in the adjacent Salzburg Basin. Austrian Journal of Earth Sciences, n°108, 68-81.

ZAGLER G. (2016) Untersberg. In SPÖTL C., PLAN L., CHRISTIAN E. (Editors), Höhlen und Karst in Österreich, Oberösterreichisches Landesmuseum Linz, 541-552

Fonctionnement de la lentille d'eau douce de Lifou à Ani-e-Wee (Lifou, Iles Loyauté, Nouvelle Calédonie). Conséquences sur le gisement de nautiles fossiles

Laurent MOREL (1), Vincent LIGNIER (2), Claire A. CHAUVEAU (3), Isabelle COUCHOUD (4) & Stéphane JAILLET (4)

(1) Laboratoire Ampère, Université de Lyon, CNRS UMR 5005, laurent.morel@univ-lyon1.fr
(2) Lycée A.& L. Lumière, Lyon 08.
(3) Université Libre de Bruxelles, Belgique
(4) Laboratoire Edytem, Université Savoie Mont Blanc, CNRS, Savoie Technolac, F-73376 Le Bourget du Lac

Résumé

L'archipel des Loyauté (Nouvelle Calédonie) est un ensemble d'îles volcaniques à couverture carbonatées karstifiées, où les interactions entre l'eau de mer et l'eau douce sont permanentes. L'eau météorique s'infiltre directement pour s'accumuler sous la forme d'une lentille d'eau douce flottant sur l'eau de mer qui imprègne la base noyée du karst. Plusieurs cénotes et grottes donnent accès à cette lentille d'eau douce. C'est au cours d'explorations spéléologiques sur l'île de Lifou, dans le trou d'eau "Ani-e-Wee", que des coquilles de nautiles fossiles ont été aperçues la première fois vers -35m. Deux missions scientifiques : Namaka 2011 et Nautilus Death Cave 2014 ont été conduites pour étudier le gisement et son lien avec le fonctionnement de la lentille d'eau douce. L'analyse croisée des variations actuelles des niveaux hydrologiques en mer et dans le cénote d'Ani-e-Wee permet de montrer la faiblesse de la connectivité entre l'océan et l'aquifère karstique actuel. C'est un argument important pour la compréhension du piège qu'a constitué le karst pour ces animaux et mieux comprendre la dynamique du karst lors de la remontée du niveau marin. Des paramètres physico-géochimiques (oxygène dissous, conductivité, température) sont exposés ainsi que les variations de hauteur de cette lentille.

Abstract

Functioning of the freshwater lens from (Ani-e-Wee, Lifou, Loyalty Islands, New Caledonia). Consequences on the nautilus fossil deposit. The Loyalty Archipelago (New Caledonia) is a set of karstified carbonate islands, where the interactions between seawater and fresh water are permanent. Meteoric water seeps directly into the form of a freshwater lens floating on seawater that permeates the drowned base of the karst. Several cenotes and caves provide access to this freshwater lens. It was during caving explorations on Lifou Island, in the water hole "Ani-e-Wee", that shells of fossil nautilus were first seen around -35. Two scientific missions: Namaka 2011 and Nautilus Death Cave 2014 were conducted to study the deposit, and its relationship with the freshwater lens behaviour. Cross-analysis of current variations in hydrological levels at sea and in the Ani-e-Wee Cenote has shown the weakness of connectivity between the ocean and the current karst aquifer. This is an important argument for understanding the trap that karst has created for these animals and better understanding the dynamics of karst when rising sea levels. Physics-geochemical parameters (dissolved oxygen, conductivity, temperature) will be exposed as well as variations in the height of this lens.

1. Introduction.

Suite à la découverte en 2010 d'un gisement de coquilles de nautiles fossiles entre 35 et 60 m de profondeur, dans un cénote de Kumo à Lifou (Nouvelle Calédonie), deux expéditions (2011, 2014) ont révélé le caractère exceptionnel de cette découverte qui semble être un cas unique au monde de fossilisation récente de nautile dans un karst littoral (7000 ans BP, Landman et *al*., 2014). Plusieurs études sont menées en parallèle : paléontologie, géologie, géomorphologie, paléo-climatologie, biologie (Jaillet et *al*., 2014 ; Lignier et *al*., 2014 ; Morel et *al*., 2016). Un axe d'étude sur l'hydrologie était nécessaire pour mieux caractériser le fonctionnement hydrodynamique de la lentille d'eau douce dans le cénote lui-même et ses relations avec la mer. Pour ce faire, les travaux se sont orientés sur 3 pistes : (i) analyse parallèle des variations du niveau d'eau (marée) et de la température dans la mer et le cénote ; (ii) profils verticaux CTD (Conductivité, Température, Profondeur), oxygène dissous, piézométrie, dans le cénote et (iii) étude géométrique et morphologique du gisement et de la halocline dans le vide souterrain (fig. 1). La caractérisation des mouvements relatifs d'eau dans la cavité constitue une piste à la compréhension des circulations d'eau actuelles entre les deux entités (mer / cavité) mais aussi pour l'analyse du trajet potentiel (aujourd'hui clos) effectué par les nautiles depuis la mer vers la cavité piège. D'autres mesures sur la chimie des eaux douce, salée et

saumâtre, afin d'estimer leur potentiel de dissolution sur les coquilles et sur la roche ont été menées. Une analyse de la position de l'interface eau douce-eau salée (halocline) et sa dynamique dans le temps est proposée. Cinq enregistrements des fluctuations des hauteurs d'eau sur une dizaine de jours ont été réalisés comparativement dans l'océan et plusieurs cavités voisines : littoral de la Baie de Santal (océan), Ani-e-Wee à -2 m et -40 m, grottes d'Athepe et de Quanono (lentille d'eau douce) (fig. 1).

Ce travail a été financé le ministère des Outre-Mer, l'université de Nouvelle Calédonie et par une collaboration avec l'IRD Nouméa.

2. Marée et piézométrie.

Les marées sont de type semi-diurne à inégalité diurne (écart entre grands et petits marnages). Il y a ainsi deux pleines mers et deux basses mers par jour, dont les hauteurs sont différentes. Tout au long de l'expédition le marnage a été enregistré avec un pas de temps d'une minute. On retrouve bien des marées de type semi-diurne à inégalité diurne avec une amplitude maximale de 1,6 m (fig. 2), sur la période de juillet 2014. Seuls trois jours sur les dix enregistrés sont présentés pour une meilleure lisibilité, les autres jours d'enregistrement n'apportant pas plus d'information. Pendant la période d'étude, les conditions météorologiques étaient stables, la pluviométrie était presque nulle. Tous les résultats présentés ont été réalisés sur la même période.

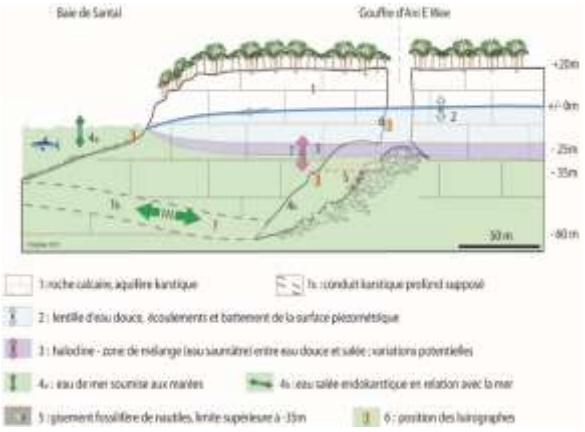

Figure 1 : Relation entre la lentille d'eau douce, l'intrusion saline et le gisement fossilifère de nautiles. Positionnement des stations de mesures de hauteurs et de températures (luirographe).

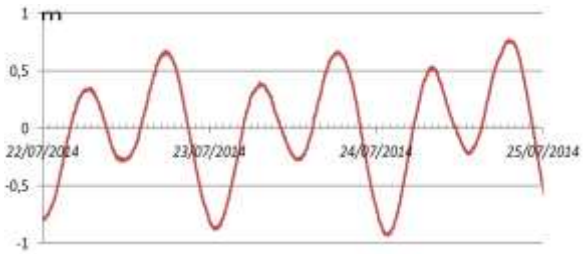

Figure 2 : Variations de la hauteur d'eau (en mètre) mesurées du 22 au 25 juillet 2014 à Ani-e-Wee /baie de Santal (océan).

On retrouve dans de nombreux endroits dans le monde l'existence de nappe d'eau douce flottant sur des eaux salées (Thomas, 2010). L'eau douce a la particularité de se mélanger difficilement avec les eaux salées. La relation de Ghyben-Herzberg permet d'estimer la profondeur du biseau salé et donc l'épaisseur de la nappe d'eau douce en suspension. Elle suppose (par simplification) que l'épaisseur de la zone de mélange (halocline) est nulle (fig. 3a). Dans l'équation P = ρ.g.$h.$, la pression est reliée à la masse volumique ρ, à la colonne d'eau h et l'accélération g. Avec une mesure de pression à deux hauteurs connues différentes, l'une dans la zone d'eau douce (dont on connaît ρ_d) et l'autre dans la zone salée (dont on connaît ρ_s), on peut calculer l'épaisseur « e » de la zone d'eau douce, pour une zone de transition nulle ou faible selon la relation :

Equation (1) : $e = \frac{P_1}{\rho d.g} + (\frac{P_2 - P_1 - \rho s.g.d}{g.(\rho d - \rho s)})$

Il faut soustraire aux mesures de pression (P_1, P_2) celle de la pression atmosphérique afin d'obtenir des valeurs de pression absolues.

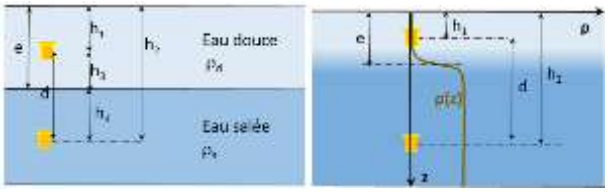

a b

Figure 3 : Enregistrement des pressions (luirographe) pour déterminer la profondeur et l'épaisseur de la halocline.

Une grande précision est nécessaire pour obtenir un calcul fiable de cette zone de transition. Mais dans la réalité, cette halocline correspond généralement à une zone de transition entre la lentille d'eau douce et l'eau de mer. Elle n'est donc pas d'épaisseur nulle. D'après les mesures de salinité, sa représentation graphique montre une forme sigmoïde (fig. 3b) et peut être décrite avec le type d'équation (courbe marron fig.3b) :

Equation 2 : $\rho(z) = \rho(0).\frac{1}{1+e^{-\lambda.z}}$

avec ρ(z) densité à la profondeur z et λ représentant la forme de la courbure de la sigmoïde.

La pression P_1 ou P_2 des enregistreurs est égale à l'intégrale de ρ(z).g.h de zéro à la profondeur h_1 ou h_2. En calculant la différence de h2-h1, soit *d* qui est connu, on obtient :

Equation 3 : $\ln\left(\frac{1+2.e^{\frac{\lambda}{g}P_2}}{1+2.e^{\frac{\lambda}{g}P_1}}\right) = \lambda.d$

On peut ainsi déduire la caractéristique de cette sigmoïde, c'est-à-dire le terme λ. Avec des mesures continues, on pourrait connaître l'évolution de cette zone de mélange. Pour augmenter la précision de cette mesure, plusieurs enregistreurs de pression pourraient être installés le long du puits dans le cénote.

On retrouve dans le gouffre d'Ani-e-Wee les deux marées journalières, inégale entre elles. Leur amplitude de 0,4 m,

est quatre fois moins importante que celle de l'océan. Un déphasage d'environ deux heures entre l'océan et Ani-r-Wee est également mesuré, montrant une faible connectivité du gouffre avec l'océan (fig.4). Sur les autres jours d'enregistrement, non présentés ici, les caractéristiques des signaux sont identiques. En étudiant les mesures de pressions de hauteur sur une journée, on identifie une faible fluctuation de l'épaisseur *e* de la zone d'eau douce. On aurait pu imaginer une hauteur constante sur une journée (en absence de précipitations). Mais ces mesures mériteraient d'être plus finement étudiées pour obtenir une meilleure estimation de ces oscillations journalières. Enfin, des mesures de température d'eau dans le cénote, à –40m de profondeur, ont été enregistrées. Elles montrent également une variation de 0,08°C (fig.5), synchrone avec celle des marées.

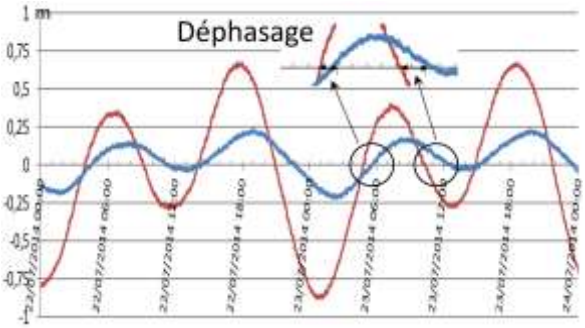

Figure 4 : Déphasage d'environ 2h entre le signal de marée de l'océan (rouge) et celui dans et sous la lentille d'eau douce à Ani-e-Wee (bleu).

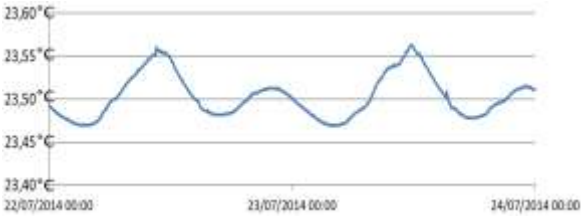

Figure 5 : Variation de la température de l'eau de mer à 40 m de profondeur à Ani-e-Wee, sous la lentille d'eau douce, par l'effet des marées.

3. Salinité, conductivité et oxygène dissous dans l'aquifère mixte du cénote.

Les mesures des différents profils présentés (salinité, conductivité et oxygène dissous) ont été réalisés sur la même période. Les mesures de salinité et de conductivité ont été réalisées en une seule plongée, avec une sonde CDT SeaBird 911 (compensée en température) doublée d'un ordinateur de plongée Vytec Suunto. Les profils obtenus présentent des courbes sigmoïdes qui attestent d'une transition progressive entre eau douce et eau salée et non une zone de transition franche (fig.6). La limite médiane se situe à -23 m pour une zone de transition de 9 m d'épaisseur environ. Avec les variations de hauteurs connues, cette halocline se situe donc bien au-dessus du site paléontologique. Cette mesure est ponctuelle et correspond à un cycle hydrologique hivernal. Une étude de l'épaisseur de la zone de transition reste à mener pour connaître sa dynamique sur un cycle annuel complet.

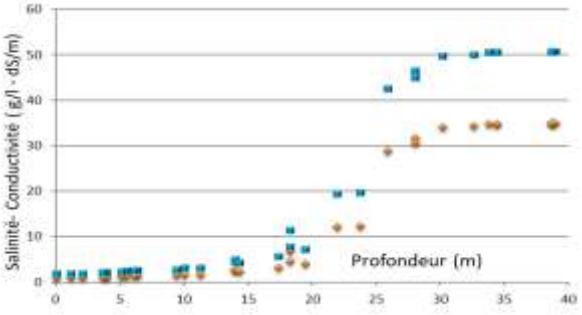

Figure 6 : Profils de salinité (bleu) et conductivité (marron) à travers la lentille d'eau douce (mesures du 22/7/2014 avec une Sonde CDTSBE911-couplée d'un ordinateur Vytec-Suunto).

Pour l'étude de l'oxygène dissous, vingt prélèvements d'eau ont été effectués par flaconnage tous les deux mètres selon le même profil, puis analysée par la méthode de Winkler, Les teneur en oxygène dissous obtenues, varient de 5,5 mg/l dans l'eau douce à 2 mg/l dans l'eau salée avec une zone de transition similaire à celle des valeurs de salinité. Ces mesures, bien corrélées avec la salinité et la température, montrent toutes la même forme de zone de transition. Un prélèvement dans l'océan sur la plage « kiki » au plus proche de la cavité montre une teneur en oxygène dissous de 4,92mg/l, valeur proche de celle obtenue à la surface de l'eau du cénote.

Dans l'aquifère salin du cénote, sous la lentille d'eau douce la valeur actuelle de l'oxygène dissous de 2 mg/l semble caractériser un milieu marin hypoxique peu propice aux organismes marins des milieux ouverts, comme les nautiles (Aminot et Kerouel, 2004).

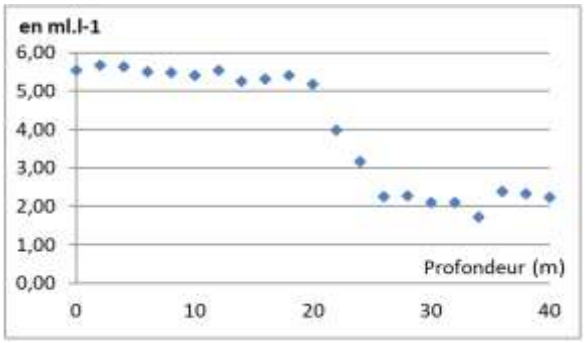

Figure 7 : Profil de teneur en oxygène dissous à travers la lentille d'eau douce (mesure du prélèvement du 22/7/2014,).

Figure 8 : Courbure des rayons de lumière montrant la variation de l'indice de diffraction dans les couches d'eau saumâtres de salinité croissante. Cénote de Quanono (Lifou).

4. Conclusions.

Les différentes mesures (déphasage, oxygène dissous) semblent attester d'une faible conductivité hydraulique karstique entre la mer et le cénote d'Ani-e-Wee. Ceci montre une faible connectivité entre l'eau de mer de la baie de Santal et l'eau de mer de l'aquifère karstique sous la lentille d'eau douce de Lifou. Dans ce secteur aucune source littorale n'est d'ailleurs connue ou mentionnée. En l'état, cette série de mesures, même ponctuelles, donne deux résultats nouveaux. Concernant l'évolution morphologique du site, ces résultats montrent un fonctionnement hydrodynamique de la lentille d'eau douce bien différent de ce qu'il a probablement été par le passé. Aujourd'hui, la connectivité entre le karst et l'océan semble faible. Le comblement sédimentaire de la baie par aggradation depuis la fin de la remontée principale du niveau marin (entre 8 et 7ka BP ; Lambeck et *al*. 2014) pourrait être à l'origine du colmatage des conduits karstiques profonds autrefois ouverts sur l'océan.

Ces conduits aujourd'hui méconnus et comblés devaient autoriser le passage des nautiles vers le karst profond. Ces observations précisent également les conditions de conservation du gisement fossilifère, notamment en ce qui concerne la position de la halocline. En effet, la profondeur actuelle de la halocline se situe bien au-dessus du gisement des coquilles (environ 10m) et ce quelle que soit la hauteur des marées. Il faudrait certes compléter ces enregistrements sur un cycle hydrologique annuel. Les mesures de dioxygène dissous confirment aussi que le milieu est hypoxique et ne permet pas une colonisation actuelle du milieu par les macro-organismes des milieux ouverts. Mais ceci participe aussi au bon état de conservation des coquilles depuis leur mise en place, malgré la présence de micro-organismes (Seuss et *al*., 2016). Le gisement de coquilles de nautiles du cénote d'Ani-e-Wee (daté à ~7000 ans BP, Landman et *al*. 2014, Lignier et *al*., 2013) s'est mis en place dans un contexte hydrodynamique différent de l'actuel et les analyses proposées ici montrent l'intérêt d'étudier finement un fonctionnement actuel pour mieux tenter d'appréhender un fonctionnement passé.

Références

AMINOT A. et KEROUEL R. (2004) Hydrologie des écosystèmes marins. Paramètres et analyses. Partie 2, Chap. III, Parag.3.

COUCHOUD I., DRYSDALE R., HELLSTROM J., CHENG H., GREIG A, LIGNIER V., JAILLET S., MOREL L. and WOODHEAD J. (2021) Age constraints on sea level during the last two glacial terminations based on submerged speleothems from New Caledonia, *UIS 2021*. S.03.

GENTHON P., WIRRMANN D., HOIBIAN T. and ALLENBACH M. (2008) Steady water level and temperature in a karstic system: The case of the coral Lifou Island (SW Pacific). *Science direct, Geoscience*, Elsevier.

JAILLET S., LIGNIER V. et MOREL L. (2014) Un faciès d'altération de type « trou de gruyère » identifié dans les grottes péri-littorales de Lifou (Iles Loyauté, Nouvelle Calédonie). *Actes des Rencontres d'Octobre*.

KUE-YOUNG K., CHUL-MIN C. and KI-HWA P. (2007) A Simple Method for Locating the Fresh Water–Salt Water Interface Using Pressure Data. *Ground water* 45(6):723-8.

LAMBECK K. ROUBY H., PURCELL A. et al. (2014) Sea level and global ice volumes from the Last Glacial Maximum to the Holocene. *PNAS 111*, 15296-15303.

LANDMAN N.H., MAPES R.H., COCHRAN J.K., LIGNIER V., HEM-BREE D.I., GOIRAN C., FOLCHER E., BRUNET P. (2014) An unusual occurrence of Nautilus macromphalus in a cenote in the Loyalty Islands. *PlosOne*, 10(3). doi: 10.1371/journal.pone.0113372

LIGNIER V., MAPES R., HEMBREE D. et al. (2013) Le cénote d'Ani-e-Wee (Lifou, Nouvelle Calédonie) et son gisement exceptionnel de Nautilus macromphalus. *Karstologia*, 61, 37-44

LIGNIER V., JAILLET S. et MOREL L. (2014) Le trou d'eau Ani-e-Wee et son gisement de nautiles fossiles (Lifou, Iles Loyauté, Nouvelle Calédonie). Bilan des missions scientifiques de 2011 et 2014. *Actes des Rencontre d'Octobre*.

MOREL L., LIGNIER V. et JAILLET S. (2016) Cénote / Mer dans un karst insulaire (Lifou, Nouvelle Calédonie). *Eurokarst 2016*.

SEUSS B., WISSHAK M., MAPES R., HEMBREE D., LANDMAN N. and LIGNIER V. (2016) Microbial Bioerosion of Erratic Sub-Fossil Nautilus Shells in a Karstic Cenote (Lifou, Loyalty Islands, New Caledonia). *Ichnos* 23 (1-2): 108-115

THOMAS C. (2010) Le karst du Yucatan : rôle du flux géothermique, des failles, de l'eau de mer et des évaporites dans sa genèse. *Karstologia* n°55, 1-18

Effects of an extreme flood on an alpine karst system

Alessia NANNONI(1), Bartolomeo VIGNA(2), Adriano FIORUCCI(2), Marco ANTONELLINI(3) & Jo DE WAELE(3)

(1) Department of Earth Sciences, University of Florence, Via La Pira 4, 50121, Florence, Italy, alessia.nannoni@unifi.it (corresponding author)
(2) Department of Environment, Land and Infrastructure Engineering (DIATI), Polytechnic of Turin, Corso Duca degli Abruzzi 24, 10129 Torino, Italy bartolomeo.vigna@polito.it, adriano.fiorucci@polito.it
(3) Department of Biological, Geological and Environmental Sciences, University of Bologna, Via Zamboni 67, 40126 Bologna, Italy m.antonellini@unibo.it, jo.dewaele@unibo.it

Abstract

The effects of an extreme storm (501 mm of rainfall in less than five days) were monitored in an alpine show cave (Bossea, Italy) to assess the characteristics of the karst aquifer. The hydrology and hydrochemistry of the main underground river were monitored during the November 2016 flood, an exceptional hydrological event (estimated recurrence time of 200 years) that caused severe damages in the whole southwestern Piedmont region. The following 2017 and 2018 spring discharge phases were monitored as well. The karst system showed an impulsive response to flooding and the contributions to flow from different hydrogeological compartments were recognized. The development of this karst system is, in fact, related to the lateral and vertical juxtaposition of rocks with different lithologies and mechanical properties, resulting in a structurally complex arrangement. A progressive increasing contribution of the non-carbonate rocks to flow during the peak of the flood was recognized, suggesting the activation of larger portions of the aquifer during high-flow conditions. The extreme flood event had not a long-term influence on the system recharge/discharge dynamics: the 2017 snow-melting phase resulted in a discharge lower than the one that occurred during the following year when no anomalous event happened.

1. Introduction

Drainage and recharge processes in karst systems are widely studied because they regulate the output signal of the system, i.e., the karst springs. Both aspects are complex due to the heterogeneity and anisotropy of karst aquifers (BERGLUND *et al.*, 2019). The heterogeneity of karst flow is enhanced in geologically complex systems like those developed in orogenetic contexts. Folding, faulting, and fracturing may control surface and subsurface catchments, preferential flow directions and water residence times. Tectonics can also put in contact geological units with different permeability and composition, giving rise to uncertainty when interpreting spring hydrodynamics (DE LA TORRE *et al.*, 2020). The behavior of tectonically complex karst aquifers is even more difficult to study when dealing with exceptional conditions such as extreme flood events or persistent droughts with long recurrence times. This study presents the results of the hydrological and hydrochemical response of a karst system developed on the Alpine chain (Bossea, Italy) to an extreme flood event that occurred in November 2016. The goal is to assess the effect of extreme meteorological conditions on the hydrodynamic response of a structurally complex karst aquifer and to recognize the contribution to discharge of different hydrogeological compartments of the catchment. This is achieved by means of multiple chemical tracers and hydrological monitoring. The hydrological monitoring of the following 2017 spring discharge phase is also reported to assess whether the flood had any influence on long-term storage/discharge dynamics. The 2018 spring discharge phase is reported to evaluate the influence of snow-melting magnitude on the system dynamics. The Bossea show cave is an excellent test site for hydrogeological investigations because it hosts an underground scientific lab since the late 70s.

2. Geological setting, flood overview and methods

The Bossea karst system (Ligurian Alps, SW Piedmont, Italy, Fig. 1a, 1b) has a mid-altitude catchment of about 5.5 km^2. The recharge area comprises losing brooks (Bertino and Roccia Bianca, Fig. 1a) with variable flowrates. The karst system architecture is controlled by Alpine tectonics: sub-vertical faults separate metamorphosed rock compartments where the folded Mesozoic carbonate blocks are laterally and vertically juxtaposed to Lower Triassic clastic and Permian volcano-clastic rocks. The compartments that are made up mostly of marble are defined as *high-hydraulic conductivity complex (H-Kc*), whereas those made up predominantly of quartzite, shale, and metavolcanics, are termed *low-hydraulic conductivity complex (L-Kc,* Fig.1a), these last acting as aquitards or forming small fractured perched aquifers. Consequently, recharge is partly diffuse and partly from allogenic streams that release water into the fractured portions of the L-Kc. The Bossea cave developed along the detachment between the folded sequence made up of marble, shale, quartzite and the underlying meta-volcanics. The main underground collector (Mora creek, TM,

Fig. 1c, d) flows along the detachment in the downstream part of the cave. The water then resurfaces along the Corsaglia stream through a set of karstified bedding junctions. The 2016 meteorological event started on November 21st and ended on November 25th. The strongest rainfall intensity near Bossea (26.8 mm/h) was recorded between November 24th and November 25th. This storm event caused floods in the upper Tanaro valley (Corsaglia stream being one of its tributaries) with a magnitude that has an estimated recurrence time of 200 years. This storm caused one of the strongest floods ever recorded in the Bossea cave (maximum discharge of 1960 L/s). Mora creek discharge (Q), water temperature (T_{wtr}), electrical conductivity (EC) were monitored during the flood and the two spring discharge phases by means of an STS integrated sensor and data logger. An automatic water sampler with a six-hours sampling frequency was installed during the 2016 flood for hydrochemical monitoring. No hydrochemical data were available for the spring events. Precipitation and air temperature data were collected in a nearby meteorological station. Air temperature is used as a proxy for rainfall temperature. Water chemical analyses (major ions, trace elements, REE) were carried out at the Polytechnic University of Turin. The lanthanides (REE) concentrations were normalized to the Post Archean Australian Shale (PAAS) to infer the rocks drained during the flood. The Matti spring hydrochemical composition was taken as reference of the non-carbonate water drained from the L-Kc (Ms, Fig. 1a).

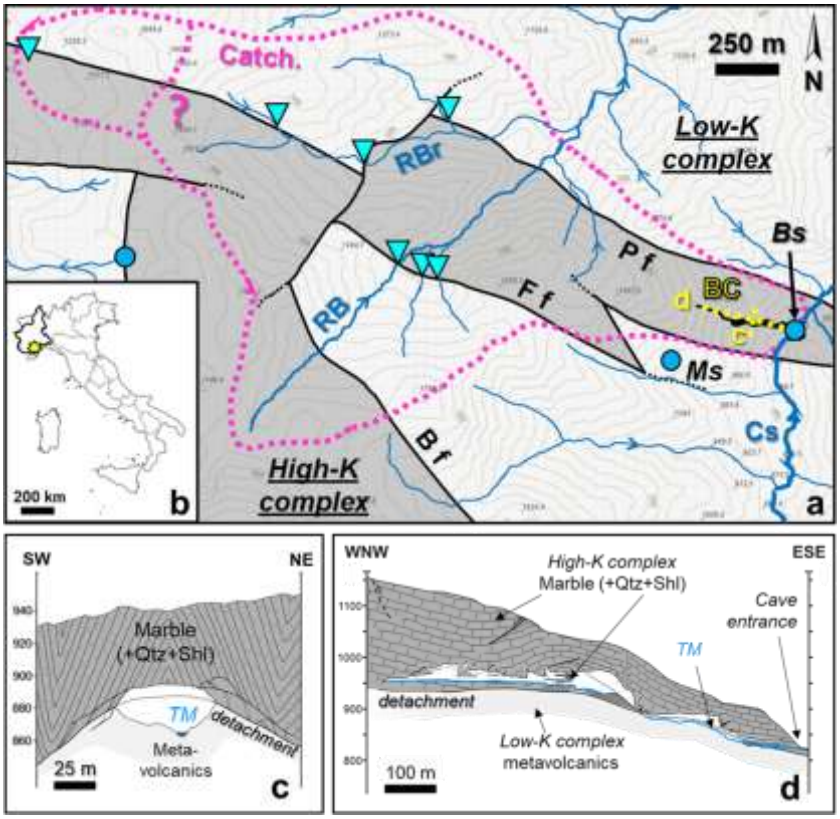

Figure 1: (a) Simplified hydrogeological map of the Bossea cave (labelled BC); springs and sinkholes are represented by light blue circles and cyan triangles, respectively (Catch. = catchment border, Bs = Bossea springs, Cs = Corsaglia stream, RB = Roccia Bianca creek, RBr = Rio Bertino creek, Ms = Matti spring, B/F/P f = Borello, Fontane and Prel faults. (b) Index map with the study site (yellow dot). (c-d) BC simplified cross-sections, their positions are marked in (a) (Qtz = quartzite, Shl = shale, TM = Mora creek); modified after ANTONELLINI et al. (2019).

3. Results

Approximately one third of 2016 precipitation fell during the November 2016 storm (Fig. 2a). TM reached its peak discharge (1960 L/s) 14 h after the highest hourly rainfall, and it returned to pre-storm values a week later (Fig. 2b). T_{wtr} started to decrease during the storm hydrograph rising limb, it increased by 0,07 °C during the peak flow, then it reached its minimum in the middle of the recession limb, returning to pre-storm values 2 months later. EC first increased sharply, then it showed a low synchronous with the maximum flood peak. Pre-storm values were reached a month after the flood. Ca/HCO_3, Sr and $\log(SO_4/HCO_3)$ decreased during the rising limb and returned to pre-storm values during the recession limb. ΣREE, Mg, and Alk/Cl increased during the flood but with different timings, whereas Ba decreased during the rising limb and did not return to pre-flood values.

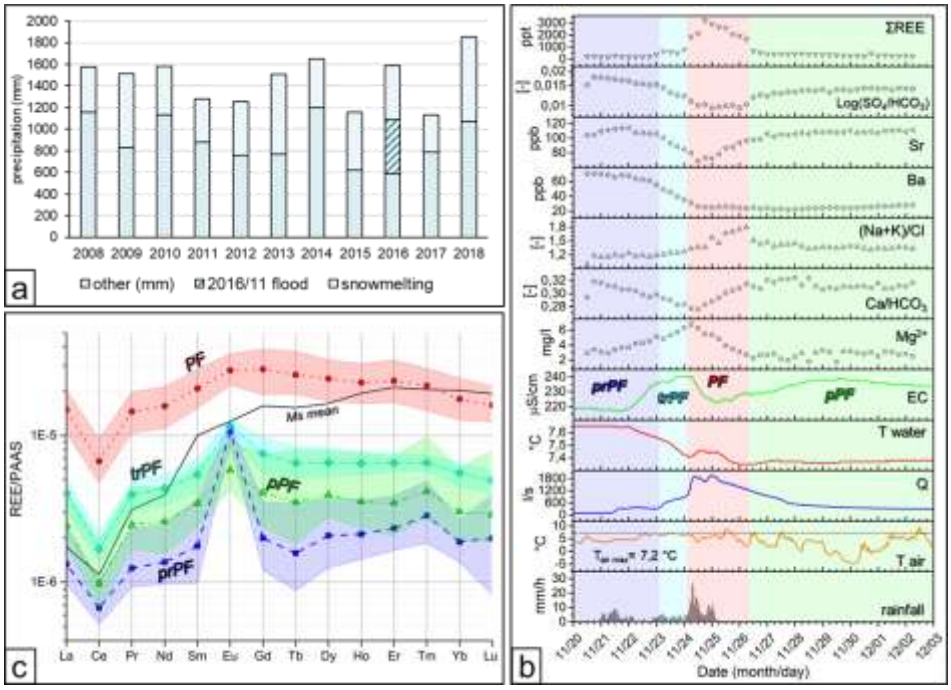

Figure 2: (a) total yearly precipitation for the 2008-2018 period; 2016 storm, and snow-melting phases contribution to the yearly budget are highlighted. (b) TM hydrographs and chemographs during the November 2016 storms; background colors refer to the different REE patterns in (c); Ms = Matti spring mean REE pattern. Samples are grouped according to their shape and time position (lines+symbols patterns = mean values for each group). Modified after NANNONI et al. (2020).

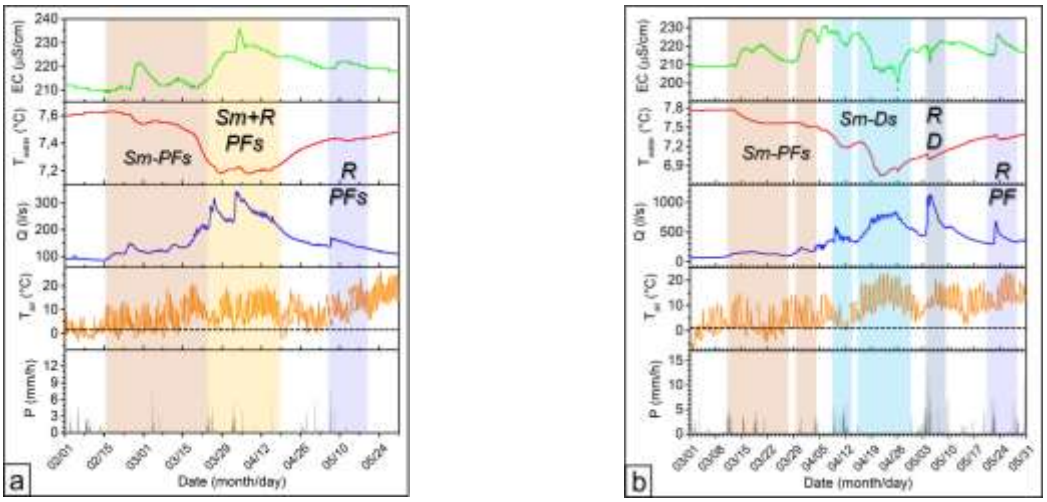

Figure 3: 2017 (a) and 2018 (b) spring discharge phases. Labels refer to the jointed interpretation of hydrographs and chemographs: Sm-PFs = snow-melting induced piston flow, Sm+R PFs = rain-controlled snow-melting and induced piston flow, Sm-DS = snow-melting induced dilution, R PF = Rain-induced piston flow.

Four normalized REE pattern groups were recognized for the 2016 event according to their shape and sampling times: pre-peak flow (prPF) with an Eu positive anomaly and rising HREE trend, transition to peak flow (trPF) with an Eu positive anomaly and an inversion of the HREE trend. The peak flow group (PF) has no Eu anomaly and shows a HREE trend like the one observed in trPF. The post-peak phase group (pPF) shows again a positive Eu anomaly (Fig.2c). The 2017 discharge phase started during mid-February and lasted until the end of May (Fig. 3a). Q varied between 70 and 350 L/s, the peak flow was reached at the beginning of April. T water started to decrease with the rise of discharge, and it reached its lowest value at the end of March. EC varied irregularly until March 21st, then it increased during high flow conditions reaching its maximum value during the flow peak. The 2018 discharge phase started at the beginning of March and finished at the end of May. Q showed a series of impulsive responses to precipitation like the flow peak at the beginning of May. Q also showed a prolonged phase of oscillation related to diurnal cycles of snow-melting not related to precipitation (Fig. 3b). During this stage, the snow cover melted because of the marked increase of air temperature. The highest Q value was reached after the temperature-induced snow-melting phase, when a strong

rainfall event occurred. Water T showed a general decrease during the whole spring season, reaching its minimum during the pure snow-melting phase. EC showed many oscillations and it reached is lowest value during the pure snow-melting phase with a trend like that of water T.

4. Discussion

The TM hydrodynamics observed during the extreme 2016 flood can be related to the contribution of different hydrogeological compartments of the aquifer. All the monitored parameters point to a piston flow phenomenon (e.g., REE spiders and trend, Alk/Cl increase, the specular EC and T trends during PF when air temperature was decreasing). The contribution of the L-Kc sectors can be recognized by comparison with the Matti spring hydrochemistry (Alk/Cl >> 1 and REE pattern).

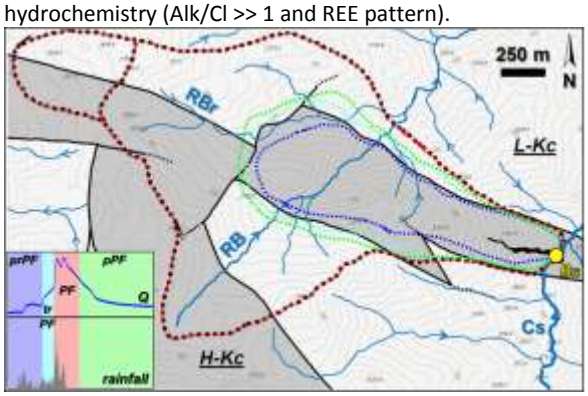

Figure 4: Bossea catchment drainage during the 2016 flood. The colored dashed lines mark the drained areas during the flood subsequent phases. The box reports the Mora creek hydrograph and the flood phases.

Four flow phases can be distinguished: a pre-peak flow phase (prPF) characterized by water inputs from the marble and possibly the shale, a transition to peak flow (trPF) phase with water drained mainly by the H-Kc, a peak flow (PF) phase that displays the strongest contribution to flow from the L-Kc, and a post-peak flow phase (pPF) during which the system recovers from the flood perturbation. Piston-flow phenomena were observed also during the 2017 and 2018 spring discharge phases, and they can be recognized by the specular trends of EC and T. PF spring dynamic is related to the combination of, a) snow-melting aided by rainfall (Sm+R PF), b) T-controlled snow-melting (Sm PFs), and c) rainfall induced (R PF). Dilution episodes (simultaneous decrease of T and EC) were observed only during and after the 2018 temperature-controlled snow-melting (Sm-Ds and R D). This could be related to the fact that snow accumulation during the 2017-2018 winter was much more intense than the previous winter. 2016/2017 hydrologic year recharge was supported mostly by the November flood and by a few, weak snowfalls, so the water input of the flood and the thin snow cover could not support normal base flow from winter to spring. This explains the extremely low base flow at the beginning of spring discharge. The scarce snow cover was rapidly melted, leading to impulsive flushing of the water stored by pressure propagation. The melting of the thick snow cover in 2018 leads first to piston flow episodes then to dilution, because the water stored in the aquifer was completely flushed from the system. Dilution in this system is limited to spring discharge, depending on snow accumulation. Even extreme floods cannot influence the system dynamics over long time intervals.

5. Conclusion

Bossea showed a piston flow behavior during the 2016 event, like for antecedent floods. This is related to the structural and morphological setting of the karst system. Progressively broader sectors are drained during the floods, but the involvement of the distal L-Kc parts is related to the duration and the intensity of the meteorological event, because infiltration needs to be efficient across most of the catchment for the non-carbonate inputs to be relevant. The recharge/discharge dynamics of the system seems not to be particularly controlled by the occurrence of extreme events on the long period.

References

ANTONELLINI M., NANNONI A., VIGNA B., DE WAELE J. (2019) Structural control on karst water circulation and speleogenesis in a lithological contact zone: The Bossea cave system (Western Alps, Italy). Geomorphology 345, 106832.

BERGLUND J. L., TORAN L., HERMAN E. K. (2019). Deducing flow path mixing by storm-induced bulk chemistry and REE variations in two karst springs: With trends like these who needs anomalies? J. Hydrol., 571, 349-364.

DE LA TORRE B., MUDARRA M., ANDREO B. (2020). Investigating karst aquifers in tectonically complex alpine areas coupling geological and hydrogeological methods. J. Hydrol. X, 6, 100047.

NANNONI A., VIGNA B., FIORUCCI A., ANTONELLINI M., DE WAELE J. (2020). Effects of an extreme flood event on an alpine karst system. J. Hydrol., 590, 125493

.

Monitoring sea-tide dynamic in a coastal cave: the Puerto Princesa Underground River, Palawan, Philippines

Leonardo PICCINI[1,2], Josè Maria CALAFORRA[1,3], Franco CUCCHI[4], Paolo FORTI[1,5]

(1) La Venta Esplorazioni Geografiche, Italy
(2) Department of Earth Science, Università di Firenze, Italy – leonardo.piccini@unifi.it
(3) Water Resources and Environmental Geology, University of Almeria, Spain - jmcalaforra@ual.es
(4) Circolo Speleologico Idrologico Friulano - Udine, Italy - franco.cucchi@tim.it
(5) Italian Institute of Speleology, Via Zamboni 67, 40125 Bologna, Italy - paolo.forti@unibo.it

Abstract

The Puerto Princesa Underground River (PPUR) is one of the most extraordinary coastal karst systems in the world. Its hydrodynamics heavily depends on the complex interactions between the flow-rate fluctuations of the river that flows through it and the internal dynamics of the tides. In fact, tides affect the whole cave, making their effects felt almost to the height of the main sink point, about 7 km far from the main out-flow entrance, which is just a few tens of meters away from the coast. Between November 2016 and April 2017, 6 probes continuously recorded changes in water level, temperature, and electrical conductivity (EC) in different points distributed along the path of the cave. Monitoring shows that water levels synchronously change along all the cave due to the pressure transmission, whereas temperature and EC fluctuations are affected by the geometry of riverbed, which impedes upstream and downstream water exchanges.

1. Introduction

The Natuturingam cave, better known as Puerto Princesa Underground River (PPUR), is one of the largest subterranean estuaries in the world (PICCINI & IANDELLI, 2011; BADINO *et al*, 2017), where tides propagate for over 7 km inside the cave (CALLIGARIS *et al*., 2018). The PPUR, consisting of more than 35 km of galleries, hosts an extremely complex ecosystem based on huge colonies of bats and swiftlets. Its natural uniqueness was recognized as World Heritage by UNESCO in 1999, while the first part of its navigable path (some 2 kilometers) has been used as a show cave since the late Seventies (Fig. 1).

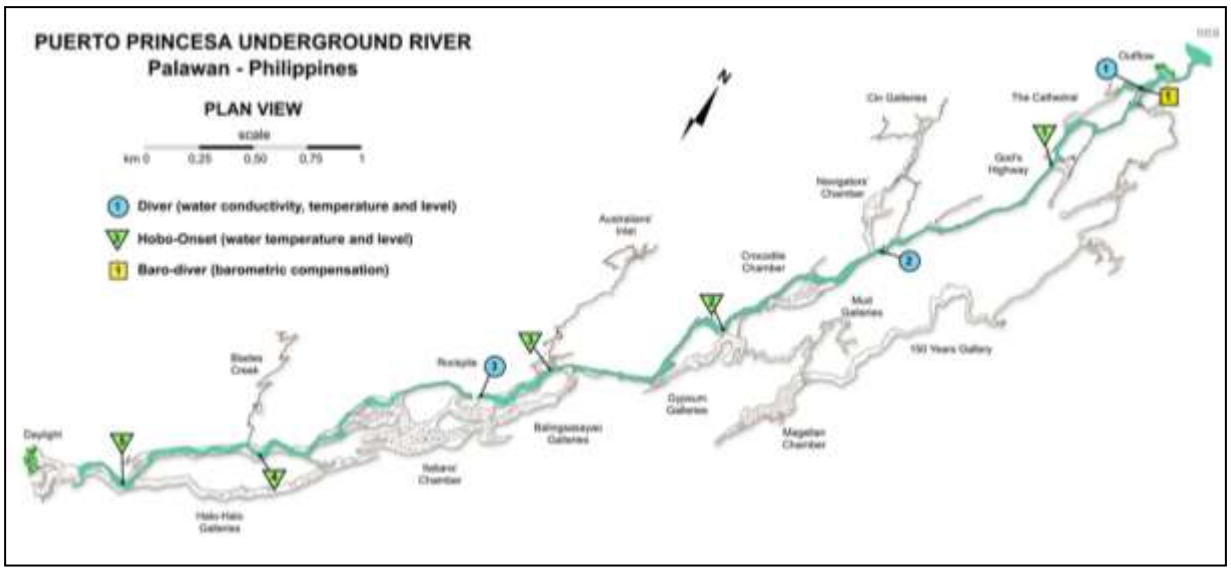

Figure 1: Location of the 3 CTD and 5 Hobo Onset which were left inside the PPUR during the first expedition (survey data processing and graphic: L. Piccini).

2. Materials and methods

Three CTD-Diver® Eijekelkamp, five 5 Hobo Onset®, and 1 Baro-Diver® Eijekelkamp were placed between November 24 to December 11 and collected again between April 27 to May 14. The diver 1 near the Outflow was partially covered by marine organisms. However, its operation was correct until the end with regards to depth and temperature, while the values of conductivity seem to be corrupted from early January 2017. The Hobo-Onset 1 and 2 were strongly corroded by sea and/or brackish water: therefore, it was impossible to download the data recorded inside.

3. Results

The diagrams on the whole CTD-Divers recording period, shows the synchrony of the oscillation curves of the sea level, with only slight differences in water level that might depend on the freshwater flow going out the cave (Fig. 2a). This is also confirmed by the three Hobo sensors places at the confluences with the Australian Inlet, with the Blades Creek, and at the Daylight (Fig. 1). These recordings, in fact, are tuned with the other three divers, underlining the fact that the tide occurs, though in reduced form, along the whole karst system (Fig. 2-a) The layout of the strobe placed 200 m downstream of the Daylight is particularly relevant, as the tide effect occurs exclusively for high tides, while it is completely absent during low tides.

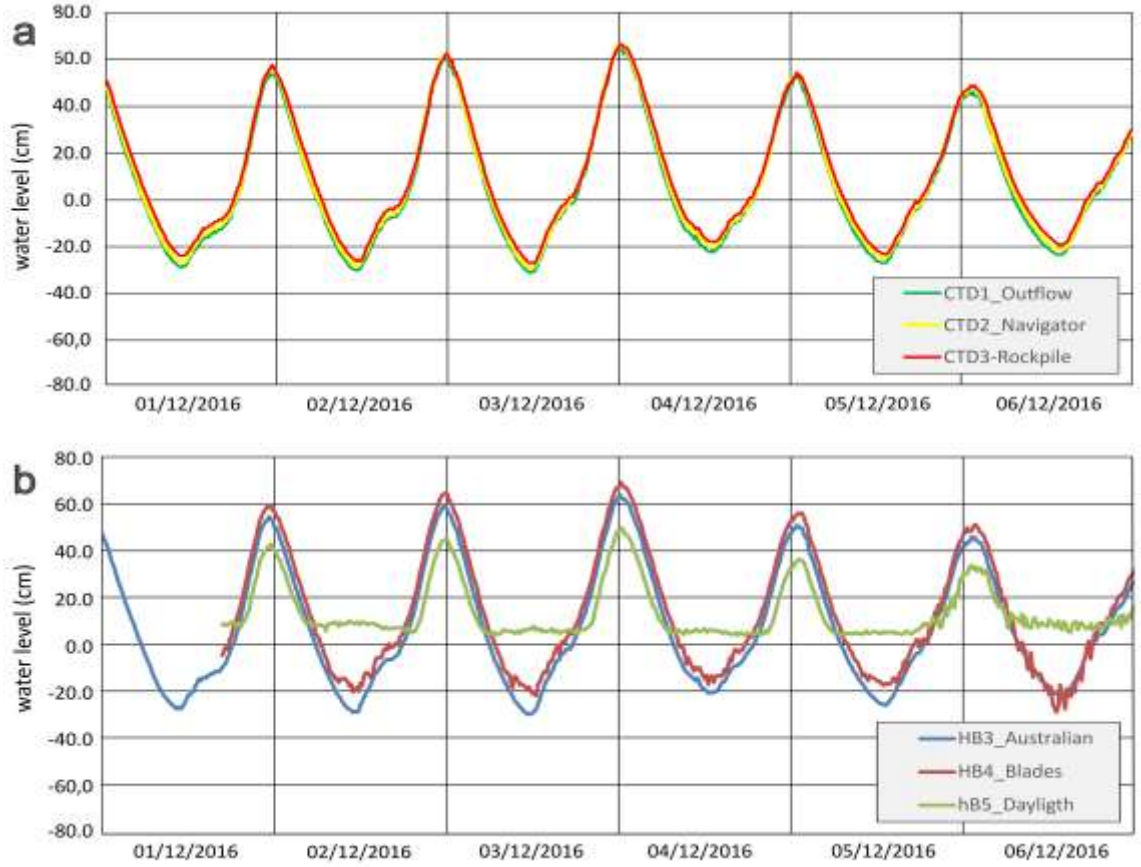

Figure 2: a - Water level fluctuations (centimeters compared to local mean level) measured at the three CTD stations from December 01 to December 12, 2016: CTD1 = PPUR Outflow, CTD2 = Navigator's Chamber, CTD3 = Rock pile. b- Water level fluctuations (centimeters compared to local mean level) measured at the three Hobo stations from December 01 to December 12, 2016: HB3 = confluence with Australian Inlet, HB4 = confluence with Blades Creek, HB5 = Daylight.

Temperatures recorded by the three CTD Divers show rather complex trends, which are, however, still clearly influenced by tidal motion (Fig. 3). A detailed analysis of the curves reveals that during the high tide phase, the temperatures are a few °C higher than the ones measured during low tide phases. This was observed in all the three stations, but it has a higher range in the CTD1 and CTD2, with 4-5°C differences, while the temperature fluctuations at CTD3 station are usually below 2°C. The smaller temperature oscillation, which occurs mainly in the second half of the diagram, is probably tied to the fact that the temperature of the lower layer of water is in a state of equilibrium with the rock, as it

is affected by less exchanges with seawater from outside. While the first month of recordings shows similar temperature variations, from the beginning of 2017 we found significant differences between the sensors placed near the outflow and the one placed at Rock pile. It can currently be stated that with the decrease in flow rate the more external sensors are strongly affected by the influence of seawater, while the internal one maintains oscillations at around 25.5°C. The different hydrodynamics of the CTD1 and CTD2 stations, which behave similarly although far from each other, compared to station CTD3 are clearly underlined by the diagram that shows the trend of electric conductivity (EC), which is once again subject to variations that are influenced by tidal motion.

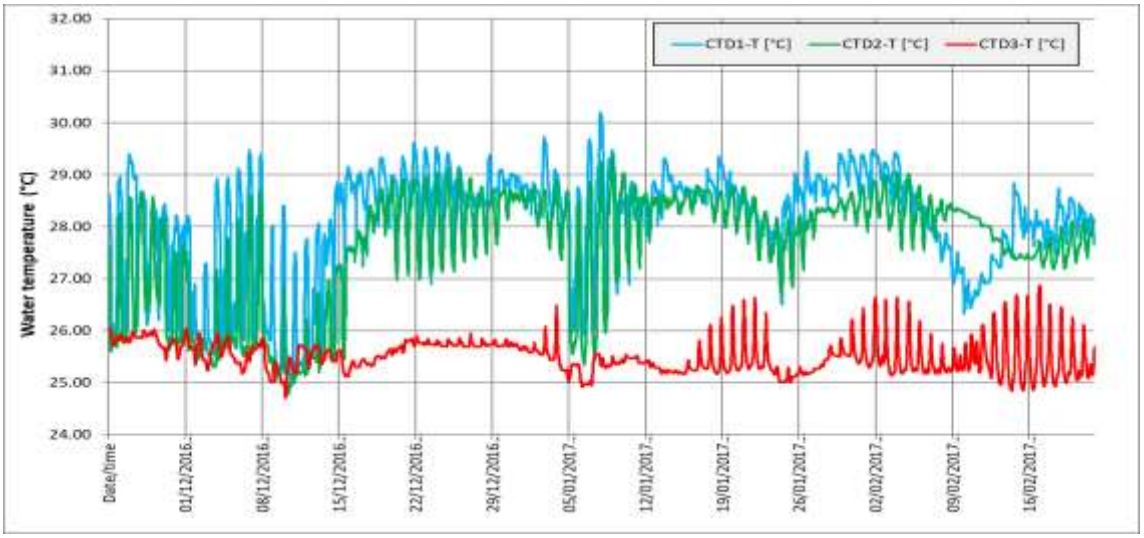

Figure 3: Water temperature measured at the three CTD stations from December 01, 2016 to February 28, 2017. CTD1 = PPUR outflow, CTD2 = Navigator's Chamber, CTD3 = Rock pile.

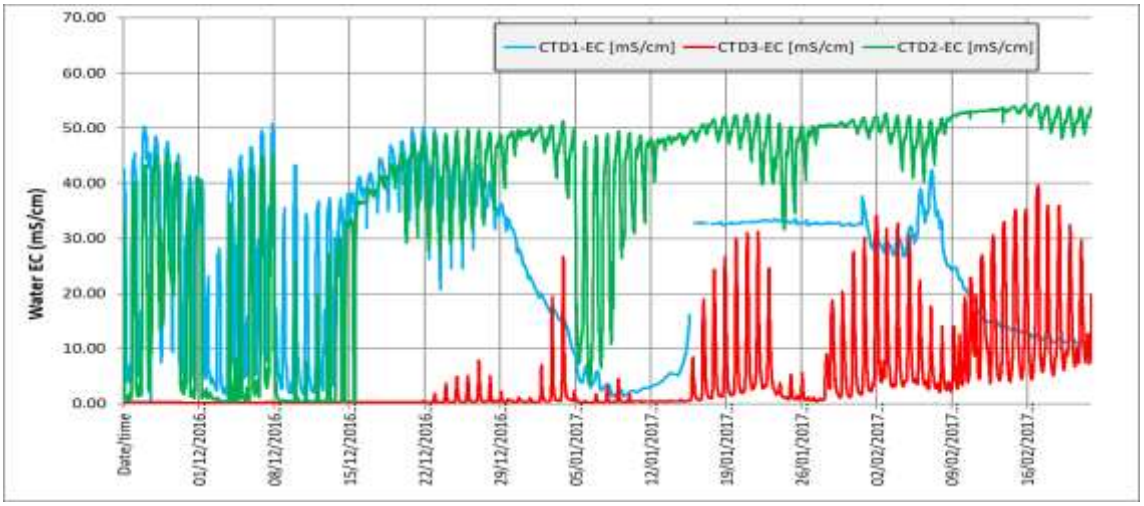

Figure 4: Electrical Conductivity measured at the three CTD stations from December 01, 2016 to February 28, 2017. From 03/01/2017 the EC sensor of CTD1 did not provide reliable measurements due to a technical damage. CTD1 = PPUR Outflow, CTD2 = Navigator's Chamber, CTD3 = Rock pile.

In the first part of the diagram, up until the end of December 2016, the CTD1 and CTD2 stations show wide oscillations in EC, due to the variation in tide levels that bring them alternatively to the higher layer of freshwater (EC circa 0.5 mS/cm), and to the underlying saltwater one (EC up to 45-50 mS/cm). The CTD3 station, on the other hand, initially shows constant EC values at around 0.2-0.3 mS/cm, which are clearly related to fresh water. The situation changes here starting from December 29, with rhythmical EC increases, which indicate the progressive intrusion of brackish water that becomes almost pure saltwater (EC > 20 mS/cm) starting from January 10, 2017. After that, compared to the CTD3 station's strong EC oscillations, the CTD2 station shows progressively less accentuated oscillations but within clearly marine values, with an EC of around 50 mS/cm.

4. Discussions

In the monitored period, the synchrony of all the water level fluctuations means that even in low flow rate conditions (below 0.3 m^3/s), there is not an upstream rising of the tide wave along the river but a general rise that involved the whole semi-submerged part of the karst system. This phenomenon is linked to the vertical movement of water in the saturated area, probably characterized by currently submerged conduits. Overall, the trend of the water level variations in the six monitoring stations shows that the PPUR behaves as one system in direct hydrostatic connection with the open sea, at least until the Blades Creek confluence. Upstream from this point, a morphological rise in the riverbed prevents the water from decreasing during low tide phases.

Concerning temperature fluctuations, the more external stations are affected by a high variation range. This phenomenon is tied to the fact that the probe alternatively finds itself in the upper and colder layer of fresh-saltwater and in the lower and warmer seawater one. Electrical conductivity fluctuations better show the dynamic of tides inside PPUR. The different behavior of the CTD1 and CTD2 sensors, compared to the CTD3 one, indicates a different effect of the tides on the interaction between fresh-brackish waters lens and the underlying saltwater. A possible explanation is that the lower layer of saltwater reached the probe only when the freshwater discharge decreased below a certain value. We must consider that in Rock pile, where the sensor was placed, the river has a smaller cross section and, consequently, with the same discharge, the height of the freshwater layer must be greater. The second possibility is connected to the occurrence of the low riverbed area located at the confluence of the Australian Inlet, which is due to the contribution of coarse fluvial sediments from this important tributary, fed by a swallow-hole which collects water from an external basin. This low riverbed area could influence the direct exchange between the waters of the inner sector and the outer sector (from the Australian Inlet confluence to the Outflow). The fact that, even in periods of extremely low water level, waters 200-250 m upstream of the Rock pile syphon appear to be completely meteoric, seems to better fit with the first hypothesis. In fact, it must be kept in mind that inside the aquifer the lens of freshwater that "floats" upon the saltwater, progressively thickens towards the inside and thus, from a specific point onward, prevents saltwater (or even brackish water) from reaching and mixing with the waters inside the cave.

5. Conclusion

Monitoring pointed out the occurrence of three different sectors inside the PPUR, whose dynamics surely also have important repercussions from a biological point of view. The first sector, from the entrance to the Australian Inlet confluence, has a behavior that is ultimately in direct connection with the open sea, demonstrating the existence of a deep, saturated area capable of quickly transmitting hydraulic head variations, which are tied to tidal oscillation.

The second sector, which develops from the Australian Inlet (or, more precisely, from an unspecified point upstream from it) to the Blades Creek confluence has a behavior that is still fully affected by the tides, with respect to water level variations, while temperatures are on average lower than sea water ones, even when, similarly to what happens in Rock pile, the halocline rises following the reduction of the freshwater layer's thickness.

The third, innermost sector, probably encompasses the area slightly downstream from the Daylight only, where the waterway flows on a rocky riverbed, whose morphology prevents the level from decreasing under a certain value. This sector does not appear to be directly connected with a deep saltwater layer.

In the monitored period, the system demonstrates the stability of the upper freshwater lens for at least four months, despite the strong fluctuations in water volume in the explorable cavity.

Acknowledgments

We gratefully thank the PPUR Park staff, the Protected Area Management Board, the local and National Authorities for the support given during our expeditions to PPUR and the GAIA Exploration Club of Manila and the La Karst Caving Group of Puerto Princesa, for the help given during the cave exploration.

References

BADINO G., DE VIVO A., FORTI P. and PICCINI L. (2017) Puerto Princesa Underground River (Palawan, Philippines): some peculiar features of a high energy, tropical coastal karst system. Geological Society of London, Spec. Publ. 466, 155-170.

CALLIGARIS C., CALAFORRA J.M., CUCCHI F., FORTI P., ZINI L. (2018) Effect of a strong rainstorm on the hydrodynamics of the Puerto Princesa Underground River (Palawan, Philippines) Acta Carsologica, 47/1, 53-67.

PICCINI L., IANDELLI N. (2011) Tectonic uplift, sea level changes and evolution of a coastal karst: the Saint Paul Mountain (Palawan, Philippines). Earth Surface Processes and Landforms, 36, 594-609.

Monitoring karst aquifers at Redstone Arsenal, a U.S. Army facility in Alabama, USA

Gheorghe M. L. PONTA(1), Stuart W. MCGREGOR(1),
Rebecca A. BEARDEN(1) & Christine F. EASTERWOOD(2)

(1) Geological Survey of Alabama, 420 Hackberry Lane, Tuscaloosa, Alabama 35401 U.S.A., gponta@gsa.state.al.us (corresponding author)
(2) US Army Garrison – Redstone Environmental Management Division 4488 Martin Road [IMRE-PWE] Redstone Arsenal, AL 35898

Abstract

Cave ecosystems at Redstone Arsenal (RSA), a U.S. Army facility in Madison County, Alabama, provide vital habitat for the federally endangered Alabama Cave Shrimp (Palaemonias alabamae) in Bobcat Cave and the Tuscumbia Darter (Etheostoma tuscumbia) in the Jaya Springs complex. The purpose of this study is to provide time series data (water level elevation, specific conductivity, and temperature) from two wells and two caves and discharge measurements and water analyses at the Jaya Springs complex to a multidisciplinary team, who will develop a management plan for a buffer zone around the spring to minimize potential urban development impacts on the caves and springs. In 2019-20, water-quality sampling indicates steady conditions in Bobcat Cave with little significant variation in chloride (0,9-4,2 mg/L), sulfate (0,7-3,7 mg/L), and nitrate (0,2-1,8 mg/L) concentrations compared to previous years, while water quality in Matthews Cave shows concentrations of chloride (1,3-5,9 mg/L), sulfate (2,1-4,5 mg/L), and nitrate (0,5-3,3 mg/L) slightly elevated over levels observed in Bobcat Cave. Preliminary water quality data for the Jaya Springs complex show the presence of chloride (3,2-5,3 mg/L), nitrate (0,089-0,919 mg/L), sulfate (0.72-5.06 mg/L), and elevated values for E.coli (39.3-307.6 Most Probable Number (MPN)/100 ml), and fecal coliform (3990-52470 Colony Forming Units (CFU)/100 ml). One water sample collected at well RS1559 stands out with specific conductance of 2140 µS/cm and total dissolved solids of 1620 mg/L. A recharge area (geographical watershed) was defined for the Jaya Springs complex based on surface watershed boundaries derived from 7.5 minutes topographic maps. Four water samples were collected at the end of the dry season (November 21, 2019) for radiocarbon analysis and the calibrated dates range between 1218 (Jaya Springs complex) and 20577 (Well RS1559) 14C age, years BP 1950, confirming the presence of shallow and intermediate aquifers in the study area.

1. Introduction and study area

Redstone Arsenal (RSA), a U.S. Army facility in Madison County, Alabama, was established in 1941 to support World War II military actions with chemical and munitions manufacturing. It later became an important site for the development of missile and rocket technology. As a result of these activities in some areas of RSA solvent releases occurred and soil and groundwater were contaminated. Overall, Comprehensive Environmental Response, Compensation and Liability Act (CERCLA) programs were established for the removal of nonaqueous-phase liquid (DNAPL) products. An extensive network of nested monitoring wells was installed (shallow, intermediate, deep) to delineate the horizontal and vertical extension of the contamination and to facilitate monitoring and cleanup. Some of these wells located in the recharge area of the Jaya Springs complex are part of our monitoring network.

RSA covers over 155 km^2. It is bounded on the south by the Tennessee River and on the west, north, and east by the cities of Madison and Huntsville (Fig. 1; Inset 1a). Activities on RSA and urbanization of areas hydrologically upgradient from the study area cause changes in runoff and potentially affect water quality.

Redstone Arsenal is situated in the Interior Low Plateaus Province Highland Rim Section Tennessee Valley Physiographic District. The area is underlain by the Mississippian-aged Tuscumbia Limestone and Fort Payne Chert, dipping south-southeast about 6 to 20 meters per kilometer (0.33 to 1-degree dip). In these formations sinkholes, springs, caves, and sinking streams are common (Fig. 1). Due to this horizontal bedding setup, water moves very slowly underground, with a velocity as low as 0,14m/hour, based on previously performed dye studies, subsequently influencing the age of the waters. Because the entire study area is underlain by karstifiable rocks, and is in a densely populated area, a high degree of risk to contamination exists.

Matthews Cave is a vadose/water table cave, with a single stream passage trending downdip. The cave is developed along a fracture-oriented north-northeast to south-southwest and the main passage narrows at the upstream and downstream ends. Fluctuations of water level during precipitation events are controlled by a small restriction located at the downstream end of the cave, creating a lake where the probe is installed.

Bobcat Cave is an incipient fissure network maze (labyrinthic) type cave developed along four fractures-oriented north-south, interconnected along two East – West fractures (50 m long each).

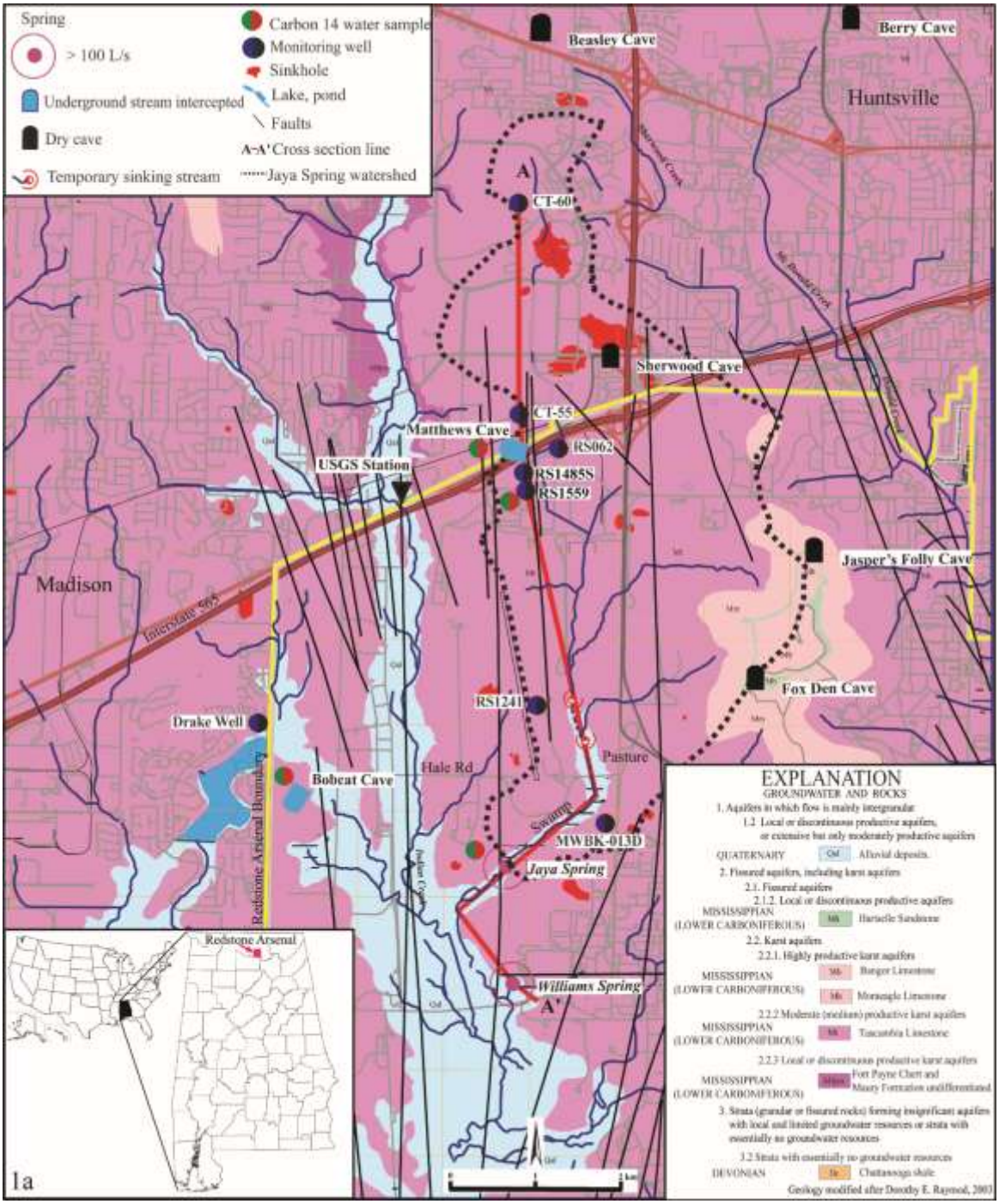

Figure 1: Simplified bedrock karst hydrogeological map of Redstone Arsenal and surrounding areas.

The *Jaya Springs complex* is a swamp recharged by several small springs, the largest and most upstream found just south of Hale Road. Their waters combine into a stream at the downstream end of the 1.5 km-long swamp.

2. Materials and methods

Time series water-level, specific conductivity, and temperature data were collected using data loggers on an hourly/daily schedule at two caves and two wells. Bobcat Cave has been monitored almost continuously since 1990, Matthews Cave since December 2019, and two wells since February 2020. The Jaya Springs complex has been monitored monthly (discharge measurements/water sampling) since December 2019. Precipitation data and gage height were obtained from the USGS 03575830 Indian Creek station located just north of RSA. Radiocarbon analysis was

performed at the University of Georgia. The quoted uncalibrated dates have been given in radiocarbon years before 1950 (years BP), using the ^{14}C half-life of 5568 years. Subsequently, these data were calibrated and corrected to 1950 (years BP).

A modified version of the International Association of Hydrogeologist legend was used on Figures 1 and 2 (Ponta, 2019). Figure 1 is a simplified bedrock karst hydrogeologic map, with the overburden/alluvial deposits which cover the entire area not displayed. A hydrogeologic cross section was produced to show the relationships among different geologic formations affecting RSA. Figure 2 also shows the water level elevation of selected wells, demonstrating the south trend of the water table towards Wheeler Lake/Tennessee River (not shown on the map, located 6,5 km south of Williams Spring). Matthews and Bobcat caves are developed at the interface between the Tuscumbia Limestone and Fort Payne Chert. Water samples from these two caves, well RS1559 (installed in Fort Payne Chert), and the Jaya Springs complex, originating in Tuscumbia Limestone, were sampled for radiocarbon and water quality analyses (Fig. 1; Fig.2). Well RS1559, with a total depth of 33 m (water sample was collected at this depth), is an existing well located 500 m south of Matthews Cave. The well is constructed in the Fort Payne Chert aquifer.

In Matthews Cave time series data were collected using one OTT ecoLog 800 datalogger with water level, specific conductance, and temperature measured hourly and that data transmitted to the GSA office daily using cellular communications technology. In Bobcat Cave time series data were collected using one OTT HydroMet datalogger installed at the south end of the cave where water level, specific conductance, and temperature are measured hourly in a lake. That data is downloaded quarterly.

The Jaya Springs complex has been monitored since November 2019 (discharge measurements and water quality). A recharge area (geographical watershed) was defined for the Jaya Springs complex based on the U.S.G.S. 7.5-minute topographic map (Fig. 1).

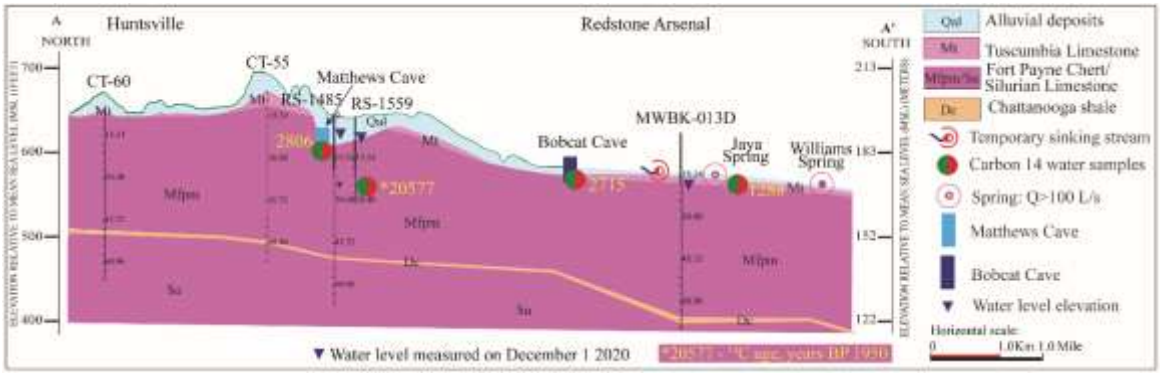

Figure 2: Simplified hydrogeological cross section.

3. Results and discussion

In December 2019, carbon in the water samples from RS1559, Matthews Cave, Bobcat Cave, and Jaya Springs complex, were aged and the calibrated dates range between 1218 (Jaya Springs complex), 2715 (Bobcat Cave), 2806 (Matthews Cave), and 20577 (Well RS1559) ^{14}C age, years BP 1950.

These findings confirm the presence of an intermediate aquifer in Matthews Cave, Bobcat Cave, and the Jaya Springs complex and a lower aquifer in well RS1559 and are backed up by water level elevation measurements in nested wells at the site. The water sample from RS1559 has a pH of 8,4, a specific conductance of 2140 µS/cm, and elevated values for chlorite (30,84 mg/L) and sulphate (682 mg/L). Nitrate was not detected.

Results of water-level investigations in Matthews Cave indicate that the hydrology of the cave is controlled by a stream originating a few hundred meters north of the cave (the sinking point is undefined) with a perceptible phreatic zone at the lower end of the cave during the dry season. Matthews Cave's temperature regime throughout the year ranged from 16,8 to 18,3°C and averaged around 17,8°C for the monitored period. Higher specific conductance values are associated with low water level elevation, which are diluted during higher water level elevation/discharge episodes. In 2019–20 Matthews Cave's chloride concentration ranged from 1,3 to 5,9 mg/L, sulfate from 2,1 to 4,5 mg/L and nitrate from 0,5 to 3,3 mg/L, values compared with previous years.

Results of water-level investigations in Bobcat Cave indicate that the hydrology of the cave is likely controlled by groundwater originating in the shallow karst terrain around the cave and a phreatic zone component recharged several kilometers away from the cave. These findings suggest that Bobcat Cave is a water table cave most of the time, with a stream component after abundant precipitation.

Bobcat Cave's temperature regime throughout the year ranged from 11,7 to 15,8°C and averaged around 13,7°C for the monitored period. Temperature generally was constant

between February and September, with large variations after storm events. In 2019–20 chloride ranged from 0,9 to 4,2 mg/L, sulfate from 0,7 to 3,7 mg/L, and nitrate from 0,2 to 1,8 mg/L. These values are slightly lower than those recorded in Matthews Cave

The discharge of the Jaya Springs complex for the period of monitoring was between 37 and 259 L/s, with pH values ranging from 7,10 to 7,80, specific conductivity between 307 to 393 µS/cm, and Total Dissolved Solids 157 to 212 mg/L. Chloride ranged from 3,2 to 5,3 mg/L, with the highest concentration at the lowest flow. Chloride values of 2 or less are naturally occurring. Concentrations of nitrate ranged from 0,089 to 0,918 mg/L. Sulfate concentrations ranged from 0,72 to 5,26 mg/L, the highest concentration detected at lowest flow. Calcium concentrations varied from 57,9 to 88,8 mg/L and the concentrations of sodium ranged between 1,93 and 2,72 mg/L. The presence of Mg2+ (ranged between 3,0 to 4,22 mg/L) in low concentrations compared to Ca2+. In natural waters unaffected by pollution, trace metals occur in low concentrations, generally <0,001 mg/L. Elevated trace metal concentrations may indicate the presence of a pollution source. Chromium was detected in one sample with a concentration of 0,0017 mg/L at a discharge of 259 L/s. The drinking water MCL (USEPA National Primary and Secondary Drinking Water Standard) for chromium (III) is 0,1 mg/L. Manganese ranged from 0,137 to 1,220 mg/L. The drinking water MCL for manganese is 0,05 mg/L. Cadmium was not detected in any samples. The CO2 concentration ranged from 5 to 23 mg/L., with the highest value corresponding to the highest flow.

The major ionic composition of water collected at the Jaya Springs complex is dominated by calcium, magnesium, and bicarbonate ions, typical of karst groundwater (calcium and magnesium bicarbonate type). Meanwhile, well RS1559 is dominated by sodium, potassium, and sulfate ions (sodium and potassium chloride or sodium sulfate type).

E. coli (39,3-307,6 MPN/100 ml) and fecal coliform (3990-52470 CFU/100 ml) were analyzed only at the Jaya Springs complex. These elevated numbers are related to a 1 km-long cow pasture located north of Hale Road at the head of the Jaya Springs complex.

4. Conclusion

Parameters investigated in this study exhibit seasonal as well as spatial variability. In the investigated aquatic systems specific conductance values varied with water level and discharge. Water-quality sampling indicates steady conditions in Bobcat Cave with little significant variation in chloride, sulfate, and nitrate concentrations compared to previous years, while water quality in Matthews Cave and the Jaya Springs complex show the presence of above-mentioned constituents, with concentrations of chloride, sulfate, and nitrate elevated over Bobcat Cave. Based on results of this limited preliminary data little effect of urban development has been observed on the Jaya Springs complex to date.

Four water samples were collected at the end of the dry season (November 21, 2019) for radiocarbon analysis and the calibrated dates range between 1218 (Jaya Spring) and 20577 (Well RS1559) ^{14}C age, years BP 1950 and suggest the presence of an intermediate and at least one lower aquifer.

Acknowledgments

The authors acknowledge the GSA Ecosystems Investigations Program and Groundwater Assessment Program teams that made this work possible. This project was prepared in cooperation with U. S. Army, Redstone Arsenal Environmental and Cultural Resources Directorate Under Contract No. W9126G-19-2-0037. We also acknowledge the Alabama Cave Survey, which provided access to their cave information database. GSA provided a monetary cost share for this research.

References

PONTA G.M.L., 2019 Karst Hydrogeology. In Ponta GML and Onac BP (eds.) Cave and Karst Systems of Romania. Springer International Publishing, Cham, pp 41-47

RAYMOND, D.E., 2003, Geologic map of the Madison 7.5-minute quadrangle, Madison County, Alabama; Geological Survey of Alabama QS29 Quadrangle Series

Relations between Isonzo river high plain phreatic aquifer and groundwater levels in the westernmost part of Classical Karst: Pozzo dei Frari case study (Gradisca d'Isonzo, NE Italy)

Rino SEMERARO[(1)], Federico VALENTINUZ[(2,3)], Stefano REJC[(3)] & Maurizio TAVAGNUTTI[(3)]

(1) rinosemeraro0@gmail.com
(2) Professional Geologist, geo.valentinuz@gmail.com
(3) Centre for Karst Research "C. Seppenhofer", Gorizia, Italy, seppenhofer@libero.it

Abstract.

As known, north-western part of the Classical Karst hydrostructure recharge comes mainly from losses of the Isonzo/Soča river and from autogenic recharge due to the diffuse infiltration on the karst plateau. To get more information a CTD-Diver coupled to a Baro-Diver probe have been installed in the Pozzo dei Frari in Gradisca d'Isonzo. To evaluate aquifer recharge variations, groundwater levels have been compared with Isonzo and Vipacco river discharge and with meteorological data. Mean EC values compared with bibliographic data indicate that the average contribution of Isonzo river to the recharge of this area of the aquifer is about 75%. The observed inverted groundwater temperature trend (with maximum values reached in November/December and minimum values in June/July) with respect to air temperature and Isonzo river temperature could be due to the recharge from Isonzo river (characterized by cold waters) that prevails in low level conditions. The observed evolution of EC after main recharge events shows a short decrease followed by a clear increase, which is interpreted as a piston effect (pushing of more mineralized waters in the shaft).

1. Introduction

Isonzo/Soča river (NE-Italy) flows from NE to SW in the alluvial High Plain at the foothill of the Classical Karst plateau. Gradisca d'Isonzo old town was built on two isolated limestone spurs, on the right bank of the river at about 30 m a.s.l. (Fig. 1). These outcrops are separated from the north-western Classical Karst by Isonzo thalweg but are geologically connected. In the limestone of Gradisca, among the natural karst shafts and artificial cavities which intercept the karst aquifer, the best known is the Pozzo dei Frari located in Campiello Emo. It is a dug well that was excavated at the end of 1400s, discovering a karst cavity with drinking water after 6 meters (Martinis, 1953). The shaft was used until the 1960s and is well known for the constant presence of the Proteus anguinus s.l. Laurenti, 1768 (Berini, 1826). To verify the possible relations with the hydrometry of Isonzo River, and the rainfalls of the area a CTD-Diver probe was installed by the Centre for Karst Researches "C. Seppenhofer" of Gorizia (Italy) in the water basin of the Pozzo dei Frari. This instrument recorded level, temperature and electrical conductivity variations.

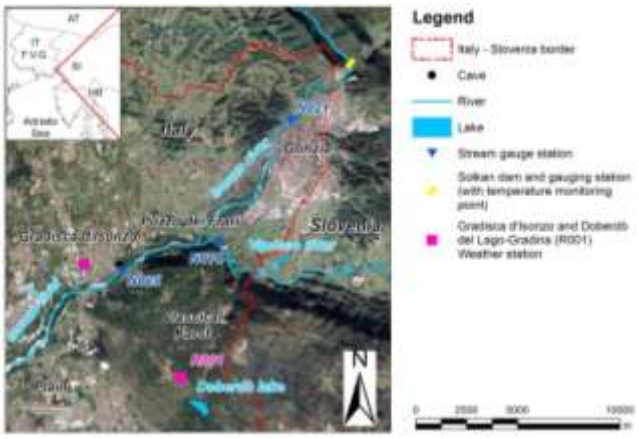

Figure 1: Geographical setting with meteorological and hydrographic stations considered in this study (modified from Google Earth, 2020 Maxar Technologies Image© CNES/Airbus).

2. Geological and hydrogeological settings

The Gradisca d'Isonzo area (Fig. 2) corresponds to the north-western border of the Classical Karst carbonate platform characterized by the outcrops of Paleocene-Eocene terms and in stratigraphic succession of the Eocene Flysch. Bedrock is covered by Quaternary alluvial sediments deposited mainly by Isonzo River in the plain. Mesozoic and Cenozoic carbonates outcrop on the NW slope of the Karst plateau on the Isonzo River left bank (Jurkovšek et al., 2016). The carbonate rockmass is fissured and karstified to varying degrees. The area beyond the Isonzo River, in front of Gradisca, has SE-NW faults crossing the north-eastern Classical Karst.

The high alluvial plain of Isonzo river is formed by coarse-grained sediments (mainly gravels, irregularly cemented in

conglomerate horizons and intercalated by sandy and clay layers). These deposits are a consequence of the rapid progradation of Isonzo River megafan in the Last Glacial Maximum (LGM - Upper Pleistocene) (Martelli et al., 2015). Bedrock deep is only estimated in the area between Gradisca and the Classical Karst plateau (Nicolich et al., 2004). Bedrock depth ranges between (average) ca. 25 m and 0 m a.s.l. around the limestone outcrop of Gradisca.

From a hydrogeological point of view, alluvial plain is characterized by a phreatic aquifer mainly recharged by Isonzo river. The direction of the gradient of the water table (direction of groundwater movement) is from ENE-WSW. In average flow conditions alluvial plain's groundwater contour lines are located between 24 and 22 m a.s.l. (Zini et al., 2014). A karstic aquifer develops in the carbonate platform rocks. In the floodplain the alluvial aquifer is in direct contact with the Classical Karst aquifer. This is demonstrated by hydrological, geochemical and speleological data (e.g., Bidovec, 1965; Morgante et al., 1966; Gemiti & Licciardello, 1977; Flora & Longinelli, 1989; Doctor et al., 2006; Calligaris et al., 2018, etc.). Data indicate that the North-Western part of the karst hydrostructure is mainly recharged from losses of Isonzo river. Urbanč et al. (2012) and Calligaris et al. (2019a) recently quantified recharge from the river to be about 10 m^3/s. Autogenic recharge from diffuse infiltration on the karst plateau should be added.

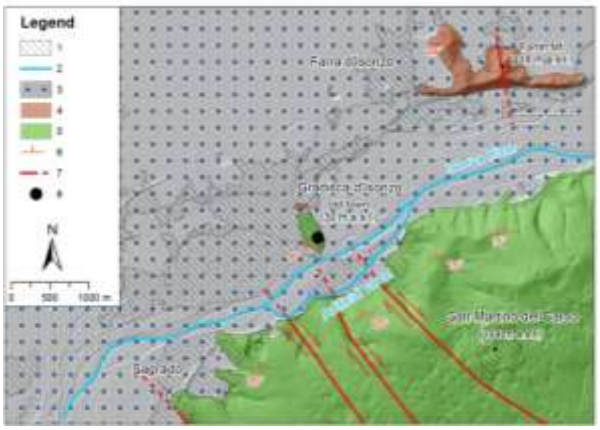

Figure 2: Geological sketch of the area: 1) urbanized area, 2) river/canal, 3) Quaternary deposits, 4) Flysch, 5) carbonate platform formations, 6) dip and strike strata, 7) fault, certain (continuous line), covered/interpreted (dashed line), 8) cave: Pozzo dei Frari.

3. Morphology of Pozzo dei Frari

The Pozzo dei Frari (2713/VG 4911 caves cadastre, WGS84 latitude 45° 53' 19.4845" and longitude 13° 30' 15.5115") (Fig. 3) is located in the city historic area. The entrance is at 29.95 m a.s.l., the depth is 19 m and the lenght is 5 m. Water level was 23.63 m a.s.l. (conventionally) during the topographic survey on November 16, 2018. The shaft develops in the Alveolinid-Nummulitid limestone in strata up to one meter thick, the natural part has an almost cylindrical section, at about 2 m above the bottom an important 112° oriented subvertical joint leads to a narrow impracticable cavity (Russo, 2019), certainly connected to the karst network. The bottom of the natural shaft is at an altitude of 10.95 m a.s.l.

Figure 3: The Pozzo dei Frari in Gradisca d'Isonzo.

4. Method and instruments

To get more information about recharge dynamics of the karst aquifer on the right bank of Isonzo river, a CTD-Diver D1271 probe produced by Eijkelkamp (Netherlands), coupled to a Baro-Diver probe, to record temperature (T), electrical conductivity (EC, K_{25}) and water levels (H) have been installed in the "Pozzo dei Frari". The technical characteristics of the CTD-Diver are the following: deep range 0-10 m, typical accuracy ± 0.05% full scale, long-term stability ± 0.2%, resolution 0.2 cm. Electrical conductivity: measuring range 0-30 mS/cm (set by the operator), accuracy ± 1%, resolution ± 0.1%. The range of the Baro-Diver probe for measuring atmospheric pressure is 150 cm of water column, accuracy of 0.5 cm and resolution 0.1 cm. The temperature range measured by both instruments is –20-80 °C, accuracy ± 0.1 °C, resolution ± 0.01 °C.

The monitoring lasted for about a year (from 16.11.2018 to 21.11.2019) and the measurement interval was set in 30 min. To evaluate aquifer recharge variations, groundwater level data have been compared with Isonzo and Vipacco river discharge and rainfalls measured by the regional monitoring network (Regione Autonoma Friuli Venezia Giulia, 2020).

5. Results of monitoring

The data recorded by the Baro-Diver probe and the CTD-Diver probe are shown in Fig. 4. During the monitoring period groundwater level oscillated between 22.87 m a.s.l. and 26.55 m a.s.l. (average level 23.62 m a.s.l.). Cumulative rainfall in the monitoring period was 1309.7 mm in Gradisca and 1250.2 mm in Doberdò while mean air temperature was respectively 14.14 °C and 14.55°C.

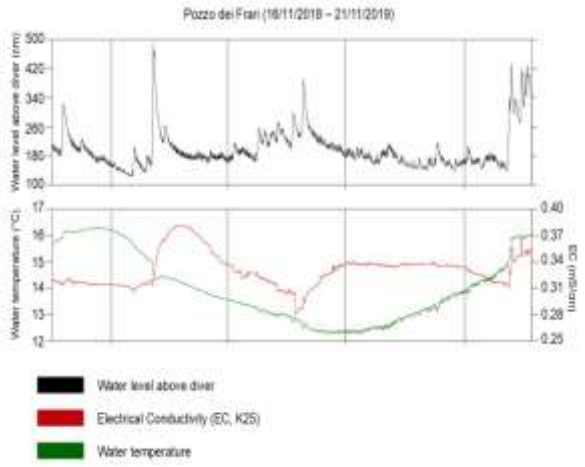

Figure 4: Data registered by CTD-Diver in the water basin of Pozzo dei Frari (water level, electrical conductivity, temperature).

The minimum and maximum air temperatures were respectively –4.5 °C and 36.9°C and have been measured in Gradisca in 26.01.2019 and in 26.06.2019. Mean Isonzo river discharge was respectively about 95.6 m^3/s at Isonzo Piuma monitoring point and 84.1 m^3/s at Gradisca monitoring point. Vipacco river medium discharge at Savogna was 13.2 m^3/s (Fig. 5). An artificial channel, departs about 1 kilometer upstream to Gradisca from a weir on the river and give back water downstream to the monitoring point (Fig. 2). The exact amount of the channel discharge is not known, but have been estimated in 10-15 m^3/s by Regione Autonoma Friuli Venezia Giulia (2020).

Despite Vipacco river inflow, in the monitoring period a decrease of Isonzo river total discharge was observed between Gorizia and Gradisca due to the water leaks from the gravelly riverbed to the alluvial plain aquifer and to the Classical Karst hydrostructure. As the exact channel's discharge in the monitoring period is not known, is not possible to calculate the amount of river losses that feed groundwater during the monitoring period. The groundwater electrical conductivity (EC K_{25}) fluctuated between 281 and 382 µS/cm (average 331 µS/cm). Groundwater temperature varied between 12.24 °C (09/07/2019) and 16.30 °C (23/12/2018).

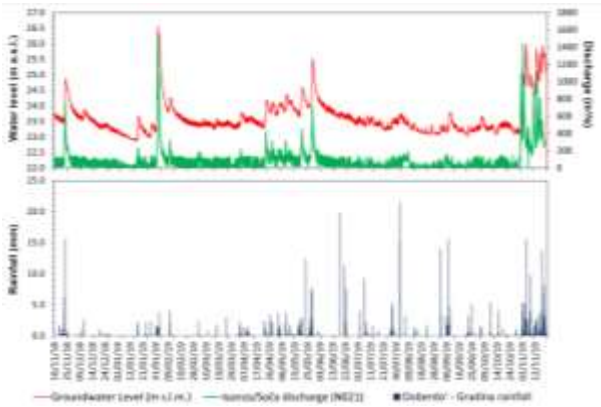

Figure 5: Comparision between water level in the Pozzo dei Frari, Isonzo river discharge (Solkan gauging station), precipitation of Doberdò Gradina (weather station).

The average value was 14.00 °C. Shaft's maximum air temperature was 22.61 °C (06/09/2019) while minimum 11.84 (03/02/2019) the medium value was 16.64 °C. Water temperature has an inverted trend with respect to air temperature, with maximum values reached in November/December and minimum values in June/July (Fig. 6). As demostrated by Calligaris et al. (2019b) Isonzo river waters that infiltrate into the karstic plateau are characterized by low EC values. Pozzo dei Frari's mean EC values are about 10 µS/cm lower than those measured in the Doberdò lake. Comparing measured values with that indicated by Calligaris et al. (2019b), an average contribution of Isonzo river to the recharge of this part of the aquifer of about 75% can be hypothesized.

Analyzing the trend of EC over time, several peaks can be observed during increases of groundwater level in the well related to flood events, the main one being observed in February 2019. The maximum Isonzo discharge was 1535.15 m^3/s, and the Pozzo dei Frari's water level increased of about 3.5 m and was registered 7 h after the maximum river discharge. After the level increase EC initially decreased and then raised reaching values up to 60 µS/cm higher than in initial conditions about 20 days after level maximum. This is an index of mobilization of more mineralized waters (piston flow effect) that enter in the shaft when the water head decrease after a flood coming from deepest layers of the aquifer or from that areas characterized by lower hydraulic conductivity. Some floods episodes are characterized by more infiltration inputs (frequent rainstorms and river water increase) e.g. from April to July 2019. In these periods in the shaft prevails low conductivity waters coming from autogenic and allogenic recharge. A drastic EC and groundwater temperature increase (due to mobilization of more mineralized waters) was observed in November 2019, after Isonzo river discharge reached 1445 m^3/s. Following Isonzo river discharge peaks maintain high water level conditions with temperature and water level fluctuations.

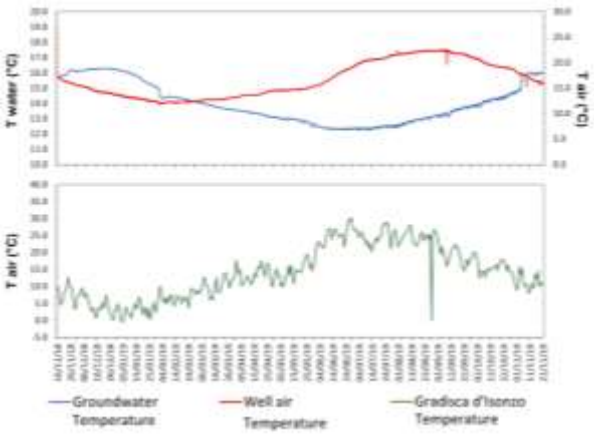

Figure 6: Comparision between groundwater temperature and air temperature of Pozzo dei Frari and mean daily atmospheric temperature of Gradisca d'Isonzo.

Soča/Isonzo river water temperature for the monitoring period measured in Solkan (Slovenia), about 4.5 km upstream for Piuma bridge (Ministrstvo za okolje in prostor, 2020) indicate that minimum temperature (3.7 °C) was observed in January and the maximum temperature in

summer (up to 17.5 °C in the period from July to September), main value was 10.1 °C.
Waters characterized by longest circulation time (likely from the deepest sectors of the aquifer) and from the autogenic recharge alternatively enter in the well during high flow conditions.
In this area of northwestern Classical Karst the Isonzo river and rainfalls contribute to the recharge of the karst aquifer and the relationship between Alluvial Plain porous aquifer and karst's groundwater flow should be investigated using chemical an isotopic methods (natural tracers) as demonstrated by Flora & Longinelli (1989) and Doctor et al. (2006) and monitoring at the same time water level, EC and water temperature in the two different phreatic and karst aquifers.

Acknowledgments

The authors thank CaRiGo–Gorizia Foundation for the contribution to the research cost. The speleologists of Centre for Karst Research "Carlo Seppenhofer" (Gorizia) Felice Bellio and Mauro Pincin for their collaboration. Luciano Russo (Trieste) for the underwater survey in cave. The Regione Autonoma Friuli Venezia Giulia Central (Directorate for Environment, Energy and Sustainable Development, Water Resources Management Service) and Alberto Deana for the meteorological and hydrographic data too. Finally, we thank the reviewers for their suggestions and for comments and critical reviews that significantly improved the manuscript.

References

BERINI G. (1826) Indagine sullo stato del Timavo e delle sue adiacenze al principio dell'era cristiana.- Opera 65 pp.

BIDOVEC F. (1965) The hydrosystem of karstic springs in the Timavo Basin.- Actes du Coll. Dubrovnik, Hydrologie des roches fissurées, AIHS-UNESCO, 1, 263–274.

CALLIGARIS C., MEZGA K., SLEJKO F.F., URBANC J. & ZINI L. (2018) Groundwater Characterization by Means of Conservative (δ18O and δ2H) and Non-Conservative (87Sr/86Sr) Isotopic Values: The Classical Karst Region Aquifer Case (Italy–Slovenia).- Geosciences 2018, 8, (321), 1–25.

CALLIGARIS C., CASAGRANDE G., LERVOLINO D., LIPPI F., OLIVO P., RAMANI M., TREU F. & ZINI L. (2019a) Water-budget as a tool to evaluate the sustainable use of groundwater resources (Isonzo Plain, NE Italy).- Rend. Online Soc. Geol. It., 47, 7–12.

CALLIGARIS C., GALLI M., GEMITI F., PISELLI S., TENTOR M., ZINI L. & CUCCHI F. (2019b) Electrical Conductivity as a tool to evaluate the various recharges of a Karst aquifer.- Rend. Online Soc. Geol. It., 47, 13–17.

CAMIS (2014) Progetto attività coordinate per la gestione del fiume Isonzo. Reg. Auton. Friuli Venezia Giulia, Adstra Eng. Srl, 44 pp.

DOCTOR D.H., ALEXANDER E.C. JR., PETRIČ M., KOGOVŠEK J., URBANC J., LOJEN S. & STICHLER W. (2006) Quantification of karst aquifer discharge component through end-member mixing analysis using natural chemistry and stable isotopes as tracers.- Hydrogeol. J., 13, 1171–1191.

FLORA O. & LONGINELLI A. (1989) Stable isotope hydrology of Classical Karst area, Trieste, Italy.- Proc. Adv. Group Meeting on the application of isotope techniques in the study of the hydrology of fracturated and fissurated rocks, I.A.E.A., Wien 1986, 203–213.

GEMITI F. & LICCIARDELLO M. (1977) Indagine sui rapporti di alimentazione delle acque del Carso Triestino e Goriziano mediante l'utilizzo di alcuni traccianti naturali.- Ann. Gruppo Grotte Ass. Trenta Ottobre, Trieste, 6, 43–61.

JURKOVŠEK B., BIOLCHI S., FURLANI S., KOLAR-JURKOVŠEK T., ZINI L., JEŽ J., TUNIS S., BAVEC M. & CUCCHI F. (2016) Geology of the Classical Karst Region (SW Slovenia – NE Italy). Map 1:50.000.- J. of Maps, 12 pp. [online] http://dx.doi.org/10.1080/17445647. 2016.1215941

MARTELLI G., GRANATI C. & POLI M.E. (2015) Geological context of the Friulan Plain.- WARBO-Life-Europ., Final Rep., Annex 58, 9–13.

MARTINIS B. (1953) Fenomeni carsici nel sottosuolo di Gradisca d'Isonzo (Gorizia).- Rass. Spel. It., 5 (3), 102–104.

MINISTRSTVO ZA OKOLJE IN PROSTOR (2020) Agencija Republike Slovenije za Okolje, Arhiv hidroloških podatkov, dnevni podak.

MORGANTE S., MOSETTI F. & TONGIORGI E. (1966) Moderne indagini idrologiche nella zona di Gorizia.- Boll. Geof. Teor. Appl., 8 (30), 114–137.

NICOLICH R., DELLA VEDOVA B. & GIUSTINIANI M. (2004) Carta del sottosuolo della Pianura Friulana. Note illustrative.- Reg. Auton. Friuli Venezia Giulia, Firenze, 32 pp.

REGIONE AUTONOMA FRIULI VENEZIA GIULIA (2020) Elaborati vari: Scala portate Fiume Isonzo e Fiume Vipacco 2013-2018 / Temperature e piogge Doberdò / Pozzo 032 Villesse 2019-2019.- Dir. Centr. Ambiente, Energia e Sviluppo Sostenibile, Unità operativa idrografica.

RUSSO L. (2019) Relazione sull'ispezione subacquea al Pozzo dei Frari di Gradisca (2713/VG 4911) del 16 novembre 2019.- Rapporto e rilievo topografico, 2 pp. (unpublished).

URBANČ J., MEZGA K. & ZINI L. (2012) An assessment of capacity of Brestovica–Klariči karst water supply (Slovenia).- Acta Carsologica, 4 (1), 89–100.

ZINI L., CUCCHI F., TREU F., BIOLCHI S., BOCCALI C., CLEVA S., ZAVAGNO E., BORGA M., MARRA F., ZOCCATELLI D., ZUECCO G., FAZZINI M., RUSSO S. & VACCARO C. (2014) Idrogeologia dell'Alta Pianura Isontina.- Progetto GEP, Edizioni Università degli Studi di Trieste, 19–27.

Hydrogeochemical and stable isotope properties of the dripwaters in the caves of the Moravian Karst (Czech Republic)

Veronika SYNKOVÁ & Pavel PRACNÝ

Department of Geological Sciences, Faculty of Science, Masaryk University, Kotlářská 267/2, 611 37, Brno, Czech Republic, vsynkova@mail.muni.cz (corresponding author)

Abstract

The dripwater hydrology and chemical parameters are used to determine water flow paths and reservoir properties of upper karst. This work was aimed to advance previous research in Moravian Karst (Czech Republic) with data on the isotopic composition of the water. The study is focused on the stable isotopic composition ($\delta^{18}O$ and $\delta^{2}H$) and hydrogeochemical properties (i.e., EC, T, discharge, pH, alkalinity, Ca^{2+} concentration or mineral saturation) of samples systematically collected quarterly between fall of 2018 and spring of 2020. The observed stable isotope composition naturally reflects the origin of the dripwater from a meteoric water. The results show higher variability of isotopic composition in seasonal drips with variable discharge, whereas one of the permanent drips shows very low isotopic variability indicating the isolated and well-mixed source of water from epikarst. Also, a somewhat similar behaviour of isotopic composition was observed in a drip with anomalous hydrochemical composition (caused most probably by prior calcite precipitation in upper cave levels). Finally, the isotopic composition of the underground river Punkva in the same cave system was studied for comparison and it shows isotopic enlightenment with respect to dripwaters.

1. Introduction

Karst dripwaters are a significant factor of speleothem origin providing diverse proxy data about paleoenvironment (e.g., FAIRCHILD *et al.* 2006). Dripwater hydrogeochemistry identifies the processes occurring on flow paths in a karst system such as CO_2 formation, dissolution, prior calcite precipitation (PCP), etc. Variations of $\delta^{18}O$ and $\delta^{2}H$ in precipitation are used to trace groundwater or air-mass trajectories. Dripwater $\delta^{18}O$ and $\delta^{2}H$ indirectly offer insight into the residence time of water in the epikarst and possible fractionation along that pathway (LACHNIET 2009).

Speleothems in the Moravian Karst (Czech Republic) are well studied, but only limited isotopic data is available, especially long-term monitoring is lacking. Despite utilizing a few analyses of $\delta^{18}O$, $\delta^{2}H$ and $\delta^{13}C$, the research of PRACNÝ *et al.* (2016a, 2016b) was focused on conventional hydrochemical parameters. An anomalous drip showing hydrogeochemical properties different from other regular drips in the Punkva Caves (Moravian Karst) was identified. The anomalous drip differs by lower saturation with respect to calcite, lower mineralization, enhanced Mg/Ca and Sr/Ca ratios, and increased $\delta^{13}C$. It was suggested that the anomalies are a result of PCP or/and water mixing in the vadose zone (e.g., FAIRCHILD *et al.* 2000).

The following study aims to supplement the previous research with long-term $\delta^{18}O$ and $\delta^{2}H$ data compared with hydrogeochemical properties of dripwater collected from the caves (Punkva, Kateřinská) and the river Punkva.

Sample	Punkva river	usual dripwaters						anomalous dripwater	d.c.
	P	A	CP1	CP2	CP3	K1	TC2	TC1	
EC [µS/cm]	508.17 ± 91.28	483.00 ± 52.36	642.67 ± 9.54	641.33 ± 14.61	643.17 ± 7.19	544.67 ± 22.59	597.17 ± 36.69	**320.80 ± 23.93**	us > an
Q [mL/hr]			430.69 ± 317.67	152.91 ± 17.57	442.43 ± 293.41	70.48 ± 17.07	346.12 ± 284.58	**717.82 ± 375.22**	us < an
T_{wall} [°C]		8.33 ± 0.80	8.23 ± 0.57	8.33 ± 0.55	8.38 ± 0.56	8.13 ± 1.15	7.77 ± 1.02	7.74 ± 1.11	
T_{water} [°C]	7.15 ± 0.70	7.72 ± 0.34	8.28 ± 0.20	8.42 ± 0.19	8.40 ± 0.15	8.47 ± 0.24	7.97 ± 0.34	7.92 ± 0.32	
pH	7.43 ± 0.23	7.75 ± 0.12	7.84 ± 0.28	7.92 ± 0.17	7.76 ± 0.20	8.07 ± 0.12	7.68 ± 0.26	7.81 ± 0.05	
alkalinity [mmol/L]	2.76 ± 1.18	3.96 ± 0.47	5.90 ± 0.18	5.76 ± 0.16	5.93 ± 0.33	4.16 ± 0.23	5.22 ± 0.19	**2.27 ± 0.80**	us > an
Ca^{2+} [mmol/L]	1.88 ± 0.55	2.40 ± 0.27	3.33 ± 0.29	3.31 ± 0.23	3.34 ± 0.23	2.60 ± 0.06	3.15 ± 0.07	**1.49 ± 0.10**	us > an
$SI_{calcite}$	0.20 ± 0.29	0.41 ± 0.11	0.78 ± 0.27	0.86 ± 0.16	0.71 ± 0.20	0.78 ± 0.14	0.56 ± 0.27	**0.05 ± 0.18**	us > an
$logPCO_{2(w)}$	−2.35 ± 0.36	−2.48 ± 0.15	−2.40 ± 0.28	−2.49 ± 0.17	−2.32 ± 0.19	−2.78 ± 0.12	−2.30 ± 0.27	−2.79 ± 0.08	
$\delta^{18}O$ [‰]	−9.16 ± 3.5	−10.07 ± 3.1	−9.96 ± 1.9	−9.95 ± 2.3	−9.86 ± 1.0	−9.81 ± 4.8	−10.12 ± 2.3	−10.03 ± 0.6	
$\delta^{2}H$ [‰]	−64.16 ± 2.7	−70.32 ± 1.2	−69.15 ± 1.2	−69.39 ± 1.2	−69.12 ± 1.5	−69.78 ± 0.8	−70.90 ± 1.0	−69.60 ± 0.9	

d.c. – drip comparison; us – usual; an – anomalous; EC – mean conductivity; Q – mean discharge; T_{wall} – mean cave wall temperature; T_{water} – mean water temperature; $SI_{calcite}$ – mean saturation indices for calcite; $logPCO_{2(w)}$ – mean saturation indices for CO_2 in water; $\delta^{18}O$ – mean ratio of ^{18}O and ^{16}O; $\delta^{2}H$ – mean ratio of ^{2}H and ^{1}H

Figure 1: Data on dripwater hydrogeochemistry and isotopic composition (mean values with the standard deviations of six measurements for each sample).

2. Study site, materials, and methods

Dripwater hydrochemistry and isotopic composition were studied in the Punkva Caves and the Kateřinská Cave (Moravian Karst, Czech Republic) and compared with the underground river Punkva. Both cave systems have been formed in Devonian limestone of Macocha Group strata in the central part of the Moravian Karst. The altitude of caves is ca. 350 m, while the plain above the cave varies between 450 and 550 m. The cave systems are situated approximately 1.6 km apart, and the WGS84 coordinates of the Punkva Caves entrance are 49.3714922N, 16.7256058E. Water samples were collected quarterly between fall of 2018 and spring of 2020. A total of 42 cave drip water and 6 river water samples were collected. In the Punkva Caves, there were six sampling sites chosen by the previous studies (three drips in the passage behind the Přední Chamber labelled CP1, CP2 and CP3; two drips in the Tunnel Corridor – TC1 and TC2; a pool located near the Angel pillar – A) (Fig. 3B). In the Kateřinská Cave, there was one sampling point in the Chaos Chamber, situated below the upper cave floor (K1). Most of the drips come from straw stalactites; the only exception is the drip TC1 which falls from a drapery about 30 cm in length. The river Punkva (P) was sampled from a surface flow ca. 700 m downstream from the entrance to the Punkva Caves.

The external temperatures (T_E) and precipitation (PR) were provided by the Cave Administration of Czechia from the Sloup (1/11/2018–18/1/2020) and Holštejn (19/1/2020–2/3/2020) stations situated 5 km from the caves.

The temperature of the dripwater (T_D) and the cave wall (T_W), electrical conductivity (EC), pH and drip rate were measured on-site. Drip discharge (Q) was calculated from the drip rate using the constant drip volume 0.14 mL measured by GENTY & DEFLANDRE (1998). The temperature of the cave wall was measured by a non-contact infrared thermometer (prec. 0.1 °C). EC and dripwater temperature were measured by a conductivity meter GMH Greisinger 3400 series (precision ± 0.5%). pH was measured by WTW pH meter 330i with sensor SenTix 61 (prec. ± 0.003 pH).

Subsequently, a laboratory analysis of alkalinity (acidimetric microtitration using 0.005 or 0.01 M HCl as a titrator) and calcium concentration (complexometric microtitration, indicator calcein) were conducted. $\delta^{18}O$ and $\delta^{2}H$ were determined at the laboratory of the Czech Geological Survey using High-Resolution Laser Absorption Spectroscopy (LWIA). Analytical uncertainties for $\delta^{18}O$ are 0.15‰ and 0.5‰ for $\delta^{2}H$. Samples collected in March 2019 were analyzed at the Stable Isotopes Laboratory of the Charles University using High-Temperature Conversion Element Analyzer (Thermo TC/EA and MAT253 mass spectrometer; analytical uncertainties are <0.2‰ for $\delta^{18}O$ values and <1.0‰ for $\delta^{2}H$ values). All values were calibrated against and reported in permill (‰) relative to V-SMOW. Saturation indices for calcite ($SI_{calcite}$) and partial pressure of CO_2 with which would the water be in equilibrium ($logPCO_{2(w)}$) were calculated using PHREEQC software and the default thermodynamic database (APPELO &PARKHURST, 2013).

Statistical analyses and graphs were generated using Statistica 12. Pearson's (r) and Spearman's (R) correlation coefficients were obtained using significance level $\alpha = 0.05$.

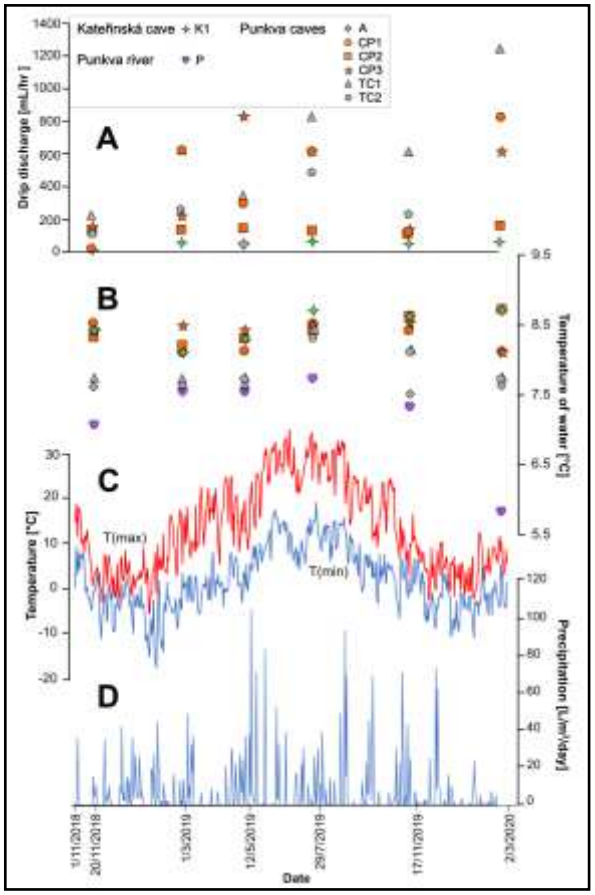

Figure 2: Meteorological and hydrological data. A) Drip discharges, B) Temperature of water, C) External maximum and minimum temperatures, D) Daily rainfall.

3. Results

Overview of hydrogeochemical properties is presented in Figure 1. The drips show negligible variability of pH (var. coeff. 0.7–3.6 %). Mean EC of the drip TC1 is 320.8 ± 23.93 µS/cm, whereas the drips CP1–3, TC2 and K1 show conductivity almost twice as high. Samples P and A show much higher EC than TC1. TC1 shows the highest mean discharge (717.82 ± 375.22 mL/hr) and medium variability (55.6 %) (Fig. 2A). The mean alkalinity of the drip TC1 is 2.27 mmol/L, while regular drips show ca. two-fold values. The value of mean Ca^{2+} for CP1 (1.49 ± 0.10 mmol/L) is only half of the values of other drips. While most of the drips show supersaturation with respect to calcite, the drip TC1 is close to equilibrium with calcite ($SI_{calcite}$ = 0.05 ± 0.18).

The T_D of drip water ranged from 7.5 °C to 8.7 °C, while the values of Punkva varied from 5.8 °C to 7.7 °C. The lowest mean T_D had the drip A (7.72 ± 0.34 °C), whereas the highest mean T_D had the K1 (8.47 ± 0.24 °C) (Fig. 1 and 2B).
The daily mean T_E was 7.08 ± 2.51 °C. Daily T_E ranged from −17.6 °C to 20.2 °C (Fig. 2C). Daily mean PR reached up to 6.12 L/m²/day. The highest monthly mean PR was 0.14 L/m²/month (May 2019), the lowest value was 0.01 L/m²/month (Jan. 2020) (Fig. 2D).
The statistically significant correlations of all data showed dependencies of $logPCO_{2(w)}$ against EC (r = 0.52; R = 0.51) and alkalinity (r = 0.56; R = 0.41). The drips CP1–3 and K1 show correlations of pH with $SI_{calcite}$ (r = 0.99), and Ca^{2+} with EC (r = 0.93; R = 0.83). The water temperature and discharge show negative correlations (r = −0.11; R = −0.39). The external and water temperature correlate (Fig. 2B and 2C). The drip discharge does not directly increase with the precipitation indicating some time delay (Fig. 2A and 2D).

Measured values of $\delta^{18}O$ and $\delta^{2}H$ plotted against the meteoric water lines are given in Figure 3A, and the data do not correspond with the closest well-defined lines from Prague and Vienna. The minimal mean $\delta^{18}O$ showed the drip TC2 (−10.12‰) while the maximal mean $\delta^{18}O$ showed the drip K1 (−9.81‰). The highest variation in $\delta^{18}O$ showed the drip K1 (var. coeff. −4.8%), although it seems to be an erroneous measurement, while the lowest variation showed the drip TC1 (−0.6%). The minimum of mean $\delta^{2}H$ was −70.90 ‰ (TC2) and the maximum was −69.12 ‰ (CP3). The highest variations in $\delta^{2}H$ showed the drip CP3 (−1.5%), whereas the minimal variation showed the drip K1 (−0.8%).
According to SMART & FRIEDRICH (1986) and BAKER *et al.* (1997), the drips CP1, CP3, TC1 and TC2 classify as seasonal drips (high flow variations and fast discharge), while CP2 and K1 show seepage flow regime (yearlong stable outflow with minor variations and large water source) (Fig. 3C).

4. Discussion

Hydrogeochemical properties of the drip TC1 differed significantly from other drips in terms of lower mineralization (expressed by EC and Ca^{2+} concentration) and alkalinity, almost negligible supersaturation with respect to calcite and slightly higher discharge (Fig. 1). This corresponds with the "anomalous" properties of TC1 observed by PRACNÝ *et al.* (2016). This anomaly was attributed to prior calcite precipitation along the flow path.
The isotopic composition showed a minimal variation of $\delta^{18}O$ and low variation of $\delta^{2}H$ compared to the rest of the drips (Fig. 3A). The stable isotopic composition could be a result of a capacious aquifer with long residence time, where water is mixed and the variability of $\delta^{18}O$ and $\delta^{2}H$ declines. This is contradicted by the high variation of TC1 discharge, which does not indicate a voluminous aquifer (Fig. 1). Another contributing mechanism might be the PCP in upper cave levels.
Apart from a sample from March 2019 (due to the extreme value, the sample was probably inappropriately sampled, stored, transported, or analyzed), the drip K1 showed constant $\delta^{18}O$ and low $\delta^{2}H$ variation (Fig. 3A). This could be a result of a voluminous aquifer with long residence time as the drip does not reflect the expected seasonal variability of isotopic composition. It might also suggest a homogenization during water mixing of meteoric water flowing through crevices in unsaturated zone as proposed by FAIMON *et al.* (2016), who assumed a complicated flow path of this drip, where the effects of surface processes are delayed or dampened.

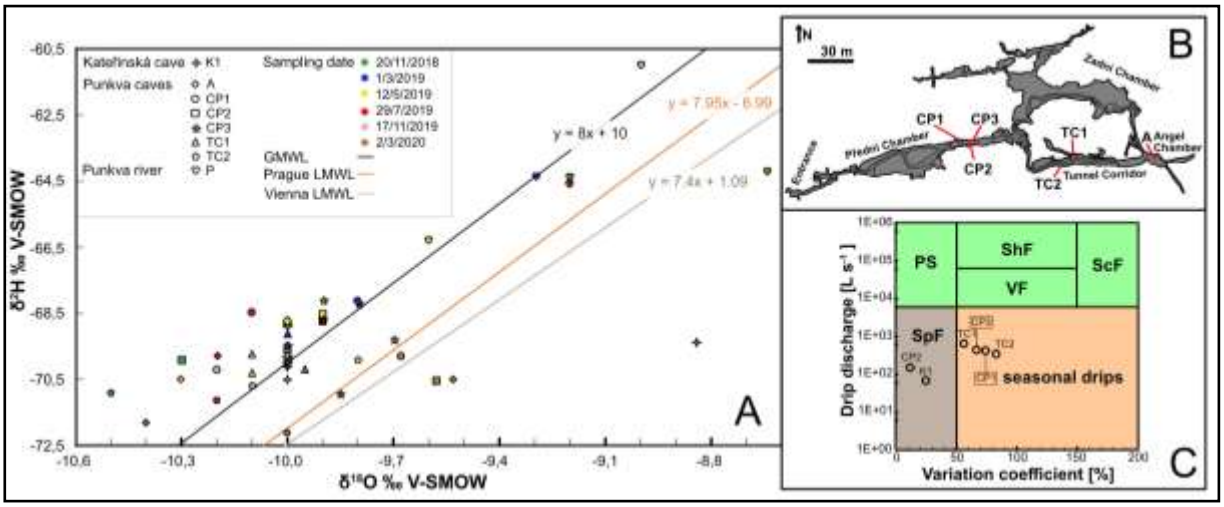

Figure 3: A) Summary of cave drip and river water $\delta^{18}O$ and $\delta^{2}H$ plotted on the meteoric water lines (GMWL – global; LMWL – local). B) Map of the dry part of Punkva Caves. C) Hydrological classification of the dripwaters from the Punkva Caves and Kateřinská Cave (Moravian Karst) based on their mean discharge and variability (PS – percolation stream, ShF – shaft flow, VF – vadose f., ScF – subcutaneous f., SpF – seepage f.). Based on SMART & FRIEDRICH (1986) and BAKER et al. (1997).

CP1–3 and K1 showed strong correlations of pH against $SI_{calcite}$ caused probably by the dependence of carbonate components on pH (increase in pH rises the CO_3^{2-} concentration and saturation).
The pH is dependent on the degassing of CO_2 from the drop and therefore on drip discharge (the longer the drop hangs on the speleothem, the more CO_2 is released). The only drip not showing correlation of pH and $SI_{calcite}$ is TC2 (caused probably by the fast discharge leading to deficient CO_2 degassing – Fig. 1).

The non-correlation of water temperature to discharge, as well as the time-delayed dependence of discharge on the precipitation, indicate a residence time of several months. CP1, CP3 and TC2 show the trend most noticeably (Fig. 2). The isotopic composition shows enlightenment of the drips. The heavier samples of the Punkva were in Oct., while the dripwaters show the heavier values in May, Jul. 2019, and Mar. 2020, indicating residence time of several months (Fig. 3A) and/or effects of evapotranspiration (ET) or different water sources for drips and the river.

5. Conclusion

The hydrogeochemical properties of the dripwaters in the Punkva Caves and the Kateřinská Cave showed very similar values and behavior as described by previous studies. The hydrochemistry of the "anomalous drip" in Punkva Caves consistently and significantly differs from the properties of "regular drips". This study shows a difference in the isotopic composition, as the anomalous drip showed low variability of $\delta^{18}O$ and $\delta^{2}H$ compared to the regular drips. This might be caused by long residence time in a large aquifer, although the hydrology seems to be too variable.

One regular drip from Kateřinská Cave showed stable discharge and constant $\delta^{18}O$, indicating voluminous well-mixed perched aquifer or complicated flow path, during which the surface effects are delayed/dampened.
The isotopic composition of dripwaters is enlightened compared to Punkva, which might be caused by ET or difference in water sources.
Based on correlations of discharge, precipitation, water temperature, and isotopic composition a several months long residence time was estimated for studied dripwaters.

Acknowledgements

We gratefully thank the Cave Administration of the Czech Republic for permission to conduct field studies and sampling.

References

APPELO C.A.J., PARKHURST D. (2013) Description of input and examples for PHREEQC ver. 3. U.S.G.S. Techniques and Methods, book 6, chap. A43, 497 p. http://pubs.usgs.gov/tm/06/a43/.

BAKER A., BARNES W.L., SMART P.L. (1997) Variations in the discharge and organic matter content of stalagmite drip waters in Lower Cave, Bristol. Hydrol. Process. 11: 1541–1555. https://doi.org/10.1002/(SICI)1099-1085(199709)11:11<1541::AID-HYP484>3.0.CO;2-Z.

FAIMON J., BODLÁKOVÁ R., PRACNÝ P., HEBELKA J. (2016) Transfer of climatic variables by dripwater : a case study from Kateřinská Cave (Moravian Karst). Environ. Earth Sci., vol. 75, p. 1151.

FAIRCHILD I., BORSATO A., TOOTH A., FRISIA S., HAWKESWORTH C.J., HUANG Y., MCDERMOTT F., SPIRO B. (2000). Controls on trace element (Sr-Mg) compositions of carbonate cave waters. Implications for speleothem climatic records. Chem. Geol. 166, 255–269. https://doi.org/10.1016/S0009-2541(99)00216-8.

FAIRCHILD I.J., SMITH C.L., BAKER A., FULLER L., SPÖTL C., MATTEY D., MCDERMOTT F. (2006) Modification and preservation of environmental signals in speleothems. Earth-Sci. Rev. 75, 105–153.

GENTY D., DEFLANDRE G. (1998) Drip flow variations under a stalactite of the Père Noël cave (Belgium). Evidence of seasonal variations and air pressure constraints. J. Hydrol., vol. 211, iss. 1–4, pp. 208–232.

LACHNIET M.S. (2009) Climatic and environmental controls on speleothem oxygen-isotope values. Quat. Sci. Rev. 28, 412–432. https://doi.org/10.1016/j.quascirev.2008.10.021.

PRACNÝ P., FAIMON J., ŠRÁČEK O., KABELKA L., HEBELKA J. (2016) Anomalous drip in the Punkva caves (Moravian Karst): relevant implications for paleoclimatic proxies. Hydrol. Process., 30: 1506–1520. Doi: 10.1002/hyp.10731.

PRACNÝ P., FAIMON J., KABELKA L., HEBELKA J. (2016) Variations of carbon dioxide in the air and dripwaters of Punkva Caves (Moravian Karst, Czech Republic). Carbonates and Evaporites 31, 375–386. https://doi.org/10.1007/s13146-015-0259-0.

SMART P., FRIEDRICH H. (1986) Water movements and storage in the unsaturated zone of a maturely karstified aquifer, Mendip Hills, England. Proceedings, Conference of environmental problems in karst terrains and their solutions, 28–30 Oct 1986. National Water Wells Assoc., Bowling Green, 57–87